

# Accuracy of macroscopic and microscopic pK<sub>a</sub> predictions of small molecules evaluated by the SAMPL6 Blind Challenge

Mehtap Isik (ORCID: [0000-0002-6789-952X](#))<sup>1,2\*</sup>, Ariën S. Rustenburg (ORCID: [0000-0002-3422-0613](#))<sup>1,3</sup>, Andrea Rizzi (ORCID: [0000-0001-7693-2013](#))<sup>1,4</sup>, M. R. Gunner<sup>6</sup>, David L. Mobley (ORCID: [0000-0002-1083-5533](#))<sup>5</sup>, John D. Chodera (ORCID: [0000-0003-0542-119X](#))<sup>1</sup>

<sup>1</sup>Computational and Systems Biology Program, Sloan Kettering Institute, Memorial Sloan Kettering Cancer Center, New York, NY 10065, United States; <sup>2</sup>Tri-Institutional PhD Program in Chemical Biology, Weill Cornell Graduate School of Medical Sciences, Cornell University, New York, NY 10065, United States; <sup>3</sup>Graduate Program in Physiology, Biophysics, and Systems Biology, Weill Cornell Medical College, New York, NY 10065, United States; <sup>4</sup>Tri-Institutional PhD Program in Computational Biology and Medicine, Weill Cornell Graduate School of Medical Sciences, Cornell University, New York, NY 10065, United States; <sup>5</sup>Department of Pharmaceutical Sciences and Department of Chemistry, University of California, Irvine, Irvine, California 92697, United States; <sup>6</sup>Department of Physics, City College of New York, New York NY 10031

\*For correspondence:  
[mehtap.isik@choderlab.org](mailto:mehtap.isik@choderlab.org) (MI)

17

---

## Abstract

Acid dissociation constant (pK<sub>a</sub>) prediction is a prerequisite for predicting many other properties of small molecules such as protein-ligand binding affinity, distribution coefficient (log D), membrane permeability, and solubility due to the necessity of predicting relevant protonation states and the free energy penalty of each state. SAMPL6 pK<sub>a</sub> Challenge was the first time that a separate challenge was conducted for evaluating pK<sub>a</sub> predictions as a part of SAMPL. It was motivated by the inaccuracies observed in prior physical property prediction challenges, such as SAMPL5 log D Challenge, caused by protonation state and pK<sub>a</sub> prediction issues. The goal of the pK<sub>a</sub> challenge was to elucidate the performance of contemporary pK<sub>a</sub> prediction methods for drug-like molecules. The challenge set was composed of 24 kinase inhibitor fragment-like small molecules and some of them were multiprotic. 11 research groups contributed blind prediction sets of 37 pK<sub>a</sub> prediction methods. Four widely used pK<sub>a</sub> prediction methods that were missing from blind predictions were added as reference methods to challenge analysis. Collecting both microscopic and macroscopic pK<sub>a</sub> predictions allowed in-depth evaluation of pK<sub>a</sub> prediction performance. This article highlights deficiencies of typical pK<sub>a</sub> prediction evaluation approaches when the difference between microscopic and macroscopic pK<sub>a</sub>s is ignored and suggests more stringent evaluation criteria for microscopic and macroscopic pK<sub>a</sub> predictions guided by the available experimental data. Top-performing submissions for macroscopic pK<sub>a</sub> predictions achieved RMSE of 0.7-1.0 units and included both quantum-mechanical and empirical approaches. These predictions included less than 8 extra/missing macroscopic pK<sub>a</sub>s for the set of 24 molecules. A large number of submissions had RMSE spanning 1-3 pK<sub>a</sub> units. Molecules with sulfur-containing heterocycles, iodo, and bromo groups suffered from less accurate pK<sub>a</sub> predictions on average considering all methods evaluated. For a subset of molecules, the available NMR-based dominant microstate sequence data was utilized to elucidate dominant tautomer prediction errors of microscopic pK<sub>a</sub> predictions which was prominent for charged tautomers. SAMPL6 pK<sub>a</sub> Challenge demonstrated the need for improving pK<sub>a</sub> prediction methods for drug-like molecules, especially for challenging moieties and multiprotic molecules. The level of pK<sub>a</sub> prediction inaccuracy observed in this challenge has potential to be detrimental to the performance of protein-ligand binding affinity predictions in two ways: (1) errors in predicted dominant charge and tautomeric state and (2) errors in the calculation of free energy correction for minor and multiple protonation states of the ligand.

## 43 0.1 Keywords

44 SAMPL · blind prediction challenge · acid dissociation constant ·  $pK_a$  · small molecule · macroscopic  $pK_a$  · microscopic  $pK_a$  · macro-  
45 scopic protonation state · microscopic protonation state

## 46 0.2 Abbreviations

47 **SAMPL** Statistical Assessment of the Modeling of Proteins and Ligands

48  **$pK_a$**   $-\log_{10}$  acid dissociation equilibrium constant

49 **SEM** Standard error of the mean

50 **RMSE** Root mean squared error

51 **MAE** Mean absolute error

52  $\tau$  Kendall's rank correlation coefficient (Tau)

53 **R<sup>2</sup>** Coefficient of determination (R-Squared)

## 54 1 Introduction

55 The acid dissociation constant ( $pK_a$ ) describes the protonation state equilibrium of a molecule given pH. Predicting  $pK_a$  is a  
56 prerequisite for predicting many other properties of small molecules such as protein-ligand binding affinity, distribution coeffi-  
57 cient ( $\log D$ ), membrane permeability, and solubility. Computer-aided drug design efforts include assessing properties of virtual  
58 molecules to guide synthesis and prioritization decisions. In such cases an experimental  $pK_a$  measurement is not possible.  
59 Therefore, accurate computational  $pK_a$  prediction methods are required.

60 For a monoprotic weak acid (HA) or base (B) dissociation equilibria shown in Equation 1, the acid dissociation constant is  
61 expressed as in Equations 2 or its common negative logarithmic form as in Equation 3. The ratio of ionization states can be  
62 calculate with HHenderson-Hasselbalch equations shown in Equation 4.



$$K_a = \frac{[A^-][H^+]}{[HA]} \quad K_a = \frac{[B][H^+]}{[BH^+]} \quad (2)$$

$$pK_a = -\log_{10} K_a \quad (3)$$

$$pH = pK_a + \log_{10} \frac{[A^-]}{[HA]} \quad pH = pK_a + \log_{10} \frac{[B]}{[BH^+]} \quad (4)$$

63 Ionizable sites are found often in drug molecules and influence their pharmaceutical properties including target affinity,  
64 ADME/Tox, and formulation properties [1]. Drug molecules with titratable groups can exist in many different charge and proto-  
65 nation states based on the pH of the environment. We rely on  $pK_a$  values to determine in which charge and protonation states  
66 the molecules exists and relative populations of these states. The pH of the human gut ranges between 1-8 and 74% of approved  
67 drugs can change ionization states withing this physiological pH range [2] and because of this  $pK_a$  values of drug molecules pro-  
68 vides essential information about their physicochemical and pharmaceutical properties. A wide distribution of acidic and basic  
69  $pK_a$  values, ranging from 0 to 12, have been observed in approved drugs [1, 2].

70 Small molecule  $pK_a$  predictions influence computational protein-ligand binding affinities in multiple ways. Errors in  $pK_a$  pre-  
71 dictions can cause modeling the wrong charge, protonation, and tautomerization states which affect hydrogen bonding oppor-  
72 tunities and charge distribution of the ligand. The prediction of the dominant protonation state and relative population of minor  
73 states in aqueous medium is dictated by the  $pK_a$  values. The relative free energy of different protonation states in the aque-  
74 ous state is a function of  $pK_a$  and pH, it contributes to the overall protein-ligand affinity in the form of a free energy penalty of  
75 reaching higher energy protonation states [3].

76 Drug-like molecules present difficulties for  $pK_a$  prediction compared to simple monoprotic molecules. Drug-like molecules  
77 are frequently multiprotic, have large conjugated systems, heterocycles, tautomerization. In addition that larger molecules  
78 with conformational flexibility can have intramolecular hydrogen bonding which shifts  $pK_a$  values. These shifts could be real or

79 modeling artifacts due to collapsed conformations caused by deficiencies in solvation models. Yet predicting  $pK_a$ s of drug-like  
80 molecules accurately is a prerequisite for computational drug discovery and design.

81 The definition of  $pK_a$  diverges into two for multiprotic molecules: macroscopic  $pK_a$  and microscopic  $pK_a$  [4–6]. Macroscopic  
82  $pK_a$  describes the equilibrium dissociation constant between different charged states of the molecule. Each charge state can be  
83 composed of multiple tautomers. Macroscopic  $pK_a$  is about the deprotonation of the molecule, not a particular titratable group.  
84 Microscopic  $pK_a$  describes the acid dissociation equilibrium between individual tautomeric states of different charges. We refer  
85 to collection of all tautomeric states of different macroscopic states (charge states) as microscopic states. Microscopic  $pK_a$  value  
86 defined between two microstates captures the deprotonation of a single titratable group with a fixed background protonation  
87 state of other titratable groups. In molecules with multiple titratable groups, the protonation state of one group can affect the  
88 proton dissociation propensity of another functional group, therefore the same titratable group may have different microscopic  
89  $pK_a$  values based on the protonation state of the rest of the molecule. Different experimental methods capture different def-  
90 initions of  $pK_a$ s as explained in more detail in this prior publication [7]. Most common  $pK_a$  measurement techniques such as  
91 potentiometric and spectrophotometric methods measure macroscopic  $pK_a$ s while NMR measurements can determine micro-  
92 scopic  $pK_a$ s and microstate populations. Therefore, it is important to pay attention to the source and definition of  $pK_a$  values  
93 to interpret their meaning correctly. Computational methods can predict both microscopic and macroscopic  $pK_a$ s. While micro-  
94 scopic  $pK_a$  predictions are more informative for determining relevant microstates/tautomers of a molecule and their relative  
95 free energies, computing predicted macroscopic  $pK_a$ s is useful for direct comparison of methods to more common macroscopic  
96 experimental measurements. In this paper, we explore approaches to assess the performance of both macroscopic and micro-  
97 scopic  $pK_a$  predictions, taking advantage of available experimental data.

98 Microscopic  $pK_a$  predictions can be converted to macroscopic  $pK_a$  predictions either directly with the equation 5 [8] or  
99 through computing the macroscopic free energy of deprotonation between ionization states with charges N and N-1 via Boltz-  
100 mann weighted sum of the relative free energy of microstates ( $G_i$ ) as in equations 6 and 7 [9].

$$K_a^{\text{macro}} = \sum_{j=1}^{N_{\text{deprot}}} \frac{1}{\sum_{i=1}^{N_{\text{prot}}} \frac{1}{K_{ij}^{\text{micro}}}} , \quad (5)$$

$$\Delta G_{N-1,N} = RT \ln \frac{\sum_i e^{-G_i/RT} \delta_{N_i, N-1}}{\sum_i e^{-G_i/RT} \delta_{N_i, N}} \quad (6)$$

$$pK_a = pH - \frac{\Delta G_{N-1,N}}{RT \ln 10} \quad (7)$$

101 In Equation 6  $\Delta G_{N-1,N}$  is the effective macroscopic protonation free energy.  $\delta_{N_i, N-1}$  is equal to 1 when the microstate i has a  
102 total charge of N-1 and null otherwise.  $\delta_{N_i, N}$  is equal to 1 when the microstate i has a total charge of N and null otherwise. RT is  
103 the ideal gas constant times the temperature.

## 104 1.1 Motivation for a blind $pK_a$ challenge

105 SAMPL (Statistical Assessment of the Modeling of Proteins and Ligands) is a series of annual computational prediction chal-  
106 lenges for the computational chemistry community. The goal of SAMPL is evaluate to current performance of the models and to  
107 bring the attention of quantitative biomolecular modeling field on major issues that limit the accuracy of protein-ligand binding  
108 models.

109 SAMPL Challenges that focus on different physical properties so far have assessed intermolecular binding models of various  
110 protein-ligand and host-guest systems, solvation models to predict hydration free energies and distribution coefficients. Poten-  
111 tial benefits of these challenges are motivating improvement computational methods and revealing unexpected contributors to  
112 error by focusing on interesting test systems. SAMPL Challenges have demonstrated the effects of force field accuracy, sampling  
113 issues, solvation modeling defects, and tautomer/protonation state predictions on protein-ligand binding predictions.

114 During the SAMPL5 log D Challenge, the performance of cyclohexane-water log D predictions were lower than expected and  
115 accuracy suffered when protonation states and tautomers were not taken into account [10, 11]. With the motivation of decon-  
116 voluting the different sources of error contributing to the large errors observed in the SAMPL5 log D Challenge, we organized

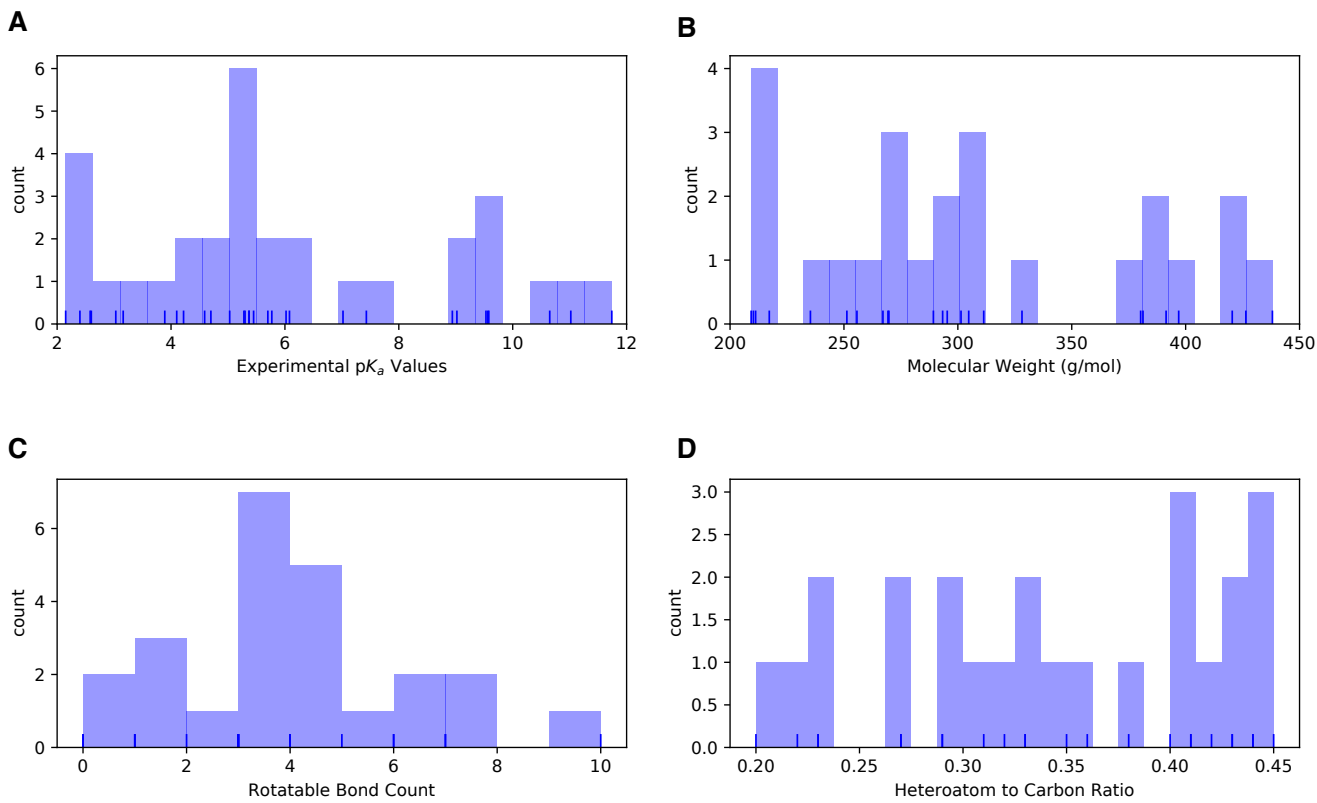


**Figure 1. Distribution of molecular properties of 24 compounds in SAMPL6  $pK_a$  Challenge.** **A** Histogram of spectrophotometric  $pK_a$  measurements collected with Sirius T3 [7]. Overlayed carpet plot indicates the actual values. Five compounds have multiple measured  $pK_a$ s in the range of 2-12. **B** Histogram of molecular weights of compounds in SAMPL6 set. Molecular weights were calculated by neglecting counter ions. **C** Histogram of the number of non-terminal rotatable bonds in each molecule. **D** The histogram of the ratio of heteroatom (non-carbon heavy atom) count to the number of carbon atoms.

separate of  $pK_a$  and log  $P$  challenges in SAMPL6 [7, 12, 13]. For this iteration of the SAMPL challenge, we have taken one step back and isolated just the problem of predicting aqueous protonation states.

This is the first time a blind  $pK_a$  prediction challenge has been fielded as part of SAMPL. In this first iteration of the challenge, we aimed to assess the performance of current  $pK_a$  prediction methods for drug-like molecules, investigate potential causes of inaccurate  $pK_a$  estimates, and determine how much current level of expected accuracy might impact protein binding affinity predictions. In binding free energy predictions, any error in predicting the free energy of accessing a minor aqueous protonation state of ligand that contributes to the complex formation will directly add to the error in the predicted binding free energy. Similarly for log  $D$  predictions, inaccurate prediction aqueous protonation state that contribute partitioning between phases or prediction of relative free energy of these states will be detrimental to the accuracy of transfer free energy predictions.

## 1.2 Approaches to predict small molecule $pK_{a,s}$

Overview of kinds of  $pK_a$  prediction methods available. Define method categories: DL, LFER, QSPR/ML, QM, QM+LEC, and QM+MM

## 2 Methods

### 2.1 Design and logistics of the SAMPL6 $pK_a$ Challenge

The SAMPL6  $pK_a$  Challenge was conducted as a blind prediction challenge focus on predicting aqueous  $pK_a$  value of 24 small molecules that resemble fragments of kinase inhibitors. The compound selection process was described in depth in the prior

132 publication reporting SAMPL6 pK<sub>a</sub> Challenge experimental data collection [7]. The distribution of molecular weights, experimen-  
133 tal pK<sub>a</sub> values, number of rotatable bonds, and heteroatom to carbon ratio are depicted in Fig. 1. The challenge molecule set  
134 was composed of 17 small molecules with limited flexibility (less than 5 non-terminal rotatable bonds) and 7 molecules with  
135 5-10 non-terminal rotatable bonds. The distribution of experimental pK<sub>a</sub> values ranged between 2-12 and roughly uniform. 2D  
136 representations of all compounds were provided in Fig. 5. Drug-like molecules are often larger and more complex than the ones  
137 used in this study, however, aimed for the

138 The dataset composition and details of the pK<sub>a</sub> measurement technique, except the identity of the small molecules, were  
139 announced about a month before the challenge start time. Experimental macroscopic pK<sub>a</sub> measurements were collected with  
140 spectrophotometric method of Sirius T3, at room temperature in ionic strength-adjusted water with 0.15 M KCl [7]. The instruc-  
141 tions for participation and the identity of the challenge molecules were released at the challenge start date (October 25, 2017).  
142 A table of molecule IDs (in the form of SM##) and their canonical isomeric SMILES was provided as input. Blind prediction  
143 submissions were accepted until January 22, 2018.

144 Following the conclusion of the blind challenge, the experimental data was made public on January 23, 2018. The SAMPL  
145 organizers and participants gathered at the Second Joint D3R/SAMPL Workshop, at UC San Diego, La Jolla, CA on February 22-23,  
146 2018 to share results. The workshop aimed to create an opportunity for participants to have discussions, evaluate the results  
147 and lessons of the challenge together. The participants reported their results and their own evaluations in the special issue of  
148 the Journal of Computer-Aided Molecular Design [14].

149 In this first iteration of pK<sub>a</sub> prediction challenge we were not sure what was the best way to capture all necessary informa-  
150 tion related to pK<sub>a</sub> predictions. Our aim was to directly evaluate macroscopic pK<sub>a</sub> predictions comparing them to experimental  
151 macroscopic pK<sub>a</sub> values and to use collected microscopic pK<sub>a</sub> prediction data for more in-depth diagnostics of method perfor-  
152 mance. Therefore, we asked participants to submit their predictions in three different submission types:

- 153 • **Type I:** microscopic pK<sub>a</sub> values and related microstate pairs
- 154 • **Type II:** fractional microstate populations as a function of pH in 0.1 pH increments
- 155 • **Type III:** macroscopic pK<sub>a</sub> values

156 For each submission type, a machine-readable submission file template was specified. For type I submissions, participants  
157 were asked to report microstate ID of protonated state, microstate ID of deprotonated state, microscopic pK<sub>a</sub>, microscopic  
158 pK<sub>a</sub> SEM. The reason and method of microstate enumeration is discussed further in Section 2.2 "Enumeration of Microstates".  
159 The SEM captures the statistical uncertainty of the predicted method. Microstate IDs were preassigned identifiers for each mi-  
160 crostates in the form of SM##\_micro##. For type II submission, submission format included a table that started with microstate  
161 ID and consecutive columns reporting natural logarithm of fractional microstate population values of each predicted microstate  
162 for 0.1 pH increments between pH 2 and 12. For type III submissions participants were asked to report molecule ID, macroscopic  
163 pK<sub>a</sub>, macroscopic pK<sub>a</sub> SEM. It was mandatory to submit predictions for all fields for each prediction, but it was not mandatory to  
164 submit predictions for all the molecules or all the submission types. Although we have accepted submissions with partial sets of  
165 molecules, it would have been a better choice to require predictions for all the molecules for better comparison of method per-  
166 formance. The submission files also included fields for naming the method, listing the software utilized, and a free text method  
167 section for the detailed documentation of each method.

168 Participants were allowed to submit predictions with multiple methods as long as they create separate submissions files.  
169 Anonymous participation to the challenge was allowed, however all participant opted to make their submissions public. All blind  
170 submissions were assigned a unique 5-digit alphanumeric submission ID, which will be used throughout this paper. Unique IDs  
171 were also assigned when multiple submissions exists for different submission types of the same method such as microscopic  
172 pK<sub>a</sub>(type I) and macroscopic pK<sub>a</sub> (type III). These submission IDs were also reported in the evaluation papers of participants and  
173 allow cross-referencing. Submission IDs, participant provided method names, and method categories are presented in Table 1.  
174 There were many instances that multiple types of submissions of the same method were provided by participants as challenge  
175 instructions requested. Although each prediction set was assigned a separate submission ID we have matched the submissions  
176 that originated from the same method according to the reports of the participant. Submission ID for both macroscopic (type III)  
177 and microscopic (type I) pK<sub>a</sub> predictions of each method (when exists) are shown in Table 1.

## 178 2.2 Enumeration of microstates

179 To capture both the pK<sub>a</sub> value and titration position of microscopic pK<sub>a</sub> predictions, we needed microscopic pK<sub>a</sub> predictions to  
180 be reported together with the pair of deprotonated and protonated microstates that describes the transition. String represen-

tations of molecules such as canonical SMILES with explicit hydrogens can be written, however, there can be inconsistencies between the interpretation of canonical SMILES written by different softwares and algorithms. In order to avoid complications while reading microstate structure files from different sources, we have decided that the safest route was pre-enumerating all possible microstates of challenge compounds, assigning the microstates IDs to each in the form of SM##\_micro##, and require participants to report microstate pairs using the provided microstates IDs.

We enumerated an initial list of microstates with Epik and OpenEye QUACPAC and took the union of results. Microstates with Epik were generated using Schrodinger Suite v2016-4, and running Epik to enumerate all tautomers within 20  $pK_a$  units of pH 7. For enumerating microstates with OpenEye QUACPAC, we had to first enumerate formal charges and for each charge enumerate all possible tautomers using the settings of maximum tautomer count 200, level 5, and carbonyl hybridization False. Then we created an union of all enumerated states written as canonical isomeric SMILES. Even though resonance structures correspond to different canonical isomeric SMILES they are not different microstates, therefore it was necessary to remove resonance structures that were replicates of the same tautomer. To detect resonance structures we converted canonical isomeric SMILES to InChI hashes with explicit and fixed hydrogen layer. Structures that describe the same tautomer but different resonance states lead to explicit hydrogen InChI hashes that are identical allowing replicates to be removed. The Jupyter Notebook used for the enumeration of microstates is provided in supplementary documents. Because resonance and geometric isomerism should be ignored when matching predicted structures microstate IDs (except SM20 which should be modelled as E-isomer), we provided microstate ID tables with canonical SMILES and 2D-depictions.

Despite pooling together enumerated charge states and tautomers with Epik and OpenEye QUACPAC to our surprise the microstate lists were still incomplete. A better algorithm that can enumerate all possible microstates would be very beneficial. In SAMPL6 Challenge participants came up with new microstates that were not present in the initial list that we provided. Based on participant requests we iteratively had to update the list of microstates and assign new microstate IDs. Every time we received a request, we shared the updated microstate ID lists with all the challenge participants.

A working  $pK_a$  microstate definition for this challenge was provided in challenge instructions for clarity. Physically meaningful microscopic  $pK_a$ s are defined between microstate pairs that can interconvert by single protonation/deprotonation event of only one titratable group. So, microstate pairs should have total charge difference of |1| and only one heavy atom that differs in the number of bound hydrogens, regardless of resonance state or geometric isomerism. All geometric isomer and resonance structure pairs that have the same number of hydrogens bound to equivalent heavy atoms are related to the same microstate. Pairs of resonance structures and geometric isomers (cis/trans, stereo) won't be considered as different microstates, as long as there is no change in the number of hydrogens bound to each heavy atom in these structures. Since we wanted to participants to report only microscopic  $pK_a$ s that are describe single deprotonation events (in contrast to transitions between microstates that are different in terms of two or more titratable protons), we have also provided a pre-enumerated list of allowed microstate pairs.

Provided microstate ID and microstate pair lists were intended to be used for reporting microstate IDs and to aid parsing of submissions. The enumerated lists of microstates were not created with the intent to guide computational predictions. This was clearly stated in the challenge instructions. However, we noticed that some participants still used the microstate lists as an input for their  $pK_a$  predictions as we received complaints from participants that due to our updates to microstate lists they needed to repeat their calculations. This would not have been an issue, if participants used  $pK_a$  prediction protocols that did not rely on an external pre-enumerated list of microstates as an input. None of the participants have reported this dependency in their method descriptions explicitly, therefore we can not identify which submissions have used the enumerated microstate lists as input and which ones has followed the instructions.

## 2.3 Evaluation approaches

Since the experimental data for the challenge was mainly composed of macroscopic  $pK_a$  values of both monoprotic and multi-protic compounds, evaluation of macroscopic and microscopic  $pK_a$  predictions was not straightforward. For only a subset of 8 molecules, dominant microstate sequence could be inferred from NMR. For the rest of the molecules the only experimental information available was the macroscopic  $pK_a$  value, while experimental data did not provide any information on which group(s) are being titrated, microscopic  $pK_a$  values, identity of associated macrostates (which charge) or microstates (which tautomers). In this comparative performance evaluation of we let the experimental data lead the challenge analysis towards various evaluation routes. To compare macroscopic  $pK_a$  predictions to experimental values we had to utilize numerical matching algorithms before we could calculate performance statistics. For the subset of molecules with experimental data about microstates, we used microstate based matching. These matching methods were described further in the next section.

231 Three types of submissions were collected during the SAMPL6  $pK_a$  Challenge. We have only utilized type I (microscopic  $pK_a$   
232 value and microstate IDs) and type III (macroscopic  $pK_a$  value) predictions in this article. Type I submissions contained the same  
233 prediction information as the the type II submissions which reported fractional population of microstates with respect to pH.

### 234 2.3.1 Matching algorithms for pairing predicted and experimental $pK_a$ s

235 Macroscopic  $pK_a$  predictions can be calculated from microscopic  $pK_a$ s for direct comparison to experimental macroscopic  $pK_a$   
236 values, although there is still a remaining issue. How to match predicted macroscopic  $pK_a$ s to experimental macroscopic  $pK_a$ s  
237 when there could multiple numbers of each reported for each molecule? Experimental data in this case did not provide any  
238 information that would indicate the titration site, the overall charge or the tautomer composition of macrostate pairs that are  
239 associated with each measured macroscopic  $pK_a$  that can guide the matching.

240 For evaluating predictions taking the experimental data as reference Fraczkiewicz et al. delinited recommendations for fair  
241 comparative analysis of computational  $pK_a$  predictions [15]. In the absence any experimental information that would aid the  
242 match, experimental and computational  $pK_a$ s should be matched preserving the order of  $pK_a$  values and minimizing sum of  
243 absolute errors.

244 We picked Hungarian matching algorithm [16, 17] to assign experimental and predicted macroscopic  $pK_a$ s with squared error  
245 cost function as suggested by Kiril Lanevskij. The algorithm is available in SciPy package (`scipy.optimize.linear_sum_assignment`) [18].  
246 This matching algorithm provides optimum global assignment that minimizes linear sum of squared errors of all pairwise  
247 matches. The reason to select squared error cost function instead of absolute error cost function is to avoid misordered matches,  
248 For instance, for a molecule with experimental  $pK_a$  values of 4 and 6, and predicted  $pK_a$ s of 7 and 8, Hungarian matching with  
249 absolute error cost function would match 6 to 7 and 4 to 9. Hungarian matching with squared error cost would match 4 to 7  
250 and 6 to 9, preserving the increasing  $pK_a$  value order between experimental and predicted values. A weakness of this approach  
251 would be failing to match experimental value of 6 to predicted value of 7, if that was the correct match based on underlying  
252 macrostates. But underlying pair of states were unknown to us both because experimental data of the challenge did not con-  
253 tain information about what charge states the transitions were happening between and also because we have not collected the  
254 pair of macrostates associated with each  $pK_a$  predictions in submissions. There is no perfect solution to numerical  $pK_a$  assign-  
255 ment problem, but we tried to determine the most fair way to penalize predictions based on their numerical deviation from the  
256 experimental values.

257 For the analysis of microscopic  $pK_a$  predictions we adopted a different matching approach. Only for the 8 molecules, we util-  
258 ized the dominant microstate sequence inerfered from NMR experiments to match computational predictions and experimental  
259  $pK_a$ s. We will refer to this assignment method as microstate matching, where experimental  $pK_a$  value is matched to the com-  
260 putational microscopic  $pK_a$  value which was reported for the dominant microstate pair observed for each transition. We have  
261 compared the results of Hungarian matching and microstate matching.

262 Inevitably the choice of matching algorithms to assign experimental and predicted values has an impact on the calculation  
263 of performance statistics. We believe the Hungarian algorithm for numerical matching and microstate-based were the best  
264 choices, providing the most unbiased matching without introducing assumptions outside of the experimental data.

### 265 2.3.2 Statistical metrics for submission performance

266 A variety of accuracy and correlation statistics were considered for analyzing and comparing performance of predictions meth-  
267 ods submitted to the SAMPL6  $pK_a$  Challenge. Calculated performance statistics of predictions were provided to participants  
268 before the workshop. Details of the analysis and scripts are maintained on the SAMPL6 Github Repository (described in Section  
269 5).

270 There are six error metrics reported for the numerical error of the  $pK_a$  values: the root-mean-squared error (RMSE), mean ab-  
271 solute error (MAE), mean error (ME), coefficient of determination ( $R^2$ ), linear regression slope ( $m$ ), and Kendall's Rank Correlation  
272 Coefficient ( $\tau$ ). Uncertainty in each performance statistic was calculated as 95% confidence intervals estimated by bootstrapping  
273 over predictions with 10000 bootstrap samples. Calculated errors statistics of all methods can be found in Table S2 for macro-  
274 scopic  $pK_a$  predictions and Tables S4 and S4 for microscopic  $pK_a$  predictions.

275 In addition to the numerical error aspect of the  $pK_a$  values, we have also evaluated predictions in terms of their ability to cap-  
276 ture the correct macrostates (ionization states) and microstates (tautomers of each ionization state) to the extend possible from  
277 the available experimental data. For macroscopic  $pK_a$ s experiments did not provide any evidence of the identity of the ionization  
278 states. However, the number of ionization states indicates the number of macroscopic  $pK_a$ s that exists between experimental  
279 range of 2.0-12.0. For instance, SM14 has two experimental  $pK_a$ s and therefore 3 different charge states were observed between

the pH range of 2.0-12.0. If a prediction reported 4 macroscopic  $pK_a$ s, it is clear that this method predicted an extra ionization state. With this perspective we reported the number of unmatched experimental  $pK_a$ s (the number of missing  $pK_a$  predictions, i.e. missing ionization states) and the number of unmatched predicted  $pK_a$ s (the number of extra  $pK_a$  predictions, i.e. extra ionization states) after Hungarian matching. The later count was restricted to only predictions with  $pK_a$  values between 2 and 12, because that was the range of the experimental method. Errors in extra or missing  $pK_a$  prediction errors highlight failure to predict the correct number of ionization states within a pH range.

For the evaluation of microscopic  $pK_a$  predictions, taking advantage of the available dominant microstate sequence data for a subset of 8 compounds, we calculated the dominant microstate prediction accuracy. Dominant microstate prediction accuracy is the ratio of correct dominant tautomer predictions for each charge state divided by, calculated over all ionization states of each molecule. In order to extract the sequence of dominant microstates from the microscopic  $pK_a$  predictions sets, we calculated the relative free energy of microstates selecting a neutral tautomer and pH 0 as reference following the Equation 8. Calculation of relative free energy of microstates was explained in more detail in a previous publication [19].

Relative free energy of state with respect to reference state B at pH 0.0 (arbitrary pH value selected as reference) can be calculated as follows:

$$\Delta G_{AB} = \Delta m_{AB} RT \ln 10 (pH - pK_a) \quad (8)$$

$\Delta m_{AB}$  is equal to the number protons in state A minus state B. R and T indicate molar gas constant and temperature, respectively. By calculating relative free energies of all predicted microstates with respect to the same reference state and pH, we were able to determine the sequence of predicted dominant microstates. The dominant tautomer of each charge state was determined as the the microstate with the lowest free energy in the subset of predicted microstates of each ionization state. This approach is feasible because the relative free energy of tautomers of the same ionization state is independent of pH and therefore the choice of reference pH is arbitrary.

We created a shortlist of top-performing methods for macroscopic and microscopic  $pK_a$  predictions. Top macroscopic  $pK_a$  predictions were selected based on the following criteria of consistence performance among different metrics: ranking in the top 10 consistently according to two error (RMSE, MAE) and two correlation metrics (R-Squared, and Kendall's Tau), and also havin a combined count of less than 8 missing or extra macroscopic  $pK_a$ s for the entire molecule set (a third of the number of compounds). These methods are presented in Table 2. A separate list of top performing methods were selected for microscopic  $pK_a$  with the following criteria: ranking in the top 10 methods when ranked by accuracy statistics (RMSE and MAE) and perfect dominant microstate prediction accuracy. These methods are presented in Table 3.

In addition to comparing the performance comparison of methods, we also wanted to compare  $pK_a$  prediction performance on the level of molecules to determine  $pK_a$ s of which molecules in the challenge set were harder to predict considering all the methods in the challenge. For this purpose, we plotted prediction error distributions of each molecule considering all prediction methods. We also calculated MAE for each molecule's over all predictions as well as for predictions from each method category.

## 2.4 Reference calculations

Including null model as helpful in comparative performance analysis of predictive methods to establish what the performance statistics look like for a baseline method for the specific dataset. Null models or null predictions employ a simple prediction model which is not expected to be particularly successful, but it is useful for providing a simple point of comparison for more sophisticated methods. The expectation is for more sophisticated or costly prediction methods to outperform the predictions from a null model, otherwise the simpler null model would be preferable. In SAMPL6  $pK_a$  Challenge there were two blind submissions that database lookup methods that were suitable to be considered as null predictions. These methods, with submission IDs 5nm4j and 5nm4j both used OpenEye pKa-Prospector database to find the most similar molecule to query molecule and report its  $pK_a$  as predicted value. We acknowledge that database lookup methods with a rich experimental database presents a challenging null model to beat, however, due to the accuracy level needed from  $pK_a$  predictions for computer-aided drug design we believe it is an appropriate performance baseline that physical and empirical  $pK_a$  prediction methods should strive to perform better than.

We have also included additional reference calculations in the comparative analysis to provide more perspective. The methods we chose to include as reference calculations were missing from the blind predictions sets although they are widely used methods by academia and industry. representing different methodological approaches: Schrodinger/Epik (nb007, nb008, nb010), Schrodinger/Jaguar (nb011, nb013), Chemaxon/Chemicalize (nb015), and Molecular Discovery/MoKa (nb016, nb017). Epik and

327 Jaguar p<sub>K</sub><sub>a</sub> predictions were collected by Bas Rustenburg, Chemicalize predictions by Mehtap Isik, and MoKa predictions by  
328 Thomas Fox, after the challenge deadline avoiding any alterations to the respective standard procedures of the methods and  
329 guidance of the experimental date. Reference calculations were not formally blind, as experimental data of the challenge has  
330 been made publically available before their collection.

331 All figures and statistics tables in this manuscript include reference calculations. As the reference calculations were not formal  
332 submissions, these were omitted from formal ranking in the challenge, but we present plots in this article which show them for  
333 easy comparison. These are labeled with submission IDs of the form *nb###* to allow easy recognition of non-blind reference  
334 calculations.

### 335 3 Results and Discussion

336 Participation to SAMPL6 p<sub>K</sub><sub>a</sub> Challenge was high with 11 research groups contributing p<sub>K</sub><sub>a</sub> prediction sets of 37 methods. A large  
337 variety of p<sub>K</sub><sub>a</sub> prediction methods were represented in SAMPL6 Challenge. We categorized these submissions into four method  
338 categories: database lookup (DL), linear free energy relationship (LFER), quantitative structure property relationship or machine  
339 learning (QSPR/ML), and quantum mechanics (QM). Quantum mechanics models were subcategorized into QM methods with  
340 and without linear empirical correction (LEC), and combined quantum mechanics and molecular mechanics (QM + MM). Table 1  
341 presents, method names, submission IDs, method categories, and also references of each approach. Integral equation-based  
342 approaches (e.g. EC-RISM) were also evaluated under the Physical (QM) category. There were 2 DL, 4 LFER, and 5 QSPR/ML  
343 methods represented in the challenge, including the reference calculations. Majority of QM calculations include linear empirical  
344 corrections (22 methods in QM + LEC category), and only 5 QM methods were submitted without any empirical corrections.  
345 There were 4 methods that used a mixed physical modeling approach of QM + MM.

346 The following sections present detailed performance evaluation of blind submissions and reference prediction methods for  
347 macroscopic and microscopic p<sub>K</sub><sub>a</sub> predictions. Performance statistics of all the methods can be found in Tables S2 and S4.  
348 Methods are referred to by their submission ID's which are provided in Table 1.

#### 349 3.1 Analysis of macroscopic p<sub>K</sub><sub>a</sub> predictions

350 The performance of macroscopic p<sub>K</sub><sub>a</sub> predictions were analyzed by comparison to experimental p<sub>K</sub><sub>a</sub> values collected by the  
351 spectrophotometric method via numerical matching following the Hungarian method. Overall p<sub>K</sub><sub>a</sub> prediction performance was  
352 lower than we have hoped for. Fig. 2 shows RMSE calculated for each prediction method represented by their submission IDs.  
353 Other performance statistics are depicted in Fig. 3. In both figures method categories were indicated by the color of the error  
354 bars. Statistics depicted in these figures can be found in Table S2. Prediction error ranged between 0.7 to 3.2 p<sub>K</sub><sub>a</sub> units in terms  
355 of RMSE, while an RMSE between 2-3 log units was observed for the majority of methods (20 out of 38 methods). Only five meth-  
356 ods achieved RMSE less than 1 p<sub>K</sub><sub>a</sub> unit. One is QM method with COSMO-RS approach for solvation and linear empirical cor-  
357 rection (*xvxzd* (DSD-BLYP-D3(BJ)/def2-TZVPD//PBEh-3c[DCOSMO-RS] + RRHO(GFN-xTB[GBSA]) + Gsolv(COSMO-RS[TZVPD]) and  
358 linear fit)), and the remaining four are empirical prediction methods of LFER (*xmyhm* (ACD/pKa Classsic), *nb007* (Schrodinger/Epk  
359 Scan)) and QSPR/ML categories (*gyuhx* (Simulations Plus), *nb017* (MoKa)). These five methods with RMSE less than 1 p<sub>K</sub><sub>a</sub> unit also  
360 are the methods that have the lowest MAE. *xvxzd* and *xmyhm* were the only two methods for which the upper 95% confidence  
361 interval of RMSE was lower than 1 p<sub>K</sub><sub>a</sub> unit.

362 In terms of correlation statistics performance of many methods have good performance, although the ranking of methods  
363 change R<sup>2</sup> and Kendall's Tau and many methods are indistinguishable from one another considering uncertainty of the correla-  
364 tion statistics. 32 out of 38 methods have R higher than and Kendall's Tau higher than 0.7 and 0.6, respectively. 8 methods have  
365 R<sup>2</sup> higher than 0.9 and 6 methods have Kendall's Tau higher than 0.8. The overlap of these two sets are the following: *gyuhx* (Sim-  
366 ulations Plus), *xvxzd* (DSD-BLYP-D3(BJ)/def2-TZVPD//PBEh-3c[DCOSMO-RS] + RRHO(GFN-xTB[GBSA]) + Gsolv(COSMO-RS[TZVPD])  
367 and linear fit), *xmyhm* (ACD/pKa Classic), *ryzue* (Adiabatic scheme with single point correction: MD/M06-2X//6-311++G(d,p)//M06-  
368 2X/6-31+G(d) for bases and SMD/M06-2X//6-311++G(d,p)//M06-2X/6-31G(d) for acids + thermal corrections), and *5byn6* (Adiabatic  
369 scheme: thermodynamic cycle that uses gas phase optimized structures for gas phase free energy and solution phase geo-  
370 metries for solvent phase free energy. SMD/M06-2X/6-31+G(d) for bases and SMD/M06-2X/6-31G(d) for acids + thermal corrections).  
371 It is worth noting that the *ryzue* and *5byn6* are QM predictions without any empirical correction. Their high correlation and rank  
372 correlation coefficient scores signal that with an empirical correction their accuracy based performance could improve. Indeed,  
373 the participants have showed that this is the case in their individual challenge analysis paper and achieved RMSE of 0.73 p<sub>K</sub><sub>a</sub>  
374 units after the challenge [28].

**Table 1. Submission IDs, names, category, and type for all the pKa prediction sets.** Reference calculations are labeled as *nb###*. The method name column lists the names provided by each participant in the submission file. The “type” column indicates if submission was or a post-deadline reference calculation, denoted by “Blind” or “Reference” respectively. The methods in the table are grouped by method category and not ordered by performance.

Method Category	Method	Microscopic pKa (Type I) Submission ID	Macroscopic pKa (Type III) Submission ID	Submission Type	Ref.
DL	Substructure matches to experimental data in pKa OpenEye pKa Prospector Database v1.0	<i>5nm4j</i>	Null	[20]	
DL	OpenEye pKa-Prospector 1.0.0.3 with Analog Search ion identification algorithm	<i>pwn3m</i>	Null	[20]	
LFER	ACD/pKa GALAS (ACD/Percepta Kernel v1.6)	<i>v8qph</i>	<i>37xm8</i>	Blind	[21]
LFER	ACD/pKa Classic (ACD/Percepta Kernel, v1.6)		<i>xmyhm</i>	Blind	[22]
LFER	Epik Scan (Schrodinger v2017-4)		<i>nb007</i>	Reference	[23]
LFER	Epik Microscopic (Schrodinger v2017-4)	<i>nb008</i>	<i>nb010</i>	Reference	[23]
QSPR/ML	OpenEye Gaussian Process	<i>6tvf8</i>	<i>hytjn</i>	Blind	[11]
QSPR/ML	OpenEye Gaussian Process Resampled		<i>q3pfj</i>	Blind	[11]
QSPR/ML	S+pKa (ADMET Predictor v8.5, Simulations Plus)	<i>hdijq</i>	<i>gyuhx</i>	Blind	[24]
QSPR/ML	Chemicalize v18.23 (ChemAxon MarvinSketch v18.23)		<i>nb015</i>	Reference	[25]
QSPR/ML	Moka v3.1.3	<i>nb016</i>	<i>nb017</i>	Reference	[26, 27]
QM	Adiabatic scheme with single point correction: SMD/M06-2X//6-311++G(d,p)//M06-2X/6-31+G(d) for bases and SMD/M06-2X//6-311++G(d,p)//M06-2X/6-31G(d) for acids + thermal corrections	<i>ko8yx</i>	<i>ryzue</i>	Blind	[28]
QM	Direct scheme with single point correction: SMD/M06-2X//6-311++G(d,p)//M06-2X/6-31G(d) for bases and SMD/M06-2X//6-311++G(d,p)//M06-2X/6-31G(d) for acids + thermal corrections	<i>w4z0e</i>	<i>xikp8</i>	Blind	[28]
QM	Adiabatic scheme: thermodynamic cycle that uses gas phase optimized structures for gas phase free energy and solution phase geometries for solvent phase free energy. SMD/M06-2X/6-31+G(d) for bases and SMD/M06-2X/6-31G(d) for acids + thermal corrections	<i>wcvnu</i>	<i>5byn6</i>	Blind	[28]
QM	Vertical scheme: thermodynamic cycle that uses only gas phase optimized structures to compute gas phase and solvation free energy. SMD/M06-2X/6-31+G(d) for bases and SMD/M06-2X/6-31G(d) for acids + Thermal corrections	<i>arcko</i>	<i>w4iyd</i>	Blind	[28]
QM	Direct scheme: solution phase free energy is determined by solution phase geometries without thermodynamic cycle SMD/M06-2X/6-31+G(d) for bases and SMD/M06-2X/6-31G(d) for acids + thermal corrections	<i>wexjs</i>	<i>y75vj</i>	Blind	[28]
QM + LEC	Jaguar (Schrodinger v2017-4)	<i>nb011</i>	<i>nb013</i>	Reference	[29]
QM + LEC	CPCM/B3LYP/6-311+G(d,p) and global fitting	<i>y4wws</i>	<i>35bdm</i>	Blind	[9]
QM + LEC	CPCM/B3LYP/6-311+G(d,p) and separate fitting for neutral to negative and for positive to neutral transformations	<i>qsicn</i>	<i>p0jba</i>	Blind	[9]
QM + LEC	EC-RISM/MP2/6-311+G(d,p)-P3NI-q-noThiols-2par	<i>kxzt</i>	<i>ds62k</i>	Blind	[30]
QM + LEC	EC-RISM/MP2/cc-pVTZ-P2-q-noThiols-2par	<i>ftc8w</i>	<i>2ii2g</i>	Blind	[30]
QM + LEC	EC-RISM/MP2/6-311+G(d,p)-P2-phi-all-2par	<i>ktpj5</i>	<i>nb001</i>	Blind*	[30]
QM + LEC	EC-RISM/MP2/6-311+G(d,p)-P2-phi-noThiols-2par	<i>wuuvc</i>	<i>nb002</i>	Blind*	[30]
QM + LEC	EC-RISM/MP2/6-311+G(d,p)-P3NI-phi-all-2par	<i>2umai</i>	<i>nb003</i>	Blind*	[30]
QM + LEC	EC-RISM/MP2/6-311+G(d,p)-P3NI-phi-noThiols-2par	<i>cm2yq</i>	<i>nb004</i>	Blind*	[30]
QM + LEC	EC-RISM/MP2/6-311+G(d,p)-P2-phi-all-1par	<i>z7fhp</i>	<i>nb005</i>	Blind*	[30]
QM + LEC	EC-RISM/MP2/6-311+G(d,p)-P3NI-phi-all-1par	<i>8toyp</i>	<i>nb006</i>	Blind*	[30]
QM + LEC	EC-RISM/MP2/cc-pVTZ-P2-phi-noThiols-2par	<i>epvmk</i>	<i>tjld0</i>	Blind	[30]
QM + LEC	EC-RISM/MP2/cc-pVTZ-P2-phi-all-2par	<i>xnoe0</i>	<i>mkhqa</i>	Blind	[30]
QM + LEC	EC-RISM/MP2/cc-pVTZ-P3NI-phi-noThiols-2par	<i>4o0ia</i>	<i>mpwiy</i>	Blind	[30]
QM + LEC	EC-RISM/B3LYP/6-311+G(d,p)-P3NI-q-noThiols-2par	<i>nxaaw</i>	<i>ad5pu</i>	Blind	[30]
QM + LEC	EC-RISM/B3LYP/6-311+G(d,p)-P3NI-phi-noThiols-2par	<i>0xi4b</i>	<i>f0gew</i>	Blind	[30]
QM + LEC	EC-RISM/B3LYP/6-311+G(d,p)-P2-phi-noThiols-2par	<i>cwyk</i>	<i>np6b4</i>	Blind	[30]
QM + LEC	PCM/B3LYP/6-311+G(d,p)	<i>gdqeg</i>	<i>yc70m</i>	Blind	[30]
QM + LEC	COSMOtherm_FINE17 (COSMOtherm C30_1701, BP/TZVPD/FINE//BP/TZVP/COSMO)	<i>t8ewk</i>	<i>0hxtm</i>	Blind	[31, 32]
QM + LEC	DSD-BLYP-D3(BJ)/def2-TZVPD//PBEh-3c[DCOSMO-RS] + RRHO[GFN-xTB[GBSA]] + Gsolv(COSMO-RS[TZVPD]) and linear fit		<i>xvxzd</i>	Blind	[33]
QM + LEC	ReScosS conformations // DSD-BLYP-D3 reranking // COSMOtherm pKa: DSD-BLYP-D3(BJ)/def2-TZVPD// PBE-D3(BJ)/def2-TZVP/COSMO + RRHO[GFN-xTB + GBSA-water] + Gsolv[COSMO-RS(FINE17/TZVPD)] level and COSMOtherm pKa applied at the single conformer pair level (COSMOtherm17.0.5 release and BP-TZVPD-FINE-C30-1701 parameterization)	<i>eyetm</i>	<i>8xt50</i>	Blind	[33]
QM + LEC	ReScosS conformations // COSMOtherm pKa: DSD-BLYP-D3(BJ)/def2-TZVPD// PBE-D3(BJ)/def2-TZVP/COSMO + RRHO[GFN-xTB + GBSA-water] + Gsolv[COSMO-RS(FINE17/TZVPD)] level and COSMOtherm pKa was applied directly on the resulting conformer sets with at least 5% Boltzmann weights for each microspecies (COSMOtherm17.0.5 release and BP-TZVPD-FINE-C30-1701 parameterization)	<i>ccpmw</i>	<i>yqkga</i>	Blind	[33]
QM + MM	M06-2X/6-31G*(for bases) or 6-31+G*(for acids) for gas phase, solvation free energy using TI with explicit solvent and GAFF, solvation free energy of proton -265.6 kcal/mol	<i>0wfzo</i>		Blind	[34]
QM + MM	M06-2X/6-31G*(for bases) or 6-31+G*(for acids) for gas phase, solvation free energy using TI with explicit solvent and GAFF, solvation free energy of proton -271.88 kcal/mol	<i>z3btx</i>		Blind	
QM + MM	M06-2X/6-31G*(for bases) or 6-31+G*(for acids) + thermal state correction for gas phase, solvation free energy using TI with explicit solvent and GAFF, solvation free energy of proton -265.6 kcal/mol	<i>758j8</i>		Blind	
QM + MM	M06-2X/6-31G*(for bases) or 6-31+G*(for acids) + thermal state correction for gas phase, solvation free energy using TI with explicit solvent and GAFF, solvation free energy of proton -271.88 kcal/mol	<i>hgn83</i>		Blind	

\* Microscopic pKa submissions were blind, however, participant requested a correction after blind submission deadline for macroscopic pKa submissions. Therefore, these were assigned submission IDs in the form of *nb##*.

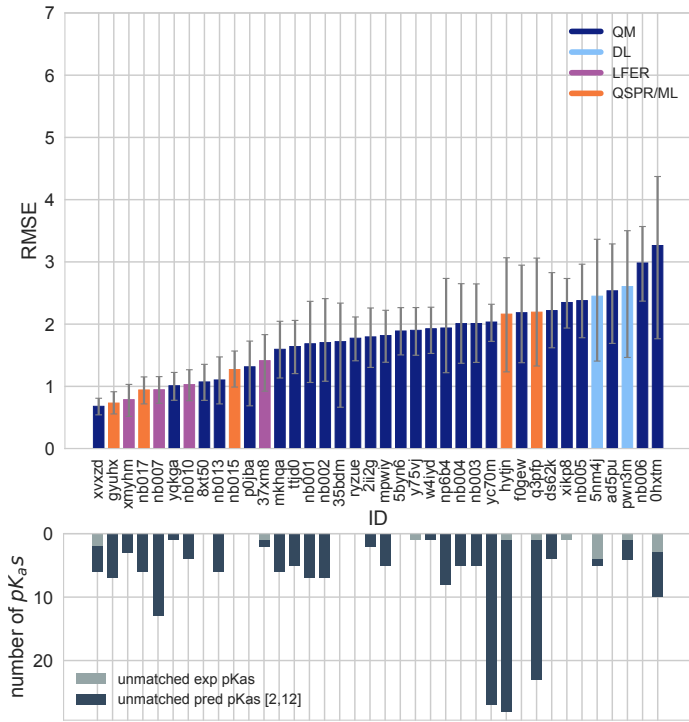


**Figure 2. RMSE and unmatched pK<sub>a</sub> counts vs. submission ID plots for macroscopic pK<sub>a</sub> predictions based on Hungarian matching.** Methods are indicated by submission IDs. RMSE is shown with error bars denoting 95% confidence intervals obtained by bootstrapping over challenge molecules. Submissions are colored by their method categories. Light blue colored database look up methods are utilized as the null prediction method. QM methods (navy) includes pure QM, QM+LEC, and QM+MM approaches. Lower bar plots show the number of unmatched experimental pK<sub>a</sub>s (light grey, missing predictions) and the number of unmatched pK<sub>a</sub> predictions (dark grey, extra predictions) for each method between pH 2 and 12. Submission IDs are summarized in Table 1. Submission IDs of the form nb### refer to non-blinded reference methods computed after the blind challenge submission deadline. All others refer to blind, prospective predictions.

Null prediction methods based on database lookup (*5nm4j* and *pwn3m*) had similar performance, roughly RMSE of 2.5 p*K*<sub>a</sub> units, MAE of 1.5 p*K*<sub>a</sub> units, R<sup>2</sup> of 0.2 and Kendall's Tau of 0.3. Many methods were observed to have prediction performance advantage over the Null predictions shown in light blue in Fig. 2 and Fig. 3 considering all the performance metrics as a whole. In terms of correlation statistics the null methods are the worst performers, except *0xhtm*. From the perspective of accuracy-based statistics (RMSE and MAE), only the top 10 methods were observed to have significantly lower errors than the null methods considering the uncertainty of error metrics expressed as 95% confidence intervals.

Distribution of macroscopic  $pK_a$  prediction signed errors observed in each submission was plotted in Fig. 7A as ridge plots based on Hungarian matching. *2ii2g*, *f0gew*, *np64b*, *p0jba*, and *yc70m* tend to overestimate and *5byn6*, *ryzue*, and *w4iyd* tend to underestimate macroscopic  $pK_a$  values.

There were four submissions of QM+LEC category that used COSMO-RS implicit solvation model. It was interesting that while three of these achieved the lowest RMSE among QM-based methods (*xvxzd*, *yqkga*, and *8xt50*) [33] and one of them showed the highest RMSE (*0hxtm* (COSMOtherm\_FINE17)) in SAMPL6 Challenge macroscopic  $pK_a$  predictions. All four methods used COSMO-RS/FINE17 level to compute solvation free energies. The major difference between the three low-RMSE methods and the *0hxtm* seems to be the protocol for determining relevant conformations for each microstate. *xvxzd*, *yqkga*, and *8xt50* methods used semi-empirical tight binding (GFN-xTB) method and GBSA continuum solvation model for geometry optimization of conformers and followed up with high level single point energy calculations with solvation free energy (COSMO-RS(FINE17/TZVPD)) and rigid rotor harmonic oscillator (RRHO[GFN-xTB(GBSA)] corrections. *yqkga*, and *8xt50* methods selected conformations for each microstate with Relevant Solution Conformer Sampling and Selection (ReSCoSS) workflow. Conformations were clustered according to shape and lowest energy conformations from each cluster according to BP86/TZVP/COSMO single point energies in any of the 10 different COSMO-RS solvents were considered as relevant conformers. More details of the ReSCoSS workflow was described by Pracht et al [33] *yqkga* method further filtered out conformers that have less than 5% Boltzmann weights at the DSD-

396 BLYP-D3/def2-TZVPD + RRHO(GFNxTB) + COSMO-RS(fine) level. *xvxzd* method used MF-MD-GC//GFN-xTB workflow and used  
397 energy thresholds of 6 kcal/mol and 10 kcal/mol, for conformer and microstate selection On the other hand, the conformational  
398 ensemble captured for each microstate seems to be much limited for *0hxtm* method, judging by the method description in the  
399 submission file. *0hxtm* method reported that relevant conformations were computed with the COSMOconf 4.2 workflow which  
400 produced multiple relevant conformers for only the neutral states of SM18 and SM22. In contrast to *xvxzd*, *yqkga*, and *8xt50*  
401 methods, the *0hxtm* method also did not include a RRHO correction. Participants of the three low-RMSE methods report that  
402 capturing the chemical ensemble for each molecule including conformers and tautomers and high level QM calculations led to  
403 more successful macroscopic  $pK_a$  prediction results and RRHO correction provided a minor improvement [33]. Comparing these  
404 results to other QM approaches in SAMPL Challenge also points to the advantage of COSMO-RS solvation approach compared  
405 to other implicit solvent models.

406 In addition the statistics related to the value of  $pK_a$ , we have also analyzed missing or extra  $pK_a$  predictions. Analysis of the  
407  $pK_a$  values with accuracy- and correlation-based error metrics was only possible after assignment of predicted macroscopic  $pK_a$ s  
408 to experimental  $pK_a$ s through the Hungarian matching, although, this approach masks  $pK_a$  prediction issues in the form of extra  
409 or missing macroscopic  $pK_a$  predictions. To capture this form of prediction errors we reported the number of unmatched ex-  
410 perimental  $pK_a$ s (missing  $pK_a$  predictions and the number of unmatched predicted  $pK_a$ s (extra  $pK_a$  predictions) after Hungarian  
411 matching for each method. Both missing and extra  $pK_a$  prediction counts were only considered for the pH range of 2-12 which  
412 was the limits of experimental measurements. The lower subplot of Fig. 2 shows the total count of unmatched experimental or  
413 predicted  $pK_a$ s for all the molecules in each prediction set. The order of submission IDs in the x-axis follows the RMSD based  
414 ranking so that the performance of each methods from both  $pK_a$  value accuracy and the number of  $pK_a$ s can be viewed together.  
415 Presence of missing or extra macroscopic  $pK_a$  predictions is a critical error, because inaccuracy in predicting the correct num-  
416 ber of macroscopic transitions shows that methods are failing predict the correct set of charge states, i.e. failing to predict the  
417 correct number of ionization states that can be observed between the specified pH range.

418 In challenge results, extra macroscopic  $pK_a$  predictions were found to be more common than missing  $pK_a$  predictions. In  
419  $pK_a$  prediction evaluations usually accuracy of ionization states predicted within a pH range seen is neglected. When predictions  
420 are only evaluated for  $pK_a$  value accuracy with numerical matching algorithms more  $pK_a$  predictions are likely to lead to lower  
421 prediction errors. Therefore, it is not surprising that methods are biased to predict extra  $pK_a$  values. The SAMPL6  $pK_a$  Challenge  
422 experimental data consists of 31 macroscopic  $pK_a$ s in total, measured for 24 molecules (6 molecules in the set have multiple  
423  $pK_a$ s). Within the 10 methods with lowest RMSE only *xvxzd* method has an error of missing predicted  $pK_a$  (2 unmatched out  
424 of 31 experimental  $pK_a$ s), and all other methods that rank top 10 according to RMSE have extra predicted  $pK_a$ s ranging from 1  
425 to 13. Two prediction sets without any extra  $pK_a$  predictions and low RMSE are *8xt50* (ReSCoSS conformations // DSD-BLYP-D3  
426 reranking // COSMOtherm pKa) and *nb015* (ChemAxon/Chemicalize).

### 427 3.1.1 Consistently well performing methods for macroscopic $pK_a$ prediction

428 Methods ranked differently when ordered by different error metrics, although there were a couple of methods that consistently  
429 ranked at the top fraction. By using a combinatorial criteria that takes all multiple statistical metrics and unmatched  $pK_a$  counts  
430 into account, we identified a short list of consistently well performing methods for macroscopic  $pK_a$  predictions, shown in Table 2.  
431 The criteria for selection was ranking in Top 10 according to RMSE, MAE,  $R^2$ , and Kendall's Tau and also having a combined  
432 unmatched  $pK_a$  (extra and missing  $pK_a$ s) count less than 8 (a third of the number of compounds). The resulted in a list of four  
433 methods which are consistently well performing across all criteria.

434 Consistently well performing methods for macroscopic  $pK_a$  prediction included methods from all categories. Two methods of  
435 the QM+LEC category were *xvxzd* (DSD-BLYP-D3(BJ)/def2-TZVPD//PBEh-3c[DCOSMO-RS] + RRHO(GFN-xTB[GBSA]) + Gsolv(COSMO-  
436 RS[TZVPD])) and linear fit) and (*8xt50*) (ReSCoSS conformations // DSD-BLYP-D3 reranking // COSMOtherm pKa) and both used  
437 COSMO-RS approach. Empirical  $pK_a$  predictions with top performance were both proprietary softwares. From QSPR and LFER  
438 categories, *gyuhx* (Simulation Plus) and *xmyhm* (ACD/pKa Classic) were the methods that made it to consistently well perform-  
439 ing methods list. Simulation Plus  $pK_a$  prediction method consisted of 10 artificial neural network ensembles trained on 16,000  
440 compounds for 10 classes of ionizable atoms. Atom type and local molecular environment was how the ionization class of each  
441 atom was determined [35]. ACD/pKa Classic which was trained on method 17,000 compounds uses Hammet-type equations  
442 and tries to capture effects related to tautomeric equilibria, covalent hydration, resonance effects, and  $\alpha$ ,  $\beta$ -unsaturated systems  
443 [22].

444 In Figure 4 prediction vs. experimental data correlation plots of macroscopic  $pK_a$  predictions with 4 consistently well-performing  
445 methods, a representative average method, and the null method(*5nm4j*). The representative method with average performance

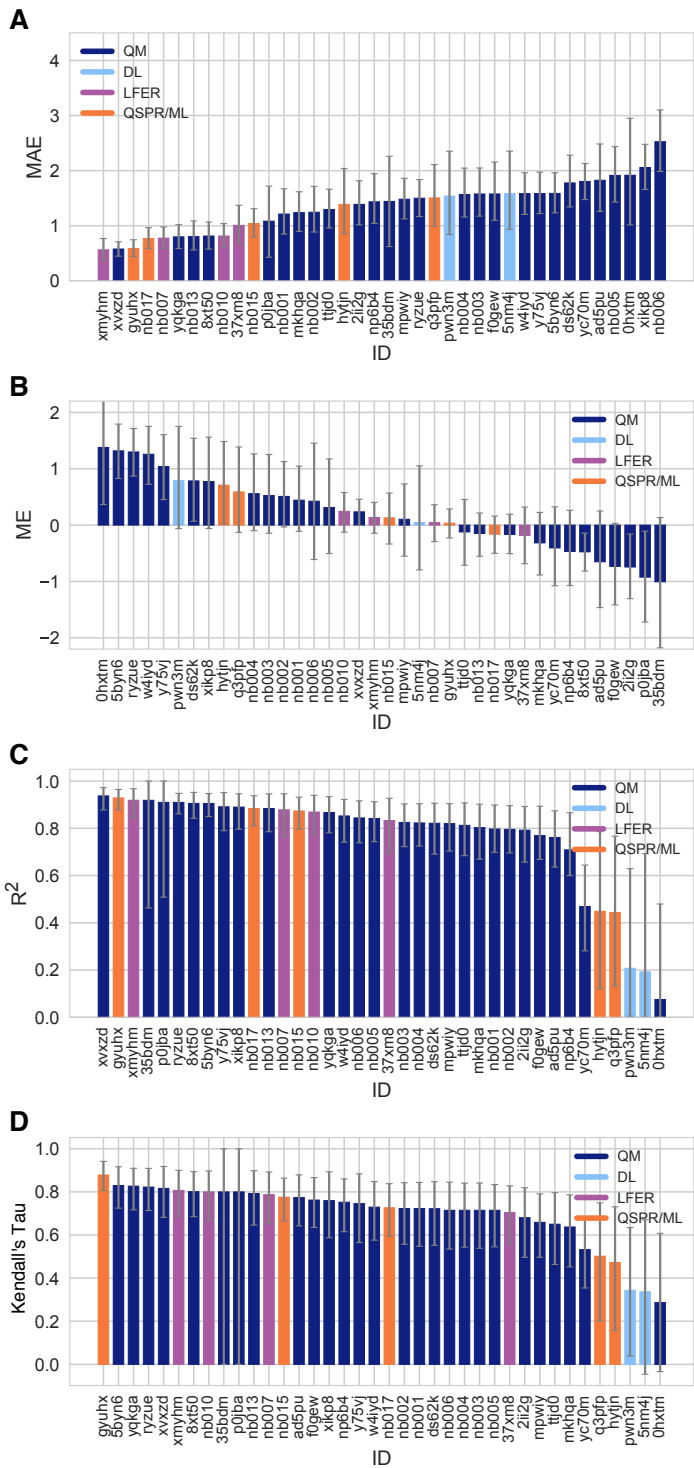


**Figure 3. Additional performance statistics for macroscopic pK<sub>a</sub> predictions based on Hungarian matching.** Methods are indicated by submission IDs. Mean absolute error (MAE), mean error (ME), Pearson's R<sup>2</sup>, and Kendall's Rank Correlation Coefficient Tau ( $\tau$ ) are shown, with error bars denoting 95% confidence intervals obtained by bootstrapping over challenge molecules. Refer to Table 1 for submission IDs and method names. Submissions are colored by their method categories. Light blue colored database look up methods are utilized as the null prediction method.

446 (2li2g (EC-RISM/MP2/cc-pVTZ-P2-q-noThiols-2par)) was selected as the method with the highest RMSE below the median of all  
447 methods.

**Table 2. Four consistently well-performing prediction methods for macroscopic  $pK_a$  prediction based on consistent ranking within the Top 10 according to various statistical metrics.** Submissions were ranked according to RMSE, MAE,  $R^2$ , and  $\tau$ . Consistently well-performing methods were selected as the ones that rank in the Top 10 in each of these statistical metrics. These methods also have less than 2 unmatched experimental  $pK_a$ s and less than 7 unmatched predicted  $pK_a$ s according to Hungarian matching. Performance statistics are provided as mean and 95% confidence intervals.

Submission ID	Method Name	RMSE	MAE	$R^2$	Kendall's Tau ( $\tau$ )	Unmatched Exp. $pK_a$ Count	Unmatched Pred. $pK_a$ Count [2,12]
xvxzd	Full quantum chemical calculation of free energies and fit to experimental $pK_a$	0.68 [0.54, 0.81]	0.58 [0.45, 0.71]	0.94 [0.88, 0.97]	0.82 [0.68, 0.92]	2	4
gyuhx	S+pKa	0.73 [0.55, 0.91]	0.59 [0.44, 0.74]	0.93 [0.88, 0.96]	0.88 [0.8, 0.94]	0	7
xmyhm	ACD/pKa Classic	0.79 [0.52, 1.03]	0.56 [0.38, 0.77]	0.92 [0.85, 0.97]	0.81 [0.68, 0.9]	0	3
8xt50	ReSCoSS conformations // DSD-BLYP-D3 reranking // COSMOtherm pKa	1.07 [0.78, 1.36]	0.81 [0.58, 1.07]	0.91 [0.84, 0.95]	0.80 [0.68, 0.89]	0	0

### 448 3.1.2 Which chemical properties are driving macroscopic $pK_a$ prediction failures?

449 In addition to comparing the performance of methods that participated in the SAMPL6 Challenge, we also wanted to analyze  
 450 macroscopic  $pK_a$  predictions from the perspective of challenge molecules and determine whether particular compounds suffer  
 451 from larger inaccuracy in  $pK_a$  predictions. The goal of this analysis is to provide guidance on which molecular properties or  
 452 moieties might be causing larger  $pK_a$  prediction error. In Fig. 5 2D depictions of challenge molecules are presented with MAE cal-  
 453 culated for their macroscopic  $pK_a$  predictions over all methods, based on Hungarian match. For multiprotic molecules MAE was  
 454 averaged over all the  $pK_a$ s. For the analysis of  $pK_a$  prediction accuracy observed for each molecule, MAE is a more appropriate  
 455 statistical value than RMSE for following global trends. This is because MAE value less sensitive to outliers than is RMSE.

456 A comparison of prediction performance of individual molecules is shown in Fig. 6. In Fig. 6A MAE each molecule is shown  
 457 considering all blind predictions and reference calculations. A cluster of molecules marked orange and red have higher than  
 458 average MAE. Molecules marked red (SM06, SM21, and SM22) are the only compounds in SAMPL6 dataset with bromo or iodo  
 459 groups and they suffered a macroscopic  $pK_a$  prediction error in the range of 1.7-2.0  $pK_a$  units in terms of MAE. Molecules marked  
 460 orange (SM03, SM10, SM18, SM19, and SM20) all have sulfur-containing heterocycles, and all molecules except SM18 of this  
 461 group have MAE larger than 1.6  $pK_a$  unit. SM18 despite containing thiazole group has a low MAE. SM18 is the only compound  
 462 with three experimental  $pK_a$ s and we suspect presence of multiple experimental  $pK_a$ s could have a masking affect on the errors  
 463 captured by MAE with Hungarian matching due to more pairing choices.

464 We analyzing MAE of each molecule for empirical(LFER and QSPR/ML) and QM-based physical methods (QM, QM+LEC, and  
 465 QM+MM) separately for more insight. Fig. 6B shows that the difficulty of predicting  $pK_a$ s of the same subset of molecules was  
 466 a trend conserved in the performance of physical methods. For QM-based methods too sulfur containing heterocycles, amide  
 467 next to aromatic heterocycles, compounds with iodo and bromo domains have lower  $pK_a$  prediction accuracy.

468 SAMPL6  $pK_a$  set consists of only 24 small molecules which limits our ability to do statistically confirm the determination of  
 469 which chemical substructures cause greater errors in  $pK_a$  predictions. Still the trends seen in this challenge distinguish molecules  
 470 with iodo, bromo, and sulfur-containing heterocycles with larger prediction errors of macroscopic  $pK_a$  value. We hope that  
 471 reporting this observation will lead to improvement of methods for similar compounds with such moieties.

472 We have also looked for correlation with molecular descriptors for finding other potential explanations for why macroscopic  
 473  $pK_a$  predictions were larger in some molecules. While testing correlation between errors and many molecular descriptors it  
 474 is important to keep the possibility of spurious correlations in mind. We haven't observed any significant correlation between  
 475 numerical  $pK_a$  predictions and the descriptors we have tested. First of all, higher number of experimental  $pK_a$ s (Fig. 6A) did not  
 476 seem to associate with lower  $pK_a$  prediction performance. But we need to keep in mind that there was a low representation  
 477 of multiprotic compounds in the SAMPL6 set (5 molecules with 2 macroscopic  $pK_a$ s and one molecule with 3 macroscopic  $pK_a$ ).  
 478 Other descriptors we checked for were presence of amide groups, molecular weight, heavy atom count, rotatable bond count,  
 479 heteroatom count, heteroatom to carbon ratio, ring system count, maximum ring size, and the number of microstates (as  
 480 enumerated for the challenge). Correlation plots and  $R^2$  values can be seen in Fig. S2. We had suspected that  $pK_a$  prediction  
 481 methods may be trained better for moderate values (4-10) than extreme values as molecules with extreme  $pK_a$ s are less likely  
 482 to change ionization states close to physiological pH. To test this we look at the distribution of absolute errors calculated for all  
 483 molecules and challenge predictions binned by experimental  $pK_a$  value 2  $pK_a$  unit increments. As can be seen in Fig. S3B, the  
 484 value of true macroscopic  $pK_a$ s was not a factor affecting prediction error seen in SAMPL6 Challenge.

485 Fig. 7B is helpful to answer the question of "Are there molecules with consistently overestimated or underestimated  $pK_a$ s?".

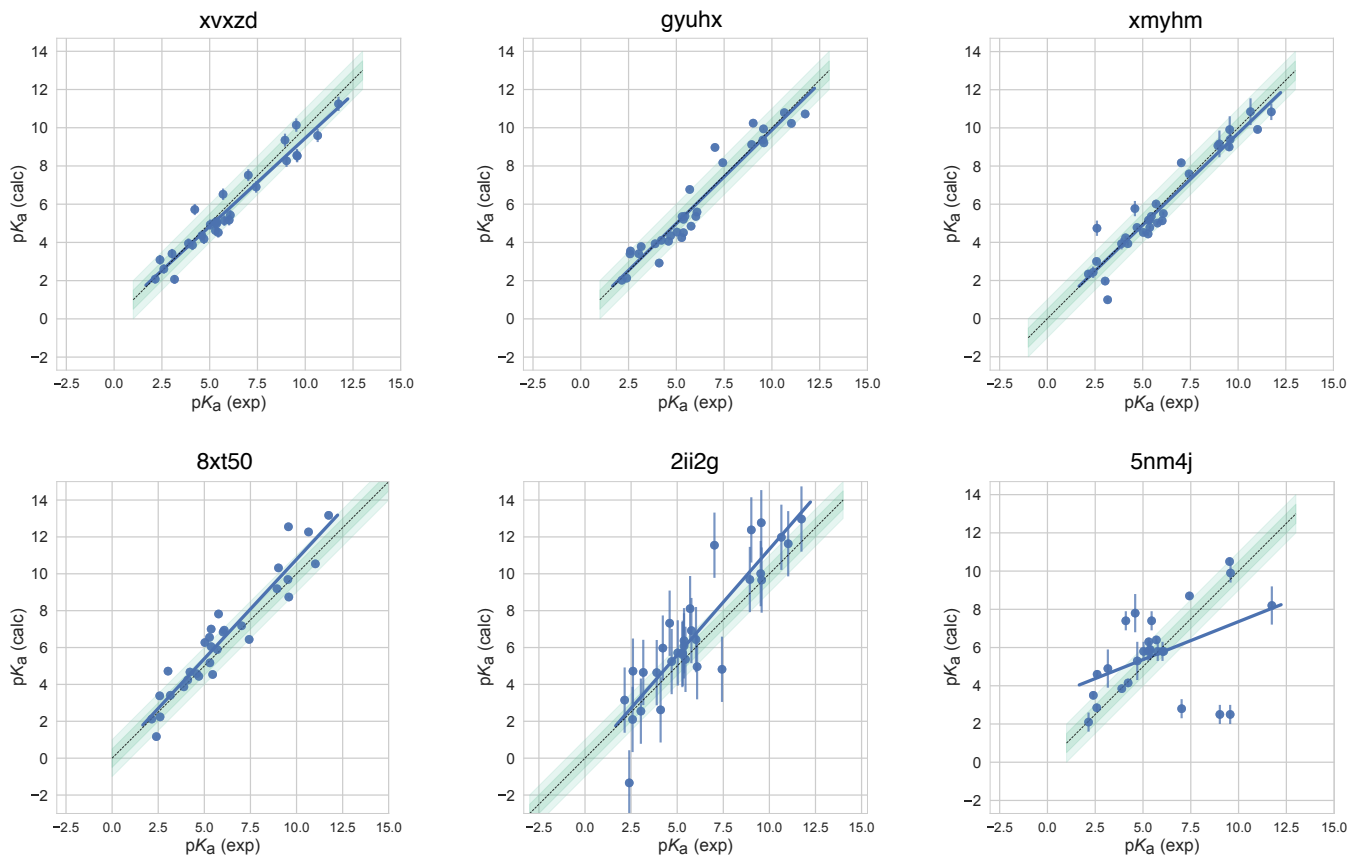


**Figure 4. Predicted vs. experimental value correlation plots of 4 consistently well-performing methods, a representative method with average performance (2ii2g), and the null method (5nm4j).** Dark and light green shaded areas indicate 0.5 and 1.0 units of error. Error bars indicate standard error of the mean of predicted and experimental values. Experimental pKa SEM values are too small to be seen under the data points. EC-RISM/MP2/cc-pVTZ-P2-q-noThiols-2par method (2ii2g) was selected as the representative method with average performance because it is the method with the highest RMSE below the median.

486 This ridge plots shows the error distribution of each experimental p $K_a$ . SM02\_pKa1, SM04\_pKa1, SM14\_pKa1, and SM21\_pKa1  
 487 were underestimated by majority of the prediction methods for more than 1 p $K_a$  unit. SM03\_pKa1, SM06\_pKa2, SM19\_pKa1, and  
 488 SM20\_pKa1 were overestimated by the majority of the preodction methods for more than 1 p $K_a$  unit. SM03\_pKa1, SM06\_pKa2,  
 489 SM10\_pKa1, SM19\_pKa1, and SM22\_pKa1 have the highest spread of errors and were less accurately predicted overall. Refer to  
 490 Ridge plots of Delta pKa error to identify compounds that were frequently mispredicted.

### 491 3.2 Analysis of microscopic p $K_a$ predictions using microstates determined by NMR for 8 molecules

492 The common approach for analysing microscopic p $K_a$  prediction accuracy has been to compare it to experimental macroscopic  
 493 p $K_a$  data, assuming experimental p $K_a$ s describe titrations of distinguishable sides and, therefore, equal to microscopic p $K_a$ s. But  
 494 this typical approach fails to evaluate the methods in microscopic level.

495 Analysis of microscopic p $K_a$  predictions of the SAMPL6 Challenge was not straight-forward due to lack of experimental  
 496 data with microscopic detail. For 24 molecules macroscopic p $K_a$ s were determined with spectrophotometric method. For 18  
 497 molecules single macroscopic titration was observed and for 6 molecules multiple experimental p $K_a$ s were reported. For 18  
 498 molecules with single experimental p $K_a$  it is probabable that the molecules are monoprotic and therefore macroscopic p $K_a$   
 499 value is equal to the microscopic p $K_a$ , but there is no direct experimental evidence to support that this is the case but only  
 500 the support from prediction methods. There is always the possibility that the macroscopic p $K_a$  observed is the result of two  
 501 different titrations overlapping closely with respect to pH. We did not want to bias the blind challenge analysis with any prediction  
 502 method. Therefore, we believe analyzing the microscopic p $K_a$  predictions via Hungarian matching to experimental values

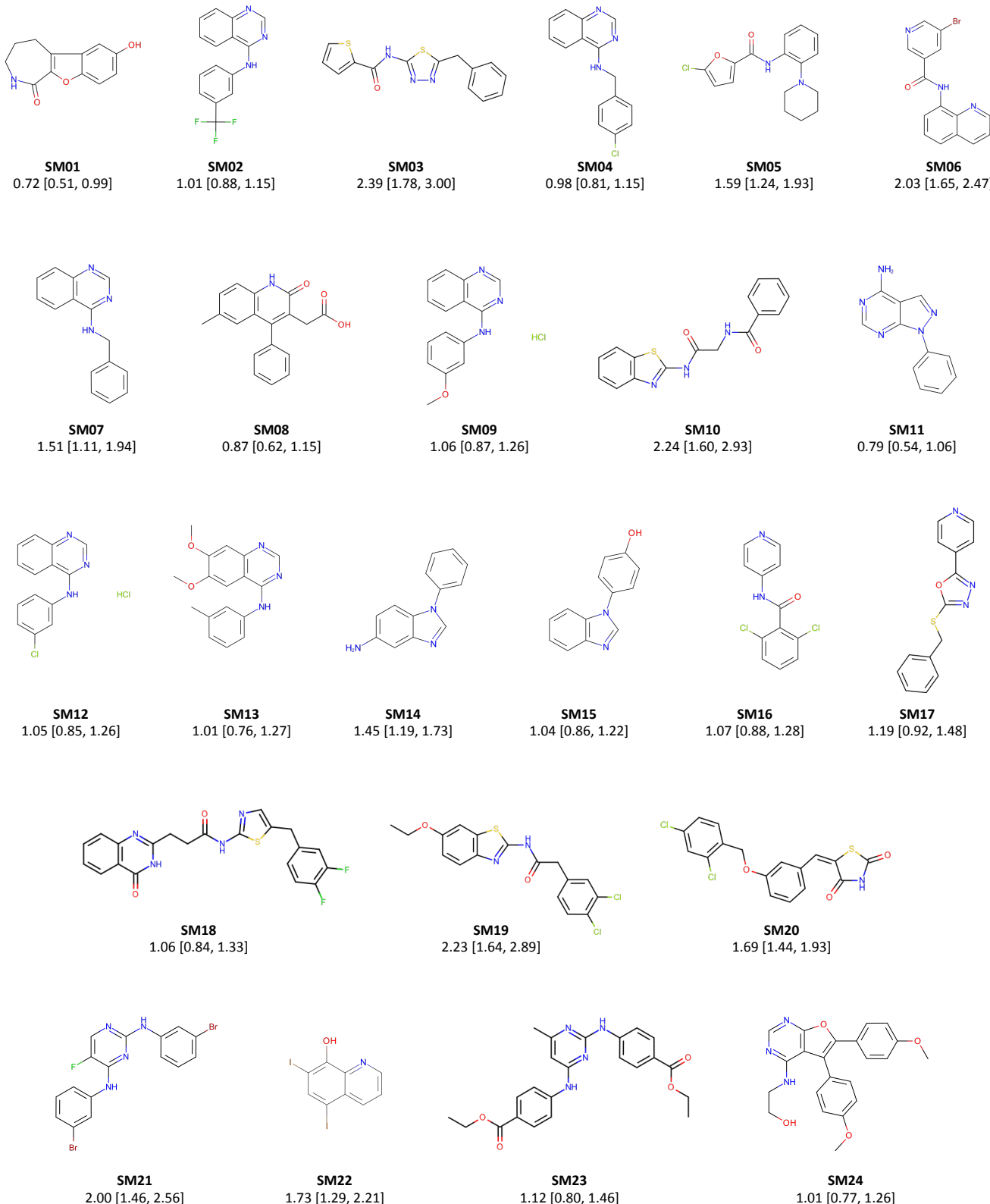
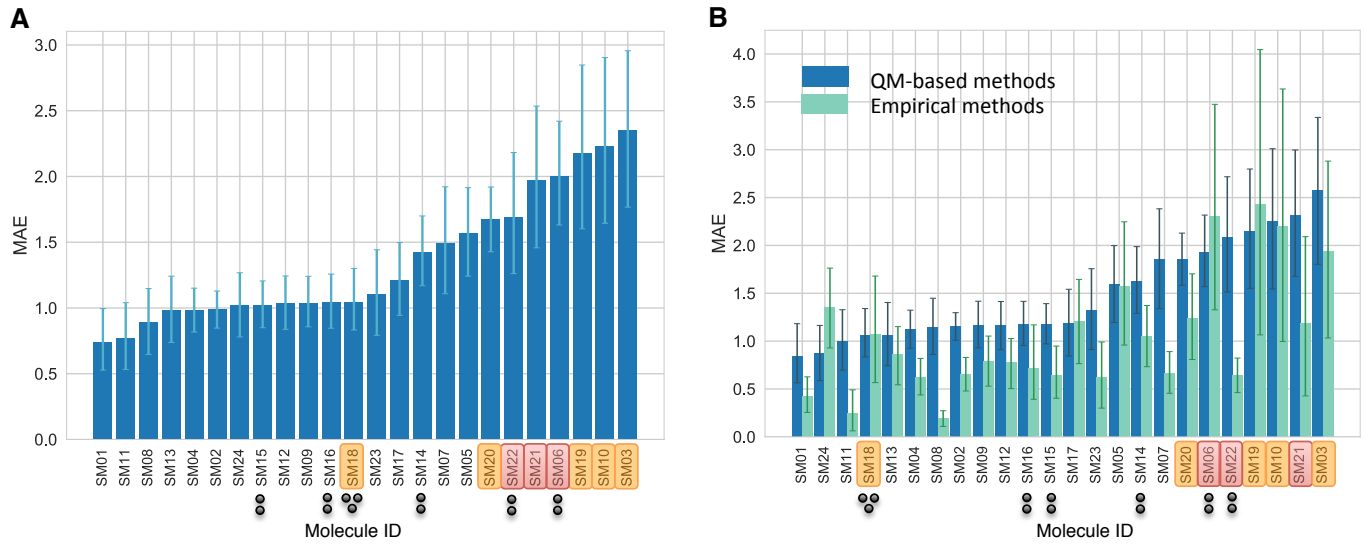
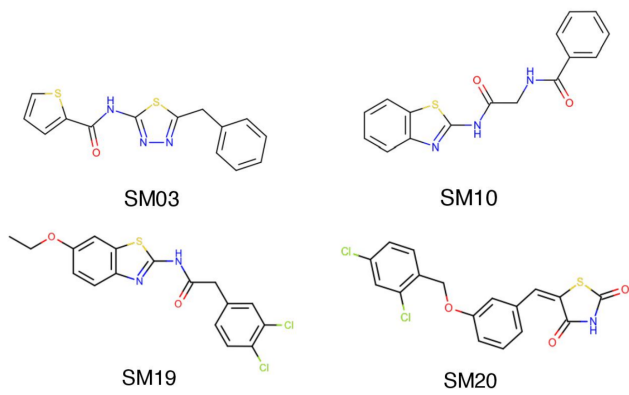


**Figure 5. Molecules of SAMPL6 Challenge with MAE calculated for all macroscopic  $pK_a$  predictions.** MAE calculated considering all prediction methods indicate which molecules had the lowest prediction accuracy in SAMPL6 Challenge. MAE values calculated for each molecule include all the matched  $pK_a$  values, which could be more than one per method for multiprotic molecules (SM06, SM14, SM15, SM16, SM18, SM22). Hungarian matching algorithm was employed for pairing experimental and predicted  $pK_a$  values. MAE values are reported with 95% confidence intervals.



**C SAMPL6 molecules with sulfur-containing heterocycles**



**D SAMPL6 molecules with bromo and iodo groups**

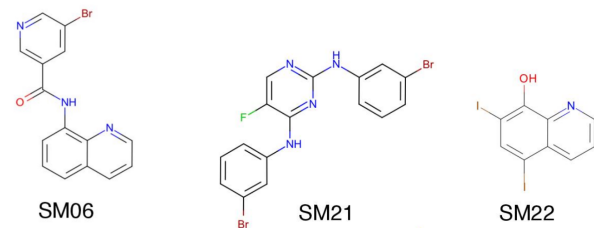


**Figure 6. Average prediction accuracy calculated over all prediction methods was lower for molecules with sulfur-containing heterocycles, bromo, and iodo groups.** (A) MAE calculated for each molecule as an average of all methods. (B) MAE of each molecule broken out by method category. QM-based methods (blue) include QM predictions with or without linear empirical correction. Empirical methods (green) include QSAR, ML, DL, and LFER approaches. (C) Depiction of SAMPL6 molecules with sulfur-containing heterocycles. (D) Depiction of SAMPL6 molecules with iodo and bromo groups.

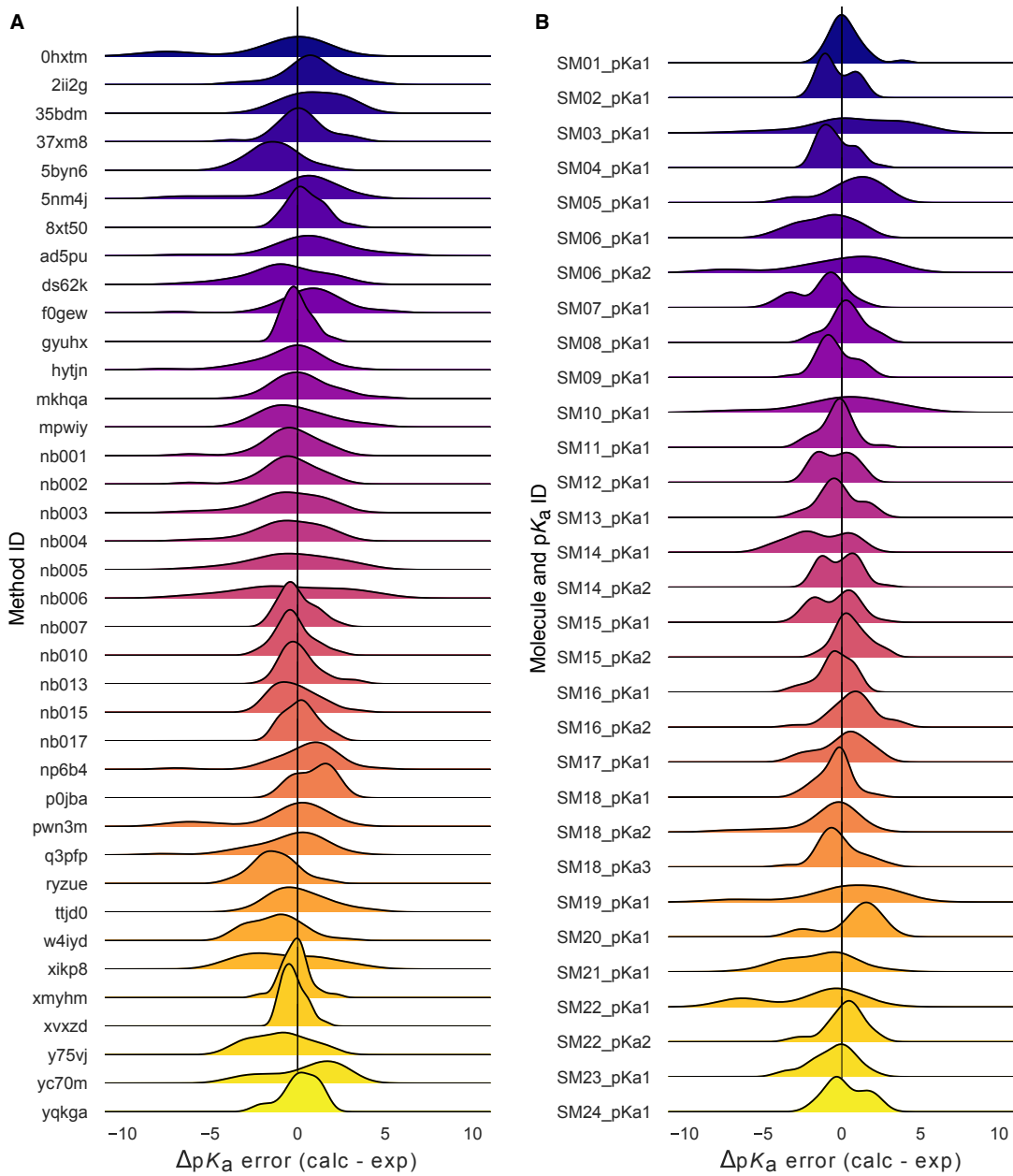


**Figure 7. Macroscopic  $pK_a$  prediction error distribution plots show how prediction accuracy varies across methods and individual molecules.** (A)  $pK_a$  prediction error distribution for each submission for all molecules according to Hungarian matching. (B) Error distribution for each SAMPL6 molecule for all prediction methods according to Hungarian matching. For multiprotic molecules,  $pK_a$  ID numbers (pKa1, pKa2, and pKa3) were assigned in the direction of increasing experimental  $pK_a$  value.

503 with the assumption that the 18 molecules have single titratable site is not the best approach. Instead analysis at the level of  
504 macroscopic  $pK_a$ s is much more appropriate when a numerical matching scheme is the only option to evaluate predictions using  
505 macroscopic experimental data.

506 For a subset of the molecules in the dataset of 8 molecules, dominant microstates were inferred from NMR experiments.  
507 This dataset was extremely useful for guiding the assignment between experimental and predicted  $pK_a$  values based on mi-  
508 crostates. In this section we present the performance evaluations of microscopic  $pK_a$  predictions for only the 8 compounds with  
509 experimentally determined dominant microstates.

### 510 3.2.1 Microstate-based matching revealed errors masked by $pK_a$ value-based matching between experimental 511 and predicted $pK_a$ s

512 Comparing microscopic  $pK_a$  predictions directly to macroscopic experimental  $pK_a$  values with numerical matching can lead to  
513 underestimation of errors. To demonstrate how numerical matching often masks the  $pK_a$  prediction errors we compared the  
514 performance analysis done by Hungarian matching to microstate-based matching for 8 molecules presented in Fig. 8A. RMSE  
515 calculated for microscopic  $pK_a$  predictions matched to experimental values via Hungarian matching is shown in Fig. 8B, while  
516 Fig. 8C shows RMSE calculated via microstate-based matching. What is important to notice is that the Hungarian matching  
517 leads to significantly lower RMSE compared to microstate-based matching. The reason is that the Hungarian matching assigns  
518 experimental  $pK_a$  values to predicted  $pK_a$  values only based on the closeness of the numerical values, without consideration  
519 of the relative population of microstates and microstate identities. Because of that a microscopic  $pK_a$  value that describes a  
520 transition between very low population microstates (high energy tautomers) can be assigned to the experimental  $pK_a$  if it has  
521 the closest  $pK_a$  value. This is not helpful, because in reality the microscopic  $pK_a$ s that influence the observable macroscopic  $pK_a$   
522 the most are the ones with higher populations (transitions between low energy tautomers).

523 The number of unmatched predicted microscopic  $pK_a$ s are shown in lower bar plots of Fig. 8B and C, to emphasize the large  
524 number of microscopic  $pK_a$  predictions submitted by many methods. In the case of microscopic  $pK_a$  the number of unmatched  
525 predictions do not indicate an error in the form of an extra predicted  $pK_a$ , because the spectrophotometric experiments do not  
526 capture all microscopic  $pK_a$ s theoretically possible (transitions between all pairs of microstates that are 1 proton apart).  $pK_a$ s  
527 of transitions to and from very high energy tautomers are very hard to measure by experimental methods, including the most  
528 sensitive methods like NMR. The reason we plotted them was more to demonstrate how the increased number of prediction  
529 value choices for Hungarian matching can lead to erroneously low RMSE values. We have also checked how often Hungarian  
530 matching led to the correct matches between predicted and experimental  $pK_a$  in terms of the microstate pairs, i.e. how often the  
531 microstate pair of the Hungarian match recapitulates the dominant microstate pair of the experiment. The overall accuracy of  
532 correct microstate pair match was found to be low for SAMPL6 Challenge submission. Fig. S4 shows that for most methods the  
533 predicted microstate pair selected by Hungarian match did not match experimentally determined microstate pair. This means  
534 the lower RMSE results obtained from Hungarian matching are low for the wrong reason. Matching experimental and predicted  
535 values on the basis of microstate IDs do not suffer from this problem.

536 The disadvantage of the evaluation through microstate-based matching approach is that the conclusions in this section are  
537 only about a subset of challenge compounds with limited diversity. This subset is composed of 6 molecules 4-aminoquinazoline  
538 and 2 molecules with benzimidazole scaffolds, and a total of 10  $pK_a$  values. The sequence of dominant microstates for SM07 and  
539 SM14 were determined by NMR experiments directly [7], and dominant microstates of their derivatives were inferred taking them  
540 as reference (Fig. 8). Although, we believe that microstate-based evaluation is more informative, the lack of a large experimental  
541 dataset limits the conclusions to a very narrow chemical diversity.

### 542 3.2.2 Accuracy of $pK_a$ predictions evaluated by microstate-based matching

543 Both accuracy and correlation based statistics were calculated for predicted microscopic  $pK_a$  values after microstate-based  
544 matching. RMSE, MAE, ME,  $R^2$ , and Kendall's Tau results of each method are shown in Fig. 8C and Fig. 9. A table of the calculated  
545 statistics can be found in Table S4. Due to small number of data points in this set, correlation based statistics calculated shows  
546 large uncertainty and provide less utility for distinguishing better performing methods. Therefore we focused more on accuracy  
547 based metrics for the analysis of microscopic  $pK_a$ s than correlation based metrics. In terms of accuracy of microscopic  $pK_a$   
548 value, all three QSPR/ML based methods (*nb016* (MoKa), *hdijyq* (Simulations Plus), *6tvf8* (OE Gaussian Process)), three QM-based  
549 methods (*nb011* (Jaguar), *ftc8w* (EC-RISM/MP2/cc-pVTZ-P2-q-noThiols-2par), *t8ewk* (COSMOlogic\_FINE17)), and one LFER method  
550 (*v8qph* (ACD/pKa GALAS)) achieved RMSE lower than 1  $pK_a$  unit. The same 6 methods also have the lowest MAE.

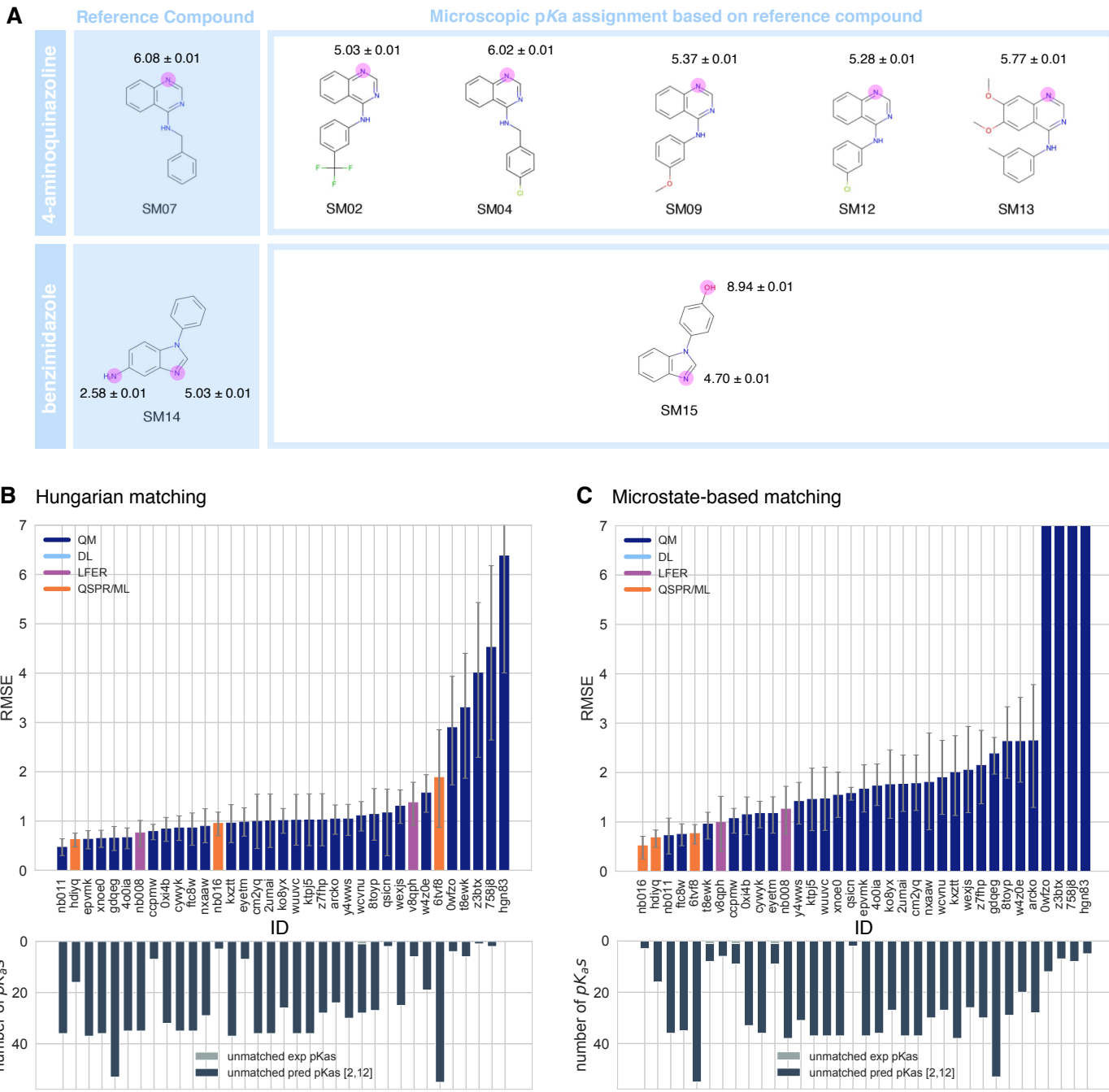


**Figure 8. NMR determination of dominant microstates allowed in depth evaluation of microscopic pKa predictions of 8 compounds.**

**A** Dominant microstate sequence of two compounds (SM07 and SM14) were determined by NMR [7]. Based on these reference compounds dominant microstates of 6 other derivative compounds were inferred and experimental pKa values were assigned to titratable groups with the assumption that only the dominant microstates have significant contributions to the experimentally observed pKa. **B** RMSE vs. submission ID and unmatched pKa vs. submission ID plots for the evaluation of microscopic pKa predictions of 8 molecules by Hungarian matching to experimental macroscopic pKas. **C** RMSE vs. submission ID and unmatched pKa vs. submission ID plots showing the evaluation of microscopic pKa predictions of 8 molecules by microstate-based matching between predicted microscopic pKas and experimental macroscopic pKa values. Submissions *0wfzo*, *z3bt8*, *758j8*, and *hgn83* have RMSE values bigger than 10 pKa units which are beyond the y-axis limits of subplot **C** and **B**. RMSE is shown with error bars denoting 95% confidence intervals obtained by bootstrapping over challenge molecules. Lower bar plots show the number of unmatched experimental pKas (light grey, missing predictions) and the number of unmatched pKa predictions (dark grey, extra predictions) for each method between pH 2 and 12. Submission IDs are summarized in Table 1.

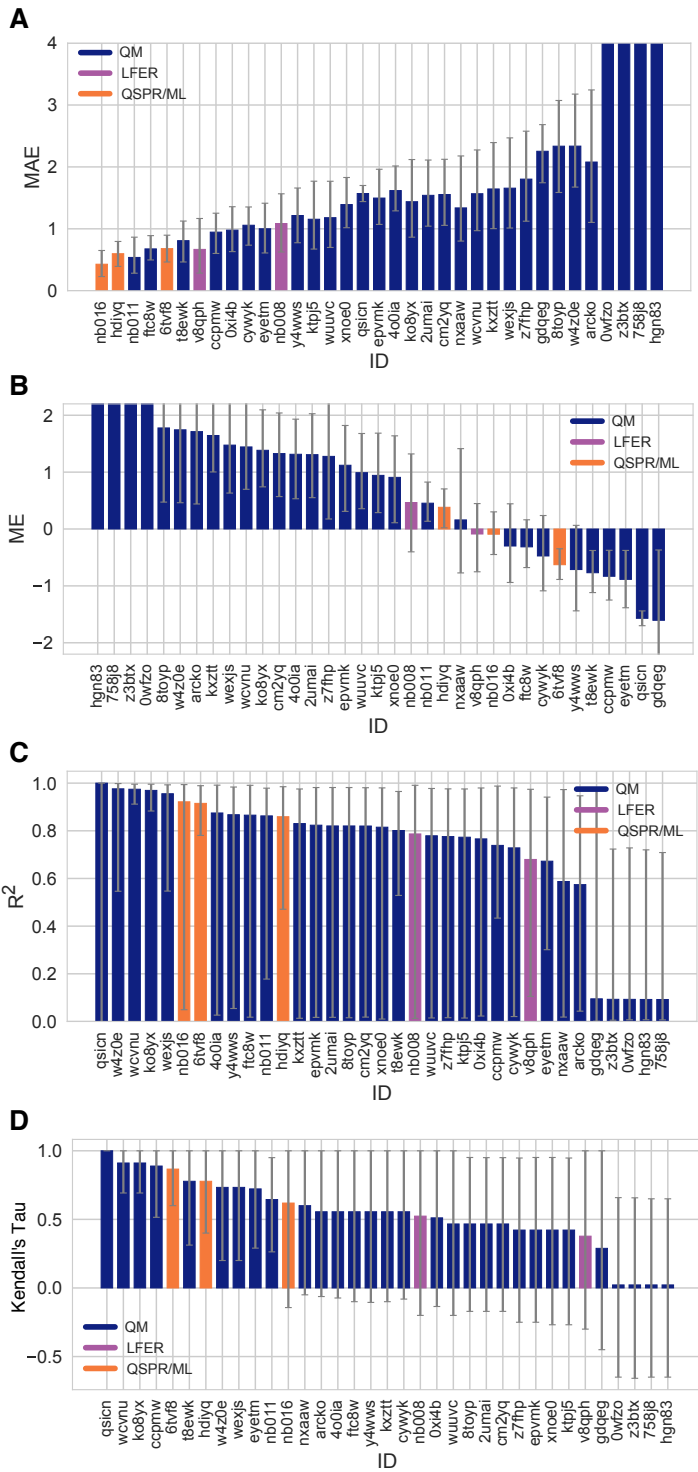


**Figure 9. Additional performance statistics for microscopic pK<sub>a</sub> predictions for 8 molecules with experimentally determined dominant microstates.** Microstate-based matching was performed between experimental pK<sub>a</sub> values and predicted microscopic pK<sub>a</sub>s. Mean absolute error (MAE), mean error (ME), Pearson's R<sup>2</sup>, and Kendall's Rank Correlation Coefficient Tau ( $\tau$ ) are shown, with error bars denoting 95% confidence intervals obtained by bootstrapping over challenge molecules. Methods are indicated by submission IDs. Submissions are colored by their method categories. Refer to Table 1 for submission IDs and method names. Submissions 0wfzo, z3btx, 758j8, and hgn83 have MAE and ME values bigger than 10 pK<sub>a</sub> units which are beyond the y-axis limits of subplots A and B. A large number and wide variety of methods have a statistically indistinguishable performance based on correlation based statistic (C and D), in part because of the relatively small dynamic range the small size of the set of 8 molecules.

551 3.2.3 Evaluating microstate prediction accuracy of methods

552 For many computational chemistry approaches including structure based modeling of protein-ligand interactions, predicting  
553 the ionization state and the exact position of protons is important to guide modeling. This is why in addition to being able to  
554 predict  $pK_a$  values accurately, we need  $pK_a$  prediction methods to be able to capture microscopic protonation states accurately.  
555 Even when the predicted  $pK_a$  value is very accurate, the predicted protonation site can be wrong. Therefore, we assessed if  
556 methods participating the SAMPL6  $pK_a$  Challenge were predicting correctly the sequence of dominant microstates, i.e. dominant  
557 tautomers of each charge state observed between pH 2 and 12.

558 Analyze which state has lowest free energy for each charge group (The sequence of "experimentally visible states")

559 Dominant microstate prediction accuracy of microscopic  $pK_a$  prediction method are shown in Fig. 10. To extract the domi-  
560 nant tautomers predicted for the sequence of ionization states of each method, first, relative free energy of microstates were  
561 calculated at reference pH 0 [19]. Then to determine dominant microstate of each charge, we have selected the lowest energy  
562 tautomer for each ionization states of the charges -1, 0, 1, and 2 (the charge range captured by NMR) experiments. Than pre-  
563 dicted and experimental dominant microstates were compared for each charge to calculate the fraction of correctly predicted  
564 dominant tautomers. This value is reported as the dominant microstate accuracy for all charges (Fig. 10A). Dominant microstate  
565 prediction errors were present the methods participating in the SAMPL6  $pK_a$  Challenge. 10 QM and 3 QSPR/ML methods did not  
566 make any mistakes in dominant microstate predictions, although, they are expected to be making mistakes in the relative ratio  
567 of tautomers (free energy difference between microstates) as reflected by  $pK_a$  value errors. While all the participating QSPR/ML  
568 methods showed good performance in dominant microstate prediction, LFER and some QM methods made mistakes. Accuracy  
569 of the prediction of the neutral dominant tautomers was perfect for all methods, except *qsicn* (Fig. 10B). But errors in predicting  
570 the major tautomer of charge +1 was much more frequent. 22 out of 35 prediction sets made at least one error in prediction the  
571 lowest energy tautomer with +1 charge. We didn't include ionization states with charges -1 and +2 in this assessment because  
572 we had only one compound with these charges in the dataset. Never the less, dominant tautomer prediction errors seems to  
573 be a bigger problem for charged tautomers than the neutral tautomer.

574 Experimental data of the sequence of dominant microstates was only available for 8 compounds. Therefore conclusions the  
575 performance of methods in terms of dominant tautomer prediction are limited to this narrow chemical diversity (benzimid-  
576 azole and 4-aminoquinazoline derivatives). We present this analysis as a prototype of how microscopic  $pK_a$  predictions should  
577 be evaluated. To reach broad conclusions about which methods are better for capturing dominant microstates and ratios of  
578 tautomers we hope that in the future more extensive evaluations can be mode with larger experimental datasets following the  
579 strategy we are demonstrating here. Even if experimental microscopic  $pK_a$  measurement data is not available, experimental  
580 dominant tautomer determinations are still informative for assessing prediction methods.

581 Focusing on dominant microstate sequence prediction accuracy from the perspective of molecules showed that major tau-  
582 tomer of SM14 cationic form was the most frequently mispredicted one. Fig. 10 shows the dominant microstate prediction  
583 accuracy calculated for individual molecules for charge states 0 and +1, averaged over all prediction methods. SM14, the  
584 molecule that exhibits highest microstate prediction error, has two experimental  $pK_a$  values that were 2.4  $pK_a$  units apart and  
585 we suspect that could be a contributor to the difficulty of predicting microstates accurately. Other molecules are monoprotic  
586 (4-aminoquinazolines) or their experimental  $pK_a$  values are very well separated (SM14, 4.2  $pK_a$  units). It would be very interesting  
587 to expand this assessment to a larger variety of drug-like molecules to discover for which structures tautomer predictions are  
588 more accurate and for which structure computational predictions are not as reliable.

589 3.2.4 Consistently-well performing methods for microscopic  $pK_a$  predictions

590 To determine consistently top-performing methods for microscopic  $pK_a$  predictions we have determined different criteria than  
591 macroscopic  $pK_a$  predictions: having perfect dominant microstate prediction accuracy, unmatched  $pK_a$  count of 0, and ranking  
592 in the top 10 according RMSE and MAE. Correlation based statistics were not found to have utility for discriminating perfor-  
593 mance due to large uncertainties in this statistics for a small dataset of 10  $pK_a$  values. Unmatched predicted  $pK_a$  count was  
594 also not a consideration, since experimental data was only informative for the  $pK_a$  between dominant microstates and did not  
595 capture the all possible theoretical transitions between microstate pairs. Table 3 reports six methods that have consistent well  
596 performance according to many metrics, although evaluated only for the 8 molecule set due to limitations of the experimen-  
597 tal dataset. Six methods were divided evenly between methods of QSPR/ML category and QM category. *nb016* (MoKa), *hdijyq*  
598 (*Simulations Plus*), and *6tvf8* (OE Gaussian Process) were QSPR and ML based methods that performed well. *nb011* (Jaguar),  
599 *0xi4b*(EC-RISM/B3LYP/6-311+G(d,p)-P2-phi-noThiols-2par), and *cwyk* (EC-RISM/B3LYP/6-311+G(d,p)-P2-phi-noThiols-2par) were  
600 QM predictions with linear empirical corrections with good performance with microscopic  $pK_a$  predictions.

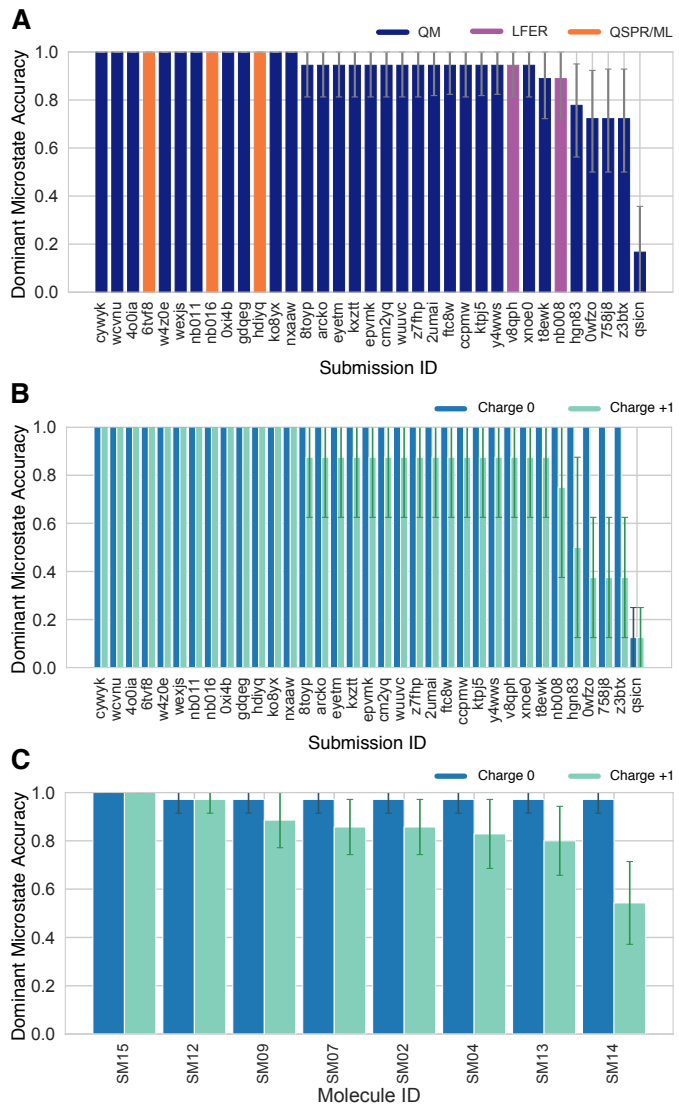


**Figure 10. Some methods predicted the sequence of dominant tautomers inaccurately.** Prediction accuracy of dominant microstate of each charged state was calculated using the dominant microstate sequence determined by NMR for 8 molecules as reference. **(A)** Dominant microstate accuracy vs. submission ID plot was calculated considering all the dominant microstates seen in the 8 molecule experimental microstate dataset. **(B)** Dominant microstate accuracy vs. submission ID plot was generated considering only the dominant microstates of charge 0 and +1 seen in the 8 molecule experimental microstate dataset. Accuracy of each molecule is broken out by total charge of the microstate. **(C)** Dominant microstate prediction accuracy calculated for each molecule averaged over all methods. In **(B)** and **(C)**, the accuracy of predicting the dominant neutral tautomer is showed in blue and the accuracy of predicting the dominant +1 charged tautomer is showed in green. Error bars denoting 95% confidence intervals obtained by bootstrapping.

Simulations Plus p $K_a$  prediction method is the only method that appeared to be consistently well performing in both the assessment for macroscopic and microscopic p $K_a$  prediction (*gyuhx* and *hdijq*). However it is worth noting that two methods that were in consistently top-performing methods list for macroscopic p $K_a$  predictions lacked equivalent submissions of their underlying microscopic p $K_a$  predictions and therefore could not be evaluated at the microstate level. These methods were (ACD/Classic p $K_a$ ) and *xvxzd*(DSD-BLYP-D3(BJ)/def2-TZVPD//PBEh-3c[DCOSMO-RS] + RRHO(GFN-xTB[GBSA]) + Gsolv(COSMO-RS[TZVPD]) and linear fit).

### 3.3 How do p $K_a$ prediction errors impact protein-ligand binding affinity predictions?

Physical modeling methods for predicting protein-ligand binding affinities rely on p $K_a$  predictions for modeling the protein and the ligand. As SAMPL6 p $K_a$  Challenge only focused on small molecule p $K_a$  prediction we will ignore the protonation state effects

**Table 3. Top performing methods for microscopic pK<sub>a</sub> predictions based on consistent ranking within the Top 10 according to various statistical metrics calculated for 8 molecule dataset.** Performance statistics are provided as mean and 95% confidence intervals. Submissions that rank in the Top 10 according to RMSE and MAE, and have perfect dominant microstate prediction accuracy were selected as consistently well-performing methods. Correlation-based statistics ( $R^2$ , and Kendall's Tau), although reported in the table, were excluded from the statistics used for determining top-performing methods. This was because correlation-based statistics were not very discriminating due to narrow dynamic range and the small number of data points in the 8 molecule dataset with NMR-determined dominant microstates.

Submission ID	Method Name	Dominant Microstate Accuracy	RMSE	MAE	R <sup>2</sup>	Kendall's Tau	Unmatched Exp. pK <sub>a</sub> Count	Unmatched Pred. pK <sub>a</sub> Count [2,12]
nb016	MoKa	1.0 [1.0, 1.0]	0.52 [0.25, 0.71]	0.43 [0.23, 0.65]	0.92 [0.05, 0.99]	0.62 [-0.14, 1.00]	0	3
hd1yq	S+pKa	1.0 [1.0, 1.0]	0.68 [0.49, 0.83]	0.60 [0.39, 0.80]	0.86 [0.47, 0.98]	0.78 [0.40, 1.00]	0	16
nb011	Jaguar	1.0 [1.0, 1.0]	0.72 [0.35, 1.07]	0.54 [0.28, 0.86]	0.86 [0.18, 0.98]	0.64 [0.26, 0.95]	0	36
6tvf8	OE Gaussian Process	1.0 [1.0, 1.0]	0.76 [0.55, 0.95]	0.68 [0.46, 0.90]	0.92 [0.78, 0.99]	0.87 [0.6, 1.00]	0	55
0xi4b	EC-RISM/B3LYP/6-311+G(d,p)-P3NI-phi-noThiols-2par	1.0 [1.0, 1.0]	1.15 [0.75, 1.50]	0.98 [0.63, 1.36]	0.77 [0.02, 0.98]	0.51 [-0.14, 1.00]	0	33
cwyk	EC-RISM/B3LYP/6-311+G(d,p)-P2-phi-noThiols-2par	1.0 [1.0, 1.0]	1.17 [0.88, 1.41]	1.06 [0.74, 1.35]	0.73 [0.02, 0.98]	0.56 [-0.08, 1.00]	0	36

of the protein for now. Many affinity prediction methods such as docking, MM/PBSA, MM/GBSA, absolute or alchemical relative free energy calculation methods predict the affinity of a fixed protonation state of the ligand to a receptor. These models strictly depend on pK<sub>a</sub> predictions for determining possible protonation states of the ligand in aqueous environment and in protein complex, as well as the free energy penalty to reach those states [3]. Accuracy of pK<sub>a</sub> predictions can become a limitation for the performance of physical models that try to capture molecular association.

In terms of the ligand protonation states, there are two ways in which the pK<sub>a</sub> prediction errors can influence the prediction accuracy for protein-ligand binding free energies as depicted in Fig. 11. First scenario is when ligand is present in aqueous solution in multiple protonation states (Fig. 11A). When only the minor aqueous protonation state contributes to protein-ligand complex formation, overall binding free energy ( $\Delta G_{bind}$ ) needs to be calculated as the sum of binding affinity of the minor state and the protonation penalty of that state ( $\Delta G_{prot}$ ).  $\Delta G_{prot}$  is a function of pH and pK<sub>a</sub>. A 1 unit of error in pK<sub>a</sub> value would lead to 1.36 kcal/mol error in overall binding affinity, if the protonation state with the minor population binds the protein. The equations in Fig. 11A show the calculation of overall affinity.

In addition to multiple protonation states being present in the aqueous environment, multiple charge states can contribute to complex formation (Fig. 11B). Then, overall free energy of binding needs to include a Multiple Protonation States Correction (MPSC) term ( $\Delta G_{corr}$ ). MPSC is a function of pH, aqueous pK<sub>a</sub> of the ligand, and the difference between the binding free energy of charged and neutral species ( $\Delta G_{bind}^C - \Delta G_{bind}^N$ ) as shown in Fig. 11B.

Using Equation 9 we can model the true MPSC ( $\Delta G_{corr}$ ) value with respect to the difference between pH and the pK<sub>a</sub> of the ligand, to see when this value has significant impact to overall binding free energy. In Fig. 12, true MPSC value that needs to be added to the  $\Delta G_{bind}^N$  is shown for ligands with varying binding affinity difference between protonation states ( $\Delta\Delta G = \Delta G_{bind}^C - \Delta G_{bind}^N$ ) and varying free energy of binding difference between the protonation states. Fig. 12A shows the simulation of a case where for a monoprotic base which has a charged state with lower affinity than the neutral state. Solid lines show the true correction. In situations where pK<sub>a</sub> is lower than pH, correction factor disappears as the ligand fully populates the neutral state ( $\Delta G_{bind} = \Delta G_{bind}^N$ ). As the pK<sub>a</sub> value gets larger than the pH, the charged state is populated more and  $\Delta G_{corr}$  value increases to approach significant  $\Delta\Delta G$ . What is interesting to note is the pH-pK<sub>a</sub> range that  $\Delta G_{corr}$  changes. It is often assumed that for a basic ligand if pK<sub>a</sub> of a ligand is more than 2 units higher than the pH, then only 1% of the population is in neutral state and it is safe to approximate the overall binding affinity with  $\Delta G_{bind}^C$  only. Based on the relative free energy difference between ligand this assumption is not always correct. As seen in Fig. 12A, responsive region of  $\Delta G_{corr}$  can span 3 pH units for a system with  $\Delta\Delta G = 1\text{kcal/mol}$  or 5 pH units for a system with  $\Delta\Delta G = 4\text{kcal/mol}$ . This highlights that the range of pK<sub>a</sub> values that impact binding affinity predictions is wider than previously appreciated. Molecules with pK<sub>a</sub>s several units away from the physiological pH can still impact the overall binding affinity significantly due to MPSC.

Despite the need to capture the contributions of multiple protonations states by including MPSC in binding affinity calculations, inaccurate pK<sub>a</sub> predictions can lead to errors in  $\Delta G_{corr}$  and overall free energy of binding prediction. In Fig. 12A dashed lines show predicted  $\Delta G_{corr}$  based on pK<sub>a</sub> error of -1 units. We have chosen a pK<sub>a</sub> error of 1 units as this is the average performance expected from the pK<sub>a</sub> prediction methods based on the SAMPL6 Challenge. Underestimated pK<sub>a</sub> causes underestimated  $\Delta G_{corr}$

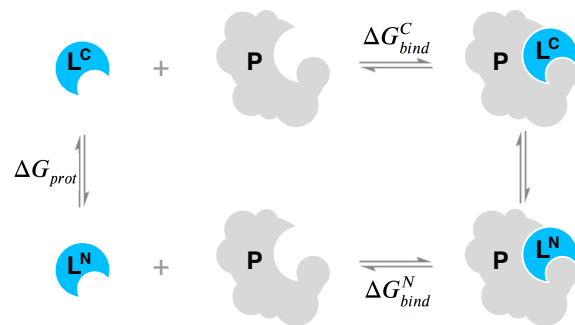
A When only the minor protonation state can bind to the protein



$$\Delta G_{bind} = \Delta G_{bind}^C + \Delta G_{prot}$$

$$\Delta G_{bind} = \Delta G_{bind}^C + RT(pH - pK_a) \ln(10)$$

B When multiple protonation states can bind to the protein



$$\Delta G_{bind} = \Delta G_{bind}^N + \Delta G_{corr}$$

$$\Delta G_{bind} = \Delta G_{bind}^N - RT \ln \frac{1 + e^{-\frac{\Delta G_{bind}^C - \Delta G_{bind}^N}{RT}} 10^{pK_a - pH}}{1 + 10^{pK_a - pH}}$$

**Figure 11. Aqueous  $pK_a$  of the ligand can influence overall protein-ligand binding affinity.** A When only the minor aqueous protonation state contributes to protein-ligand complex formation, overall binding free energy ( $\Delta G_{bind}$ ) needs to be calculated as the sum of binding affinity of the minor state and the protonation penalty of that state. B When multiple charge states contribute to complex formation, overall free energy of binding includes a multiple protonation states correction (MPSC) term ( $\Delta G_{corr}$ ). MPSC is a function of pH, aqueous  $pK_a$  of the ligand, and the difference between the binding free energy of charged and neutral species ( $\Delta G_{bind}^C - \Delta G_{bind}^N$ ).

and overestimated affinities for a varying range of pH -  $pK_a$  values depending on binding affinity difference between protonation states( $\Delta\Delta G$ ). In Fig. 12B dashed lines shows how the magnitude of the absolute error caused by calculating  $\Delta G_{corr}$  with an inaccurate  $pK_a$  varies with respect to pH. Different colored lines show simulated results with varying binding affinity difference between protonation states. For a system whose charged state has lower affinity than the neutral state ( $\Delta\Delta G = 2$  kcal/mol), the absolute error caused by underestimated  $pK_a$  by 1 units only can be up to 0.9 kcal/mol. For a system whose charged state has even lower affinity than the neutral state ( $\Delta\Delta G = 4$  kcal/mol), the absolute error caused by underestimated  $pK_a$  by 1 units only can be up to 1.2 kcal/mol. The magnitude of errors contributing to overall binding affinity are too large to be neglected. Improving the accuracy of small molecule  $pK_a$  prediction methods can help to minimize the error in predicted MPSC.

With the current level of  $pK_a$  prediction accuracy as observed in SAMPL6 Challenge, is it advantageous to include MPSC in affinity predictions that may be include errors caused by  $pK_a$  predictions? We provide a comparison of the two choices to answer this question: (1) Neglecting MPSC completely and assuming overall binding affinity is captured by  $\Delta G_{bind}^N$ , (2) including MPSC with potential error in overall affinity calculation. The magnitude of error caused by Choice 1 (ignoring MPSC) is depicted as solid line in Fig. 12B and the magnitude of error caused by MPSC computed with inaccurate  $pK_a$  is depicted as dashed lines. What is the best strategy? Error due to choice 1 is always larger than error due to choice 2 for all pH- $pK_a$  values. In this scenario including MPSC improves overall binding affinity prediction. The error caused my inaccurate  $pK_a$  is smaller than the error caused by neglecting MPSC.

The same question about whether or not an MPSC calculated based on an inaccurate  $pK_a$  should be included in binding affinity predictions can be asked for different circumstances underestimating or overestimated  $pK_a$  values, charged states with higher or lower affinities than the neutral states. We tried to capture these 4 circumstances in four quadrants of Fig. 12. In the case of overestimated  $pK_a$  values (Fig. 12E-H) it can be seen that for the most of the pH- $pK_a$  range it is more advantageous to include the predicted MPSC in affinity calculations, except a smaller window where the opposite choice would be more advantageous. For instance, for the system with  $\Delta\Delta G = 2$  kcal/mol and overestimated  $pK_a$  (Fig. 12E) for the pH- $pK_a$  region between -0.5 and 2, including predicted  $\Delta G_{corr}$  causes more error than ignoring MPSC.

In reality we do not know the exact magnitude or the direction of the error of our predicted  $pK_a$ , therefore using simulated MPSC error plots to make the decision about when to include MPSC in binding affinity predictions is not possible. But based on the analysis of extreme cases, with 1 unit of  $pK_a$  error including MPSC correction is more often than not helpful in improving binding affinity predictions. The detrimental effect of  $pK_a$  inaccuracy is still significant, however, future improvements in  $pK_a$  prediction methods can improve the accuracy of MPSC and binding affinity predictions of ligands which have multiple proto-

672 nation states that contribute to aqueous or complex populations. Achieving  $pK_a$  value prediction accuracy of 0.5 units would  
673 significantly help the binding affinity models to incorporate more accurate MPSC terms.

### 674 3.4 Take-away lessons from SAMPL6 $pK_a$ Challenge

675 SAMPL6  $pK_a$  Challenge showed that in general  $pK_a$  prediction performance of computational methods are lower than expected  
676 for drug-like molecules. Multiple titration sutes, tautomerization, frequent presence of heterocycles and extended conjugation  
677 patterns, as well as high number of rotatable bonds, and the possibility of intramolecular hydrogen bonds are factors that  
678 complicate  $pK_a$  prediction of drug-like molecules. For macroscopic  $pK_a$  predictions have not yet reached experimental accuracy.  
679 Inter-method variability of macroscopic  $pK_a$  measurements can be around 0.5  $pK_a$  units [15]. There was not a single method in  
680 SAMPL6 Challenge that achieved RMSE around 0.5 or lower for macropscoptic  $pK_a$  predictions for the 24 molecule set of kinase  
681 inhibitor fragment-like molecules. Lower RMSE values were observed in the microscopic  $pK_a$  evaluation section of this study  
682 for some methods however the 8 molecule set used for that analysis poses a very limited dataset to reach conclusions about  
683 general expectations for drug-like molecules.

684 As the majority of experimental data was in the form of macroscopic  $pK_a$  values, we had to adopt a numerical matching  
685 algorithm (Hungarian matching) to pair predicted and experimental values to calculate performance statistics of macroscopic  
686  $pK_a$  predictions. Accuracy, correlation, and extra/missing  $pK_a$  prediction counts were the main metrics for macroscopic  $pK_a$   
687 evaluations. An RMSE range of 0.7 to 3.2  $pK_a$  units. Only five methods achieved RMSE between 0.7-1  $pK_a$  units, while an RMSE  
688 between 1.5-3 log units was observed for the majority of methods. All four methods of LFER category and three out of 5 QSPR/ML  
689 methods achieved RMSE less than 1.5  $pK_a$  units. All the QM methods that achieved this level of performance included linear  
690 empirical corrections to rescale and unbias their  $pK_a$  predictions.

691 Based on consideration of multiple error metrics, we compiled a short list of consistently-well performing methods for macro-  
692 scopic  $pK_a$  evaluations. Two methods from QM+LEC methods, one QSPR/ML, two empirical methods achieved consistent per-  
693 formance according to many metrics. The common features of the two empirical methods were their large training sets (16000-  
694 17000 compounds) and being commercial prediction models.

695 There were four submissions of QM-based methods that utilized COSMO-RS implicit solvation model. It was interesting  
696 that while three of these achieved the lowest RMSE among QM-based methods (*xvxzd*, *yqkga*, and *8xt50*) [33] and one of them  
697 showed the highest RMSE (*0hxtm* (COSMOtherm\_FINE17)) in SAMPL6 Challenge macroscopic  $pK_a$  predictions. Comparison of  
698 these methods indicates that capturing conformational ensemble of microstates, high level QM calculations, and RRHO cor-  
699 rections were factors contributing to better macroscopic  $pK_a$  predictions. Linear empirical corrections applied QM calculations  
700 imporved results, especially when the linear correction is calibrated for an experimental dataset using the same level of theory  
701 ast the deprotonation free energy predictions (as in *xvxzd*). This challenge also points to the advantage of COSMO-RS solvation  
702 approach compared to other implicit solvent models.

703 Evaluation of macroscopic  $pK_a$  prediction accuracy of individual molecules on average considering all the predictions in  
704 SAMPL6 Challenge provided insight into which molecules posed greater difficulty for  $pK_a$  predictions.  $pK_a$  prediction errors  
705 were higher for compounds with sulfur-containing heterocycles, iodo, and bromo groups. This trend was also conserved when  
706 only QM-based methods were analyzed. SAMPL6  $pK_a$  dataset consisted of only 24 small molecules which limited our ability  
707 to statistically confirm this conclusion, however, we believe it is worth reporting molecular features that coincided with larger  
708 errors even if we can not evaluate the driving reason for these failures.

709 Utilizing a numerical matching algorithm to pair experimental and predicted macroscopic  $pK_a$  values was a necessity, how-  
710 ever, this approach did not capture all aspects of prediction errors. Computing the number of missing or extra  $pK_a$  predictions  
711 remaining after Hungarian matching, provided a window of observing macroscopic  $pK_a$  prediction errors such as number of  
712 macroscopic transitions or ionization states expected in a pH interval. In  $pK_a$  evaluation studies it is very typical to just focus  
713 on  $pK_a$  value errors evaluated after matching, and to ignore  $pK_a$  prediction errors that the matching protocol can not capture.  
714 SAMPL6  $pK_a$  Challenge results showed sporadic presence of missing  $pK_a$  predictions and very frequent case of extra  $pK_a$  predic-  
715 tions. Both indicates failures to capture the correct sequence of ionizations states. The traditional way of evaluating  $pK_a$ s that  
716 only focuses on the  $pK_a$  value error after some sort of numerical match between predictions and experimental values may have  
717 motivated these types of errors as there would be no penalty for missing a macroscopic deprotonation and predicting an extra  
718 one. This problem does not seem to be specific to any method category.

719 We have used the 8 molecule subset of SAMPL6 compounds with NMR-based dominant microstate sequence information  
720 to demonstrate the advantage of evaluating  $pK_a$  prediction on the level of microstates. Comparison of statistics computed by  
721 Hungarian matching and microstate-based matching on 8 molecule dataset showed how Hungarian matching, despite being the

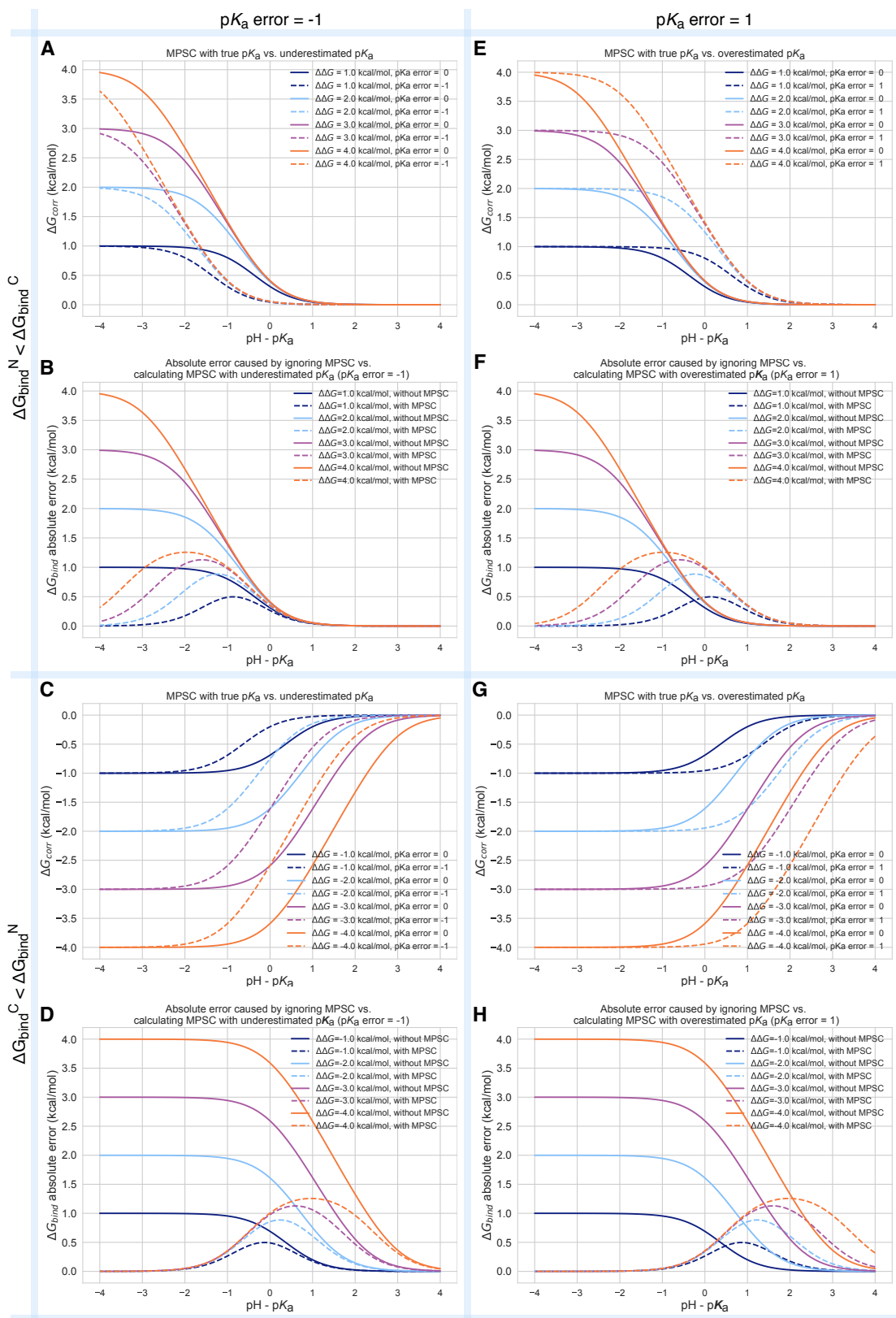


**Figure 12. Inaccuracy of  $pK_a$  prediction ( $\pm 1$  unit) affects the accuracy of MPSC and overall protein-ligand binding free energy calculation in varying amounts based on aqueous  $pK_a$  value and relative binding affinity of individual protonation states ( $\Delta\Delta G = \Delta G_{bind}^C - \Delta G_{bind}^N$ ). All calculations are made for 25°C, and for a ligand with single basic titratable group. **A, C, E, and G** show MPSC ( $\Delta G_{corr}$ ) calculated with true vs. inaccurate  $pK_a$ . **B, D, F, and H** show comparison of the absolute error to  $\Delta G_{bind}$  caused by ignoring the MPSC completely (solid lines) vs. calculating MPSC based in inaccurate  $pK_a$  value (dashed lines). These plots provide guidance on when it is beneficial to include MPSC correction based on  $pK_a$  error,  $pH - pK_a$ , and  $\Delta\Delta G$ .**

optimal matching algorithm, can mask errors in  $pK_a$  predictions. Errors computed by microstate-based matching were larger compared to numerical matching algorithms in terms of RMSE. Microscopic  $pK_a$  analysis with numerical matching algorithms may mask errors due to higher number of guesses made. Numerical matching based on  $pK_a$  values also ignores information regarding the relative population of states. Therefore, it can lead to  $pK_a$ s defined between very low energy microstate pairs to be matched to the experimentally observable  $pK_a$  between microstates of higher populations. Of course the predicted  $pK_a$  value could be correct however the predicted microstates would be wrong. Such mistakes caused by Hungarian matching were observed frequently in SAMPL6 results and therefore we decided microstate-based matching of  $pK_a$ values provides a more realistic picture of method performance.

Analysis of dominant microstate prediction accuracy of microscopic  $pK_a$  showed that some QM and LFER methods made mistakes in predicting the dominant tautomers of the ionization states seen experimentaly. Dominant tautomer prediction seemed to be a more prominant problem for charged tautomers than the neutral tautomer. The easiest way to extract dominant microstate sequence from predictions is to calculate relative free energy of microstates at any reference pH, and determining the lowest energy state in each ionization state. Errors in dominant microstate predictions was very rare for neutral tautomers, but more frequent in cationic tautomers with +1 charge of the 8 molecule set. SM14 was the molecule with the lowest dominant microstate prediction accuracy, while dominant microstates predictions for SM15 were perfect for all molecules. SM14 and SM15 both have two experimental  $pK_a$ s and benzimidazole scaffold. The difference between them is the distance between the experimental  $pK_a$  values which is smaller for SM14. This results makes sense from the perspective of relative free energies of microstates. Closer  $pK_a$  values mean that the free energy difference between different microstates are smaller for SM14, and therefore any error in predicting the relative free energy of tautomers is more likely to cause reordering of relative populations of microstates and impact the accuracy of dominant microstate predictions. It would have been extremely informative to evaluate the tautomeric ratios and relative free energy predictions of microstates, however, experimental data was missing for this approach.

According to statistics calculated with microstate-based matching, we determined a shortlist of consistently well-performing methods for microscopic  $pK_a$  predictions of 8 molecule set. These methods that ranked in top 10 according to RMSE, MEA, and had perfect dominant microstate prediction accuracy included three methods from QM+LEC category and three from QSPR/ML category. Simulations Plus  $pK_a$  prediction method was the only method that appeared to be consistently well performing in both the assessment for macroscopic and microscopic  $pK_a$  prediction (*gyuhx* and *hdlyq*), although, due to the size of the experimental datasets evaluation of macroscopic  $pK_a$  prediction carried more weight in this performance assessment. Still microscopic  $pK_a$  evaluation can provide much more in depth analysis and can be more informative about capturing reasons for failure.

The performance levels of microscopic and macroscopic  $pK_a$  prediction as seen in SAMPL6  $pK_a$  Challenge assessment can be detrimental to the accuracy of protein-ligand affinity predictions and other pH-dependent physicochemical property predictions such as distribution coefficients, membrane permeability, and solubility. Protein-ligand binding affinity predictions rely on  $pK_a$  predictions in two ways: determination of relevant aqueous microstates and the free energy penalty to reach these states. Microscopic  $pK_a$  predictions with better accuracy are needed for accurate incorporation of multiple protonation state correction (MPSC) to overall binding affinity calculations. We simulated the effect of overestimating or underestimating  $pK_a$  of a ligand by one unit on overall binding affinity prediction for a ligand where both cation and neutral states contribute to binding affinity.  $pK_a$  prediction error of this magnitude (assuming dominant tautomers were predicted correctly) could cause up to 0.9 and 1.2 kcal/mol error in overall binding affinity when relative binding affinity of protonation states are 2 or 4 kcal/mol different, respectively. For the case of 4 kcal/mol binding affinity difference between protonation states the pH- $pK_a$  range that the error would be larger than 0.5 kcal/mol suprizingly spans around 3.5 pH units. We demonstrated that the range of pH- $pK_a$  value that MPSC needs to be incorporated in binding affinity predictions can be wider than the widely assumed range of 2 pH units, based on the affinity difference between protonation states. At the level of 1 unit  $pK_a$  error incorporating MSPC would improve binding affinity predictions more often than not. If microscopic  $pK_a$  could be predicted with 0.5  $pK_a$  units of accuracy, MPSC calculations would be much more reliable.

There are multipe factors to consider when deciding which  $pK_a$  prediction method to utilize. These factors include the accuracy of microscopic and macroscopic  $pK_a$  values, accuracy of the number and the identity of ionization states predicted within the experimental pH interval, the accuracy of microstates predicted within the experimental pH interval, accuracy of tautomeric ratio (i.e. relative free energy between microstates), how costly is the calculation in terms of time and resources, and whether one has access to software licenses that might be required.

We were disappointed to see that all top performing empirical methods were developed as commercial software that require a licenses to run, and there were not any open-source alternatives for empirical  $pK_a$  predictions. Since then two publications

773 reported open source machine learning based  $pK_a$  prediction methods, however one can only predict the most acidic or most  
774 basic macroscopic  $pK_a$  values of a molecule [36] and the second one is only trained for predicting  $pK_a$  values of monoprotic  
775 molecules [37]. Recently a  $pK_a$  prediction methodology was published that describes a mixed approach of semi-empirical QM  
776 calculations and machine learning that can predict macroscopic  $pK_a$ s of both mono-and polyprotic species [38]. The authors  
777 reported RMSE of 0.85 for the retrospective analysis performed on the SAMPL6 dataset.

### 778 3.5 Suggestions for future challenge design and evaluation of $pK_a$ predictions

779 The first  $pK_a$  challenge of SAMPL series was useful for understanding the current state of the field and led to many lessons. We  
780 believe the highest benefit can be achieved if further iteration so of small molecule  $pK_a$  prediction challenges can be organized,  
781 creating motivation for improving protonation state prediction methods for drug-like molecules. In future challenges it is desire-  
782 able to increase chemical diversity to cover more of common scaffolds ?? and functional groups ?? seen in drug-like molecules,  
783 and gradually increasing the complexity of molecules.

784 Future challenges should promote stringent evaluation for  $pK_a$  prediction methods from the perspective of microscopic  $pK_a$   
785 and microstate predictions. It is necessary to assess the capability of  $pK_a$  prediction methods to capture the free energy profile of  
786 microstates of multiprotic molecules. This is critical because  $pK_a$  predictions are often utilized to determine relevant protonation  
787 states and tautomers of small molecules that must be captured in other physical modeling approaches, such as protein-ligand  
788 binding affinity or distribution coefficient predictions.

789 In this paper, we demonstrated how experimental microstate information can guide the analysis further than the typical  $pK_a$   
790 evaluation approach that has been used so far. The traditional  $pK_a$  evaluation approach only focuses on the numerical error  
791 of the  $pK_a$  values and neglects the difference between macroscopic and microscopic  $pK_a$  definitions. This is mainly caused by  
792 lack of  $pK_a$  datasets with microscopic detail. To improve  $pK_a$  and protonation state predictions of multiprotic molecules it is  
793 necessary to embrace the difference between macroscopic and microscopic  $pK_a$  definitions and select strategies for experimen-  
794 tal data collection and prediction evaluation accordingly. In SAMPL6 Challenge the analysis was limited by the availability of  
795 experimental microscopic data as well. As usual macroscopic  $pK_a$  values were abundant (24 molecules) and limited data on mi-  
796 croscopic states was available (8 molecules), although the later opened new avenues for evaluation. For future blind challenges  
797 for multiprotic compounds, striving collect experimental datasets with microscopic  $pK_a$ s would be very beneficial. Benchmark  
798 datasets of microscopic  $pK_a$ s are currently missing. This limits the improvement of  $pK_a$  and tautomer prediction methods for  
799 multiprotic molecules. If collection of experimental microscopic  $pK_a$ s is not possible due to time and resource cost of such NMR  
800 experiments, at least supplementing the more automated macroscopic  $pK_a$  measurements with NMR-based determination of  
801 the dominant microstate sequence or tautomeric ratios of each ionization state can create very useful benchmark datasets.  
802 This supplementary information can allow microstate-based assignment between experimental and predicted  $pK_a$ s and more  
803 realistic assessment of method performance.

804 If the only available experimental data is in the form of macroscopic  $pK_a$  values, the best way to evaluate computational  
805 predictions is by calculating predicted macroscopic  $pK_a$  predictions. With the conversion of microscopic  $pK_a$  to macroscopic  
806  $pK_a$ s all the structural information about the titration site is lost and only remaining information is the total charge of macro-  
807 scopic ionization states. Unfortunately, most macroscopic  $pK_a$  measurements including potentiometric and spectrophotometric  
808 methods do not capture the absolute charge of the macrostates. Spectrophotometric method does not measure charge  
809 at all. Potentiometric method can only capture the relative charge change between methods. Only pH-dependent solubility  
810 based  $pK_a$  estimations can differentiate the neutral and charged states from one another. So it is very common to have ex-  
811 perimental datasets of macroscopic  $pK_a$  without any charge or protonation position information regarding the macrostates.  
812 This causes an issue of assigning predicted and experimental  $pK_a$  values before any error statistics can be calculated. As deline-  
813 ated by Fraczkiewicz et. al. the most fair and reasonable solution for  $pK_a$  matching problem involves an assignment algorithm  
814 that preserves the order of predicted and experimental microstates and uses the principle of smallest differences to pair val-  
815 ues [15]. We recommend Hungarian matching with squared error cost function. The algorithm is available in SciPy package  
816 (`scipy.optimize.linear_sum_assignment`) [18]. In addition to the analysis of numerical error statistics after Hungarian matching,  
817 at the very least number of missing and extra  $pK_a$  predictions must be reported based on unmatched  $pK_a$  values. Missing or  
818 extra  $pK_a$  predictions point to a problem with capturing the right number of ionization states within the pH interval of the ex-  
819 perimental measurements. We have demonstrated that for microscopic  $pK_a$  predictions performance analysis based in Hungarian  
820 matching results in overly optimistic and misleading results, instead the employed microstate-based matching provided a more  
821 realistic assessment.

822 For capturing all the necessary information related to  $pK_a$  predictions we allowed three different submission types in SAMPL6:

(1) macroscopic  $pK_a$  values, (2) microscopic  $pK_a$  values and microstate pair identities, (3) fractional population of microstates with respect to pH. We realized later that collecting fractional populations of microstates was redundant, as microscopic  $pK_a$  and microstate pairs values capture all the necessary information to construct fractional population vs. pH curves. Only microscopic and macroscopic  $pK_a$  values were used for the challenge analysis presented in this paper. While exploring ways to evaluate SAMPL6  $pK_a$  Challenge results, we developed a better way to capture microscopic  $pK_a$  predictions as presented in an earlier paper [19]. This alternative reporting format consists of charge and relative free energy of microstates with respect to a reference microstate and pH predicted by  $pK_a$  predictions. This approach presents the most concise method of capturing all necessary information regarding microscopic  $pK_a$  predictions and allows calculation of predicted microscopic  $pK_a$ s, microstate population with respect to pH, macroscopic  $pK_a$ s, macroscopic population with respect to pH, and tautomer ratios. Still there may be methods developed to train to predict macroscopic  $pK_a$ s directly instead of computing it from microstate predictions that justifies allowing a macroscopic  $pK_a$  reporting format. In future challenges, we recommend collection of  $pK_a$  predictions in two submission types: (1) macroscopic  $pK_a$  values and (2) microstates, their total charge, and relative free energies with respect to a specified reference microstate and pH.

In SAMPL6 because we were worried about parsing submitted microstates in SMILES from different sources correctly, we created an pre-enumerated list of microstates and assigned them microstate IDs. There were two disadvantages of this approach. First, this list of enumerated microstates were used as an input by some participants which was not our intentions. Second, the first iteration of enumerated microstates was not complete. We had to add new microstates and assign them microstate IDs for a couple of rounds until reaching a complete list. In future challenges, a better way of handling the problem of capturing predicted microstates would be asking participants to submit a mol2 file that represents the microstate with explicit hydrogens. The organizers must only provide the microstate that was selected as the reference state for the relative microstate free energy calculations.

In the SAMPL6  $pK_a$  Challenge there was not a requirement that prediction sets should report predictions for all compounds. Some participants reported predictions for only a subset of compounds which may have led these methods to look more accurate than others, due to missing predictions. In the future it will be better to allow submissions of only complete sets for better comparison of method performance.

A wide range of methods participated the SAMPL6  $pK_a$  Challenge from very fast QSPR methods to QM methods with high-level of theory and extensive exploration of conformational ensembles. In the future, it would be interesting to capture computing costs in terms of average compute hours per molecule. This can provide guidance to future users of  $pK_a$  prediction methods for selection of which method to use.

To maximize the lessons that can be learned from blind challenges we believe in the utility of evaluating predictions of different physicochemical properties for the same molecules in consecutive challenges. In SAMPL6 we organized both  $pK_a$  and  $\log P$  challenges. Unfortunately only a subset of compounds in  $pK_a$  datasets were suitable for the potentiometric  $\log P$  measurements. Still for the subset of compounds that were common in both challenges comparing prediction performance can lead to beneficial insights especially for physical modeling techniques if there are common aspects that are beneficial or detrimental to prediction performance. For example, in SAMPL6  $pK_a$  and  $\log P$  Challenges COSMO-RS and EC-RISM solvation models achieved good performance. Having a variety of experimental measurements of physicochemical properties can also help identifying sources of errors. For example, dominant microstates determined for  $pK_a$  challenge can provide information to check if correct tautomers are modeling in a  $\log P$  or  $\log D$  challenge.  $pK_a$  prediction is a requirement for  $\log D$  prediction and experimental  $pK_a$  values can help diagnosing the source of errors in  $\log D$  predictions better. The physical challenges in SAMPL7, which is currently running with a deadline of September 30th, 2020, follow this principle and include both  $pK_a$ ,  $\log P$ , and membrane permeability properties for a set of monoprotic compounds. We hope that future  $pK_a$  challenges can focus on multiprotic drug-like compounds with microscopic  $pK_a$  measurements for an in depth analysis.

## 4 Conclusion

The first SAMPL6  $pK_a$  Challenge focused on kinase inhibitor like molecules to assess the performance of  $pK_a$  predictions for drug-like molecules. With wide participation we had an opportunity to prospectively evaluate  $pK_a$  predictions spanning various empirical and QM based approaches. A small number of popular  $pK_a$  prediction methods that were missing from blind submissions were added as reference calculations after the challenge deadline.

The experimental dataset consisted of spectrophotometric measurements of 24 molecules and some of which were multiprotic. There was also experimental data on dominant microstate sequence of a subset of the challenge molecules, but not

872 direct microscopic  $pK_a$  measurements. We have performed comparative analysis of methods represented in the blind challenge  
873 in terms of both macroscopic and microscopic  $pK_a$  prediction performance avoiding any assumptions about the experimental  
874  $pK_a$ s.

875 As the majority of the experimental data was macroscopic  $pK_a$  values, we had to utilize Hungarian matching to assign pre-  
876 dicted and experimental values before calculating accuracy and correlation based statistics. In addition to evaluating error in  
877 predicted  $pK_a$  values, we also reported the macroscopic  $pK_a$  errors that were not captured by the match between experimental  
878 and predicted  $pK_a$  values. These were extra or missing  $pK_a$  predictions which are important indicators that predictions are failing  
879 to capture the correct ionization states.

880 We utilized the experimental dominant microstate sequence data of 8 molecules to evaluate microscopic  $pK_a$  predictions in  
881 more detail. This experimental data allowed us to use microstate-based matching for evaluating the accuracy of microscopic  $pK_a$   
882 values in a more realistic way. We have determined that QM and LFER predictions had lower accuracy in determining the dom-  
883 inant tautomer of the charged microstates than the neutral states. For both macroscopic and microscopic  $pK_a$  predictions we  
884 have determined methods that were consistently well-performing according to multiple statistical metrics. Focusing on the com-  
885 parison of molecules instead of methods for macroscopic  $pK_a$  prediction accuracy indicated molecules with sulfur-containing  
886 heterocycles, iodo, and bromo groups suffered from lower  $pK_a$  prediction accuracy.

887 Overall performance level observed for  $pK_a$  predictions in this challenge is concerning for the application of  $pK_a$  prediction  
888 methods in computer-aided drug design. Many methods for capturing target affinities and physicochemical properties rely on  
889  $pK_a$  predictions for determining relevant protonation states and the free energy penalty of such states. 1 unit of  $pK_a$  error is an  
890 optimistic estimate of current macroscopic  $pK_a$  predictions for drug-like molecules based on SAMPL6 Challenge where errors  
891 in predicting correct number of ionization states or determining the correct dominant microstate were also common to many  
892 methods. In the absence of other sources of errors, we showed that 1 unit over- or underestimation of the  $pK_a$  of a ligand can  
893 cause significant errors in the overall binding affinity calculation due to errors in multiple protonation state correction factor.

894 All information regarding the challenge structure, experimental data, blind prediction submission sets, and evaluation of  
895 methods are available in the SAMPL6 GitHub Repository for future follow up analysis and to serve as a benchmark dataset for  
896 testing methods.

897 In this article we aimed to demonstrate not only the comparative analysis of the  $pK_a$  prediction performance of contemporary  
898 methods for drug-like molecules, but also to propose a stringent  $pK_a$  prediction evaluation strategy that takes into account dif-  
899 ferences in microscopic and macroscopic  $pK_a$  definitions. We hope that this study will guide and motivate further improvement  
900 of  $pK_a$  prediction methods.

## 901 5 Code and data availability

- 902 • SAMPL6  $pK_a$  challenge instructions, submissions, experimental data and analysis is available at  
<https://github.com/samplchallenges/SAMPL6>

## 903 6 Overview of supplementary information

904 Contents of the Supplementary Information:

- 905 • TABLE S1: SMILES and InChI identifiers of SAMPL6  $pK_a$  Challenge molecules.
- 906 • TABLE S2: Evaluation statistics calculated for all macroscopic  $pK_a$  prediction submissions based on Hungarian match for  
907 24 molecules.
- 908 • TABLE S3: Evaluation statistics calculated for all microscopic  $pK_a$  prediction submissions based on Hungarian match for 8  
909 molecules with NMR data.
- 910 • TABLE S4: Evaluation statistics calculated for all microscopic  $pK_a$  prediction submissions based on microstate match for 8  
911 molecules with NMR data.
- 912 • FIGURE S1: Dominant microstates of 8 molecules were determined based on NMR measurements.
- 913 • FIGURE S2: MAE of macroscopic  $pK_a$  predictions of each molecule did not show any significant correlation with any molec-  
914 ular descriptor.
- 915 • FIGURE S3: The value of macroscopic  $pK_a$  was not a factor affecting prediction error seen in SAMPL6 Challenge according  
916 to the analysis with Hungarian matching.
- 917 • FIGURE S4: There was low agreement between experimental dominant microstate pairs and the predicted microstate pairs  
918 selected by Hungarian algorithm for microscopic  $pK_a$  predictions.

919 Extra files included in SAMPL6-supplementary-documents.tar.gz:  
920   • SAMPL6-pKa-chemical-identifiers-table.csv  
921   • macroscopic-pKa-statistics-24mol-hungarian-match.csv  
922   • microscopic-pKa-statistics-8mol-hungarian-match-table.csv  
923   • microscopic-pKa-statistics-8mol-microstate-match-table.csv  
924   • experimental-microstates-of-8mol-based-on-NMR.csv  
925   • enumerate-microstates-with-Epik-and-OpenEye-QUACPAC.ipynb  
926   • molecule\_ID\_and\_SMILES.csv

## 927 7 Author Contributions

928 Conceptualization, MI, JDC, CB, DLM ; Methodology, MI, JDC ; Software, MI, AR, ASR ; Formal Analysis, MI, ASR, AR ; Investigation,  
929 MI ; Resources, JDC; Data Curation, MI ; Writing-Original Draft, MI, JDC; Writing - Review and Editing, MI, ASR, AR, CB, DLM, JDC;  
930 Visualization, MI, AR ; Supervision, JDC, DLM, CB, ASR ; Project Administration, MI ; Funding Acquisition, JDC, DLM.

## 931 8 Acknowledgments

932 Complete acknowledgments section. Caitlin Bannan for guidance on working microstate definition for the challenge, Thomas Fox for  
MoKa reference calculations, Kiril Lanevskij for hungarian algorithm

933 MI, ASR, and JDC acknowledge support from the Sloan Kettering Institute. JDC acknowledges support from NIH grant P30  
934 CA008748. MI acknowledges Doris J. Hutchinson Fellowship. We thank Brad Sherborne for his valuable insights at the conception  
935 of the pK<sub>a</sub> challenge and connecting us with Timothy Rhodes and Dorothy Levorse who were able to provide resources and  
936 expertise for experimental measurements performed at MRL. We acknowledge Paul Czodrowski who provided feedback on  
937 multiple stages of this work: challenge construction, purchasable compound selection and manuscript. MI, ASR, AR and JDC are  
938 grateful to OpenEye Scientific for providing a free academic software license for use in this work.

939 Mike Chui

## 940 9 Disclosures

941 JDC is a member of the Scientific Advisory Board for Schrödinger, LLC. DLM is a member of the Scientific Advisory Board of  
942 OpenEye Scientific Software.

943 Table ref: [21, 22, 24, 25, 27]

## 944 References

- 945 [1] Manallack DT, Pranker RJ, Yuriev E, Oprea TI, Chalmers DK. The Significance of Acid/Base Properties in Drug Discovery. *Chem Soc Rev.* 2013; 42(2):485–496. doi: [10.1039/C2CS35348B](https://doi.org/10.1039/C2CS35348B).
- 946 [2] Manallack DT, Pranker RJ, Nassta GC, Ursu O, Oprea TI, Chalmers DK. A Chemogenomic Analysis of Ionization Constants-Implications for  
947 Drug Discovery. *ChemMedChem.* 2013 Feb; 8(2):242–255. doi: [10.1002/cmdc.201200507](https://doi.org/10.1002/cmdc.201200507).
- 948 [3] de Oliveira C, Yu HS, Chen W, Abel R, Wang L. Rigorous Free Energy Perturbation Approach to Estimating Relative Binding Affinities  
949 between Ligands with Multiple Protonation and Tautomeric States. *Journal of Chemical Theory and Computation.* 2019 Jan; 15(1):424–435.  
950 doi: [10.1021/acs.jctc.8b00826](https://doi.org/10.1021/acs.jctc.8b00826).
- 951 [4] Darvey IG. The Assignment of pKa Values to Functional Groups in Amino Acids. *Biochemical Education.* 1995 Apr; 23(2):80–82. doi:  
952 [10.1016/0307-4412\(94\)00150-N](https://doi.org/10.1016/0307-4412(94)00150-N).
- 953 [5] Bodner GM. Assigning the pKa's of Polyprotic Acids. *Journal of Chemical Education.* 1986 Mar; 63(3):246. doi: [10.1021/ed063p246](https://doi.org/10.1021/ed063p246).
- 954 [6] Murray R. Microscopic Equilibria. *Analytical Chemistry.* 1995 Aug; p. 1.
- 955 [7] Işık M, Levorse D, Rustenburg AS, Ndukwe IE, Wang H, Wang X, Reibarkh M, Martin GE, Makarov AA, Mobley DL, Rhodes T, Chodera JD.  
956 pKa Measurements for the SAMPL6 Prediction Challenge for a Set of Kinase Inhibitor-like Fragments. *Journal of Computer-Aided Molecular  
957 Design.* 2018 Oct; 32(10):1117–1138. doi: [10.1007/s10822-018-0168-0](https://doi.org/10.1007/s10822-018-0168-0).
- 958 [8] Bochevarov AD, Watson MA, Greenwood JR, Philipp DM. Multiconformation, Density Functional Theory-Based pK<sub>a</sub> Prediction in Application to Large, Flexible Organic Molecules with Diverse Functional Groups. *Journal of Chemical Theory and Computation.* 2016 Dec;  
959 12(12):6001–6019. doi: [10.1021/acs.jctc.6b00805](https://doi.org/10.1021/acs.jctc.6b00805).

- 962 [9] Selwa E, Kenney IM, Beckstein O, Iorga BI. SAMPL6: Calculation of Macroscopic pKa Values from Ab Initio Quantum Mechanical Free  
963 Energies. Journal of Computer-Aided Molecular Design. 2018 Oct; 32(10):1203–1216. doi: [10.1007/s10822-018-0138-6](https://doi.org/10.1007/s10822-018-0138-6).
- 964 [10] Pickard FC, König G, Tofoleanu F, Lee J, Simonett AC, Shao Y, Ponder JW, Brooks BR. Blind Prediction of Distribution in the SAMPL5  
965 Challenge with QM Based Protomer and pK a Corrections. Journal of Computer-Aided Molecular Design. 2016 Nov; 30(11):1087–1100. doi:  
966 [10.1007/s10822-016-9955-7](https://doi.org/10.1007/s10822-016-9955-7).
- 967 [11] Bannan CC, Mobley DL, Skillman AG. SAMPL6 Challenge Results from \$\$pK\_a\$\$ Predictions Based on a General Gaussian Process Model.  
968 Journal of Computer-Aided Molecular Design. 2018 Oct; 32(10):1165–1177. doi: [10.1007/s10822-018-0169-z](https://doi.org/10.1007/s10822-018-0169-z).
- 969 [12] Işık M, Levorse D, Mobley DL, Rhodes T, Chodera JD. Octanol-Water Partition Coefficient Measurements for the SAMPL6 Blind Prediction  
970 Challenge. Journal of Computer-Aided Molecular Design. 2020 Apr; 34(4):405–420. doi: [10.1007/s10822-019-00271-3](https://doi.org/10.1007/s10822-019-00271-3).
- 971 [13] Işık M, Bergazin TD, Fox T, Rizzi A, Chodera JD, Mobley DL. Assessing the Accuracy of Octanol-Water Partition Coefficient Predictions in the  
972 SAMPL6 Part II Log P Challenge. Journal of Computer-Aided Molecular Design. 2020 Apr; 34(4):335–370. doi: [10.1007/s10822-020-00295-0](https://doi.org/10.1007/s10822-020-00295-0).
- 973 [14] Special Issue: SAMPL6 (Statistical Assessment of the Modeling of Proteins and Ligands); October 2018. Volume 32, Issue 10. Journal of  
974 Computer-Aided Molecular Design.
- 975 [15] Fraczkiewicz R. In Silico Prediction of Ionization. In: *Reference Module in Chemistry, Molecular Sciences and Chemical Engineering* Elsevier;  
976 2013. doi: [10.1016/B978-0-12-409547-2.02610-X](https://doi.org/10.1016/B978-0-12-409547-2.02610-X).
- 977 [16] Kuhn HW. The Hungarian Method for the Assignment Problem. Naval Research Logistics Quarterly. 1955 Mar; 2(1-2):83–97. doi:  
978 [10.1002/nav.3800020109](https://doi.org/10.1002/nav.3800020109).
- 979 [17] Munkres J. Algorithms for the Assignment and Transportation Problems. J SIAM. 1957 Mar; 5(1):32–28.
- 980 [18] SciPy v1.3.1, Linear Sum Assignment Documentation; Sep 27, 2019. The SciPy community. [https://docs.scipy.org/doc/scipy-1.3.1/reference/generated/scipy.optimize.linear\\_sum\\_assignment.html](https://docs.scipy.org/doc/scipy-1.3.1/reference/generated/scipy.optimize.linear_sum_assignment.html).
- 981 [19] Gunner MR, Murakami T, Rustenburg AS, Işık M, Chodera JD. Standard State Free Energies, Not pKas, Are Ideal for Describing Small  
982 Molecule Protonation and Tautomeric States. Journal of Computer-Aided Molecular Design. 2020 May; 34(5):561–573. doi: [10.1007/s10822-020-00280-7](https://doi.org/10.1007/s10822-020-00280-7).
- 983 [20] OpenEye pKa Prospector;. OpenEye Scientific Software, Santa Fe, NM. Accessed on Jan 23, 2018. <https://www.eyesopen.com/pka-prospector>.
- 984 [21] ACD/pKa GALAS (ACD/Percepta Kernel v1.6);. Advanced Chemistry Development, Inc., Toronto, ON, Canada, 2018. <https://www.acdlabs.com/products/percepta/predictors/pKa/>.
- 985 [22] ACD/pKa Classic (ACD/Percepta Kernel v1.6);. Advanced Chemistry Development, Inc., Toronto, ON, Canada, 2018. <https://www.acdlabs.com/products/percepta/predictors/pKa/>.
- 986 [23] Shelley JC, Cholleti A, Frye LL, Greenwood JR, Timlin MR, Uchimaya M. Epik: A Software Program for pK a Prediction and Protonation State  
987 Generation for Drug-like Molecules. Journal of Computer-Aided Molecular Design. 2007 Dec; 21(12):681–691. doi: [10.1007/s10822-007-9133-z](https://doi.org/10.1007/s10822-007-9133-z).
- 988 [24] Simulations Plus ADMET Predictor v8.5;. Simulations Plus, Lancaster, CA, 2018. <https://www.simulations-plus.com/software/admetpredictor/physicochemical-biopharmaceutical/>.
- 989 [25] Chemicalize v18.23 (ChemAxon MarvinSketch v18.23);. ChemAxon, Budapest, Hungary, 2018. <https://docs.chemaxon.com/display/docs/pKa+Plugin>.
- 990 [26] Milletti F, Storchi L, Sforza G, Cruciani G. New and Original p K a Prediction Method Using Grid Molecular Interaction Fields. Journal of  
991 Chemical Information and Modeling. 2007 Nov; 47(6):2172–2181. doi: [10.1021/ci700018y](https://doi.org/10.1021/ci700018y).
- 992 [27] MoKa;. Molecular Discovery, Hertfordshire, UK, 2018. <https://www.moldiscovery.com/software/moka/>.
- 993 [28] Zeng Q, Jones MR, Brooks BR. Absolute and Relative pKa Predictions via a DFT Approach Applied to the SAMPL6 Blind Challenge. Journal of  
994 Computer-Aided Molecular Design. 2018 Oct; 32(10):1179–1189. doi: [10.1007/s10822-018-0150-x](https://doi.org/10.1007/s10822-018-0150-x).
- 995 [29] Bochevarov AD, Harder E, Hughes TF, Greenwood JR, Braden DA, Philipp DM, Rinaldo D, Halls MD, Zhang J, Friesner RA. Jaguar: A High-  
996 Performance Quantum Chemistry Software Program with Strengths in Life and Materials Sciences. International Journal of Quantum  
997 Chemistry. 2013 Sep; 113(18):2110–2142. doi: [10.1002/qua.24481](https://doi.org/10.1002/qua.24481).
- 998 [30] Tielker N, Eberlein L, Güssregen S, Kast SM. The SAMPL6 Challenge on Predicting Aqueous pKa Values from EC-RISM Theory. Journal of  
999 Computer-Aided Molecular Design. 2018 Oct; 32(10):1151–1163. doi: [10.1007/s10822-018-0140-z](https://doi.org/10.1007/s10822-018-0140-z).

- 1007 [31] **Klamt A**, Eckert F, Diedenhofen M, Beck ME. First Principles Calculations of Aqueous  $pK_a$  Values for Organic and Inorganic Acids Using  
1008 COSMO-RS Reveal an Inconsistency in the Slope of the  $pK_a$  Scale. *The Journal of Physical Chemistry A*. 2003 Nov; 107(44):9380–9386. doi:  
1009 [10.1021/jp034688o](https://doi.org/10.1021/jp034688o).
- 1010 [32] **Eckert F**, Klamt A. Accurate Prediction of Basicity in Aqueous Solution with COSMO-RS. *Journal of Computational Chemistry*. 2006 Jan;  
1011 27(1):11–19. doi: [10.1002/jcc.20309](https://doi.org/10.1002/jcc.20309).
- 1012 [33] **Pracht P**, Wilcken R, Udvarhelyi A, Rodde S, Grimme S. High Accuracy Quantum-Chemistry-Based Calculation and Blind Prediction of  
1013 Macroscopic  $pK_a$  Values in the Context of the SAMPL6 Challenge. *Journal of Computer-Aided Molecular Design*. 2018 Oct; 32(10):1139–  
1014 1149. doi: [10.1007/s10822-018-0145-7](https://doi.org/10.1007/s10822-018-0145-7).
- 1015 [34] **Prasad S**, Huang J, Zeng Q, Brooks BR. An Explicit-Solvent Hybrid QM and MM Approach for Predicting  $pK_a$  of Small Molecules in SAMPL6  
1016 Challenge. *Journal of Computer-Aided Molecular Design*. 2018 Oct; 32(10):1191–1201. doi: [10.1007/s10822-018-0167-1](https://doi.org/10.1007/s10822-018-0167-1).
- 1017 [35] **Robert Fraczkiewicz MW**, SAMPL6  $pK_a$  Challenge: Predictions of ionization constants performed by the S+pKa method implemented in  
1018 ADMET Predictor software; February 22, 2018. The Joint D3R/SAMPL Workshop 2018. <https://drugdesigndata.org/about/d3r-2018-workshop>.
- 1019 [36] **Mansouri K**, Cariello NF, Korotcov A, Tkachenko V, Grulke CM, Sprankle CS, Allen D, Casey WM, Kleinstreuer NC, Williams AJ. Open-  
1020 Source QSAR Models for  $pK_a$  Prediction Using Multiple Machine Learning Approaches. *Journal of Cheminformatics*. 2019 Dec; 11(1). doi:  
1021 [10.1186/s13321-019-0384-1](https://doi.org/10.1186/s13321-019-0384-1).
- 1022 [37] **Baltruschat M**, Czodrowski P. Machine Learning Meets  $pK_a$  [Version 2; Peer Review: 2 Approved]. *F1000Research*. 2020; 9 (Chem Inf  
1023 Sci)(113). doi: [10.12688/f1000research.22090.2](https://doi.org/10.12688/f1000research.22090.2).
- 1024 [38] **Hunt P**, Hosseini-Gerami L, Chrien T, Plante J, Ponting DJ, Segall M. Predicting  $pK_a$  Using a Combination of Semi-Empirical Quan-  
1025 tum Mechanics and Radial Basis Function Methods. *Journal of Chemical Information and Modeling*. 2020 Jun; 60(6):2989–2997. doi:  
1026 [10.1021/acs.jcim.0c00105](https://doi.org/10.1021/acs.jcim.0c00105).
- 1027 [39] OEMolProp Toolkit 2017.Feb.1;. OpenEye Scientific Software, Santa Fe, NM. <http://www.eyesopen.com>.

**Table S1. SMILES and InChI identifiers of SAMPL6 pK<sub>a</sub> Challenge molecules.** A CSV version of this table can be found in *SAMPL6-supplementary-documents.tar.gz*.

SAMPL6 Molecule ID	Isomeric SMILES	InChI
SM01	c1cc2c(cc1O)c3c(o2)C(=O)NCCC3	InChI=1S/C12H11NO3/c14-7-3-4-10-9(6-7)8-2-1-5-13-12(15)11(8)16-10/h3-4,6,14H,1-2,5H2,(H,13,15)
SM02	c1ccc2c(c1)c(ncn2)Nc3cccc(c3)C(F)(F)	InChI=1S/C15H10F3N3/c16-15(17,18)10-4-3-5-11(8-10)21-14-12-6-1-2-7-13(12)19-9-20-14/h1-9H,(H,19,20,21)
SM03	c1ccc(cc1)Cc2nnnc(s2)NC(=O)c3cccs3	InChI=1S/C14H11N3OS2/c18-13(11-7-4-8-19-11)15-14-17-16-12(20-14)9-10-5-2-1-3-6-10/h1-8H,9H2,(H,15,17,18)
SM04	c1ccc2c(c1)c(ncn2)NCc3ccc(cc3)Cl	InChI=1S/C15H12ClN3/c16-12-7-5-11(6-8-12)9-17-15-13-3-1-2-4-14(13)18-10-19-15/h1-8,10H,9H2,(H,17,18,19)
SM05	c1ccc(c(c1)NC(=O)c2ccc(o2)Cl)N3CCCCC3	InChI=1S/C16H17ClN2O2/c17-15-9-8-14(21-15)16(20)18-12-6-2-3-7-13(12)19-10-4-1-5-11-19/h2-3,6-9H,1,4-5,10-11H2,(H,18,20)
SM06	c1cc2ccnc2c(c1)NC(=O)c3cc(cnc3)Br	InChI=1S/C15H10BrN3O/c16-12-7-11(8-17-9-12)15(20)19-13-5-1-3-10-4-2-6-18-14(10)13/h1-9H,(H,19,20)
SM07	c1ccc(cc1)CNc2c3cccc3ncn2	InChI=1S/C15H13N3/c1-2-6-12(7-3-1)10-16-15-13-8-4-5-9-14(13)17-11-18-15/h1-9,11H,10H2,(H,16,17,18)
SM08	Cc1ccc2c(c1)c(c(c=O)[nH]2)CC(=O)O)c3cccc3	InChI=1S/C18H15NO3/c1-11-7-8-15-13(9-11)17(12-5-3-2-4-6-12)14(10-16(20)21)18(22)19-15/h2-9H,10H2,1H3,(H,19,22)(H,20,21)
SM09	COc1cccc(c1)Nc2c3cccc3ncn2.Cl	InChI=1S/C15H13N3O.CIH/c1-19-12-6-4-5-11(9-12)18-15-13-7-2-3-8-14(13)16-10-17-15;/h2-10H,1H3,(H,16,17,18);1H
SM10	c1ccc(cc1)C(=O)NCC(=O)Nc2nc3cccc3s2	InChI=1S/C16H13N3O2S/c20-14(10-17-15(21)11-6-2-1-3-7-11)19-16-18-2-8-4-5-9-13(12)22-16/h1-9H,10H2,(H,17,21)(H,18,19,20)
SM11	c1ccc(cc1)n2c3c(cn2)c(ncn3)N	InChI=1S/C11H9N5/c12-10-9-6-15-16(11(9)14-7-13-10)8-4-2-1-3-5-8/h1-7H,(H,2,12,13,14)
SM12	c1ccc2c(c1)c(ncn2)Nc3cccc(c3)Cl.Cl	InChI=1S/C14H10ClN3.CIH/c15-10-4-3-5-11(8-10)18-14-12-6-1-2-7-13(12)16-9-17-14;/h1-9H,(H,16,17,18);1H
SM13	Cc1cccc(c1)Nc2c3cc(c(c3ncn2)OC)OC	InChI=1S/C17H17N3O2/c1-11-5-4-6-12(7-11)20-17-13-8-15(21-2)16(22-3)9-14(13)18-10-19-17/h4-10H,1-3H3,(H,18,19,20)
SM14	c1ccc(cc1)n2ncn3c2ccc(c3)N	InChI=1S/C13H11N3/c14-10-6-7-13-12(8-10)15-9-16(13)11-4-2-1-3-5-11/h1-9H,14H2
SM15	c1ccc2c(c1)ncn2c3ccc(cc3)O	InChI=1S/C13H10N2O/c16-11-7-5-10(6-8-11)15-9-14-12-3-1-2-4-13(12)15/h1-9,16H
SM16	c1cc(c(c(c1)Cl)C(=O)Nc2ccncc2)Cl	InChI=1S/C12H8Cl2N2O/c13-9-2-1-3-10(14)11(9)12(17)16-8-4-6-15-7-5-8/h1-7H,(H,15,16,17)
SM17	c1ccc(cc1)CSc2nnc(o2)c3ccncc3	InChI=1S/C14H11N3OS/c1-2-4-11(5-3-1)10-19-14-17-16-13(18-14)12-6-8-15-9-7-12/h1-9H,10H2
SM18	c1ccc2c(c1)c(=O)[nH]c(n2)CCC(=O)Nc3ncc(s3)Cc4ccc(c(c4)F)F	InChI=1S/C21H16F2N4O2S/c22-15-6-5-12(10-16(15)23)9-13-11-24-21(30-13)27-19(28)8-7-18-25-17-4-2-1-3-14(17)20(29)26-18/h1-6,10-11H,7-9H2,(H,24,27,28)(H,25,26,29)
SM19	CCOc1ccc2c(c1)sc(n2)NC(=O)Cc3ccc(c(c3)Cl)Cl	InChI=1S/C17H14Cl2N2O2S/c1-2-23-11-4-6-14-15(9-11)24-17(20-14)21-6(22)8-10-3-5-12(18)13(9)7-10/h3-7,9H,2,8H2,1H3,(H,20,21,22)
SM20	c1cc(cc(c1)OCc2ccc(cc2Cl)Cl)/C=C/3\C(=O)NC(=O)S3	InChI=1S/C17H11Cl2NO3S/c18-12-5-4-11(14(19)8-12)9-23-13-3-1-2-10(6-13)7-15-16(21)20-17(22)24-15/h1-8H,9H2,(H,20,21,22)/b15-7+
SM21	c1cc(cc(c1)Br)Nc2c(cnc(n2)Nc3cccc(c3)Br)F	InChI=1S/C16H11Br2FN4/c17-10-3-1-5-12(7-10)21-15-14(19)9-20-16(23-15)22-13-6-2-4-11(18)8-13/h1-9H,(H,20,21,22,23)
SM22	c1cc2c(cc(c(c2nc1)O))l	InChI=1S/C9H5l2NO/c10-6-4-7(11)9(13)8-5(6)2-1-3-12-8/h1-4,13H
SM23	CCOC(=O)c1ccc(cc1)Nc2cc(cnc(n2)Nc3ccc(cc3)C(=O)OCC)C	InChI=1S/C23H24N4O4/c1-4-30-21(28)16-6-10-18(11-7-16)25-20-14-15(3)24-23(27-20)26-19-12-8-17(9-13-19)22(29)31-5-2/h6-14H,4-5H2,1-3H3,(H2,24,25,26,27)
SM24	COc1ccc(cc1)c2c3c(ncn3oc2c4ccc(cc4)OC)NCCO	InChI=1S/C22H21N3O4/c1-27-16-7-3-14(4-8-16)18-19-21(23-11-12-26)24-13-25-22(19)29-20(18)15-5-9-17(28-2)10-6-15/h3-10,13,26H,11-12H2,1-2H3,(H,23,24,25)

Microstate ID of Deprotonated State (A)	Microstate ID of Protonated State (HA)	Molecule ID	pKa (exp)	pKa SEM (exp)	pKa ID	Microstate identification source
		SM07	6.08	0.01	SM07_pKa1	NMR measurement
		SM14	5.3	0.01	SM14_pKa2	NMR measurement
		SM14	2.58	0.01	SM14_pKa1	NMR measurement
		SM02	5.03	0.01	SM02_pKa1	Estimated based on SM07 NMR measurement
		SM04	6.02	0.01	SM04_pKa1	Estimated based on SM07 NMR measurement
		SM09	5.37	0.01	SM09_pKa1	Estimated based on SM07 NMR measurement
		SM12	5.28	0.01	SM12_pKa1	Estimated based on SM07 NMR measurement
		SM13	5.77	0.01	SM13_pKa1	Estimated based on SM07 NMR measurement
		SM15	8.94	0.01	SM15_pKa2	Estimated based on SM14 NMR measurement
		SM15	4.7	0.01	SM15_pKa1	Estimated based on SM14 NMR measurement

**Figure S1. Dominant microstates of 8 molecules were determined based on NMR measurements.** Dominant microstate sequence of 6 derivatives were determined taking SM07 and SM14 as reference. Matched experimental pK<sub>a</sub> values were determined by spectrophotometric pK<sub>a</sub> measurements [7]. A CSV version of this table can be found in SAMPL6-supplementary-documents.tar.gz.

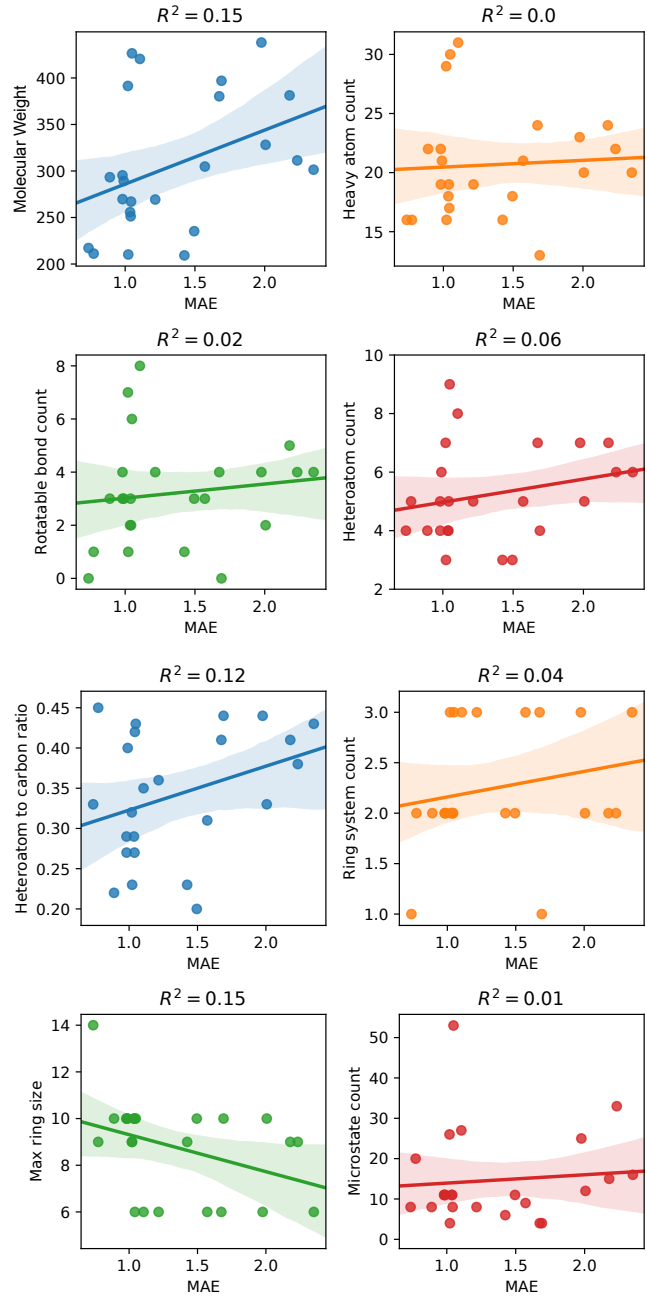


**Figure S2. MAE of macroscopic  $pK_a$  predictions of each molecule did not show any significant correlation with any molecular descriptor.**  
 Plots show regression lines, 96% confidence intervals of the regression lines, and  $R_2$ . The following molecular descriptors were calculated using OpenEye OEMolProp Toolkit [39].

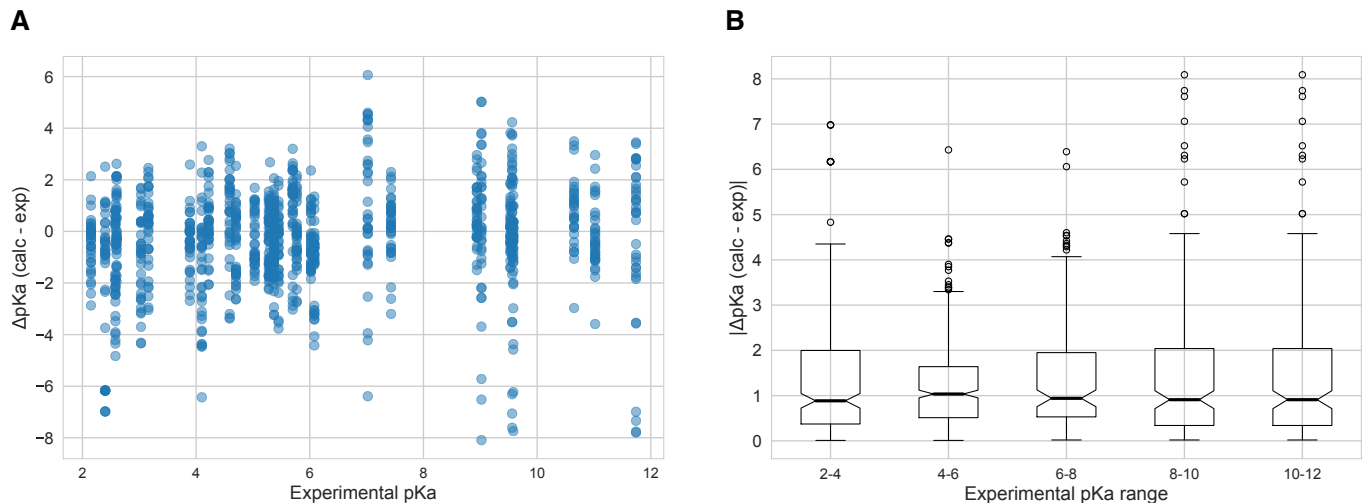


**Figure S3. The value of macroscopic  $pK_a$ s was not a factor affecting prediction error seen in SAMPL6 Challenge according to the analysis with Hungarian matching.** There was not clear trend between  $pK_a$  prediction error and the true  $pK_a$  error. Very high and very low  $pK_a$  values have similar inaccuracy compared to  $pK_a$  values close to 7. **A** Scatter plot of macroscopic  $pK_a$  prediction error calculated with Hungarian matching vs. experimental  $pK_a$  value **B** Box plot of absolute error of macroscopic  $pK_a$  predictions binned into 2  $pK_a$  unit intervals of experimental  $pK_a$ .

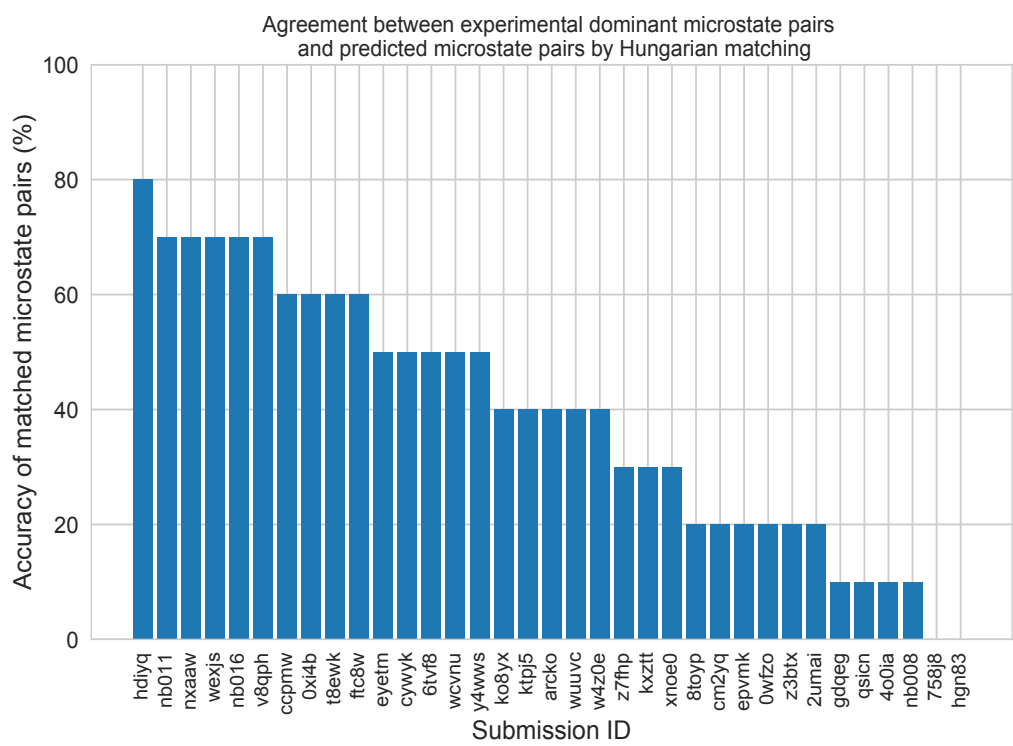


**Figure S4. There was low agreement between experimental dominant microstate pairs and the predicted microstate pairs selected by Hungarian algorithm for microscopic  $pK_a$  predictions.** This analysis could only be performed for 8 molecules with NMR data. Hungarian matching algorithm which matches predicted and experimental values considering only the closeness of the numerical value of  $pK_a$  and it often leads to predicted  $pK_a$  matches that described a different microstates pair than the experimentally observed dominant microstates..

**Table S2. Evaluation statistics calculated for all macroscopic pK<sub>a</sub> prediction submissions based on Hungarian match for 24 molecules.** Methods are represented via their SAMPL6 submission IDs which can be cross referenced with Table 1 for method details. There are eight error metrics reported: the root-mean-squared error (RMSE), mean absolute error (MAE), mean (signed) error (ME), coefficient of determination ( $R^2$ ), linear regression slope (m), Kendall's Rank Correlation Coefficient ( $\tau$ ), unmatched experimental pK<sub>a</sub>s (number of missing pK<sub>a</sub> predictions) and unmatched predicted pK<sub>a</sub>s (number of extra pK<sub>a</sub> predictions between 2 and 12. This table is ranked by increasing RMSE. A CSV version of this table can be found in *SAMPL6-supplementary-documents.tar.gz*.

Submission ID	RMSE	MAE	ME	R <sup>2</sup>	m	Kendall's Tau	Unmatched exp. pK <sub>a</sub> s	Unmatched pred. pK <sub>a</sub> s [2,12]
<i>xvxzd</i>	0.68 [0.54, 0.81]	0.58 [0.45, 0.71]	0.24 [-0.01, 0.45]	0.94 [0.88, 0.97]	0.92 [0.84, 1.02]	0.82 [0.68, 0.92]	2	4
<i>gyuhx</i>	0.73 [0.55, 0.91]	0.59 [0.44, 0.74]	0.03 [-0.23, 0.28]	0.93 [0.88, 0.96]	0.98 [0.90, 1.08]	0.88 [0.80, 0.94]	0	7
<i>xmyhm</i>	0.79 [0.52, 1.03]	0.56 [0.38, 0.77]	0.13 [-0.14, 0.41]	0.92 [0.85, 0.97]	0.96 [0.86, 1.08]	0.81 [0.68, 0.90]	0	3
<i>nb017</i>	0.94 [0.72, 1.16]	0.77 [0.58, 0.97]	-0.16 [-0.49, 0.16]	0.88 [0.81, 0.94]	0.94 [0.82, 1.08]	0.73 [0.60, 0.84]	0	6
<i>nb007</i>	0.95 [0.73, 1.15]	0.78 [0.60, 0.97]	0.05 [-0.29, 0.37]	0.88 [0.77, 0.95]	0.84 [0.77, 0.92]	0.79 [0.65, 0.89]	0	13
<i>yqkga</i>	1.01 [0.78, 1.23]	0.80 [0.59, 1.03]	-0.17 [-0.51, 0.19]	0.87 [0.78, 0.93]	0.93 [0.77, 1.08]	0.83 [0.72, 0.91]	0	1
<i>nb010</i>	1.03 [0.77, 1.26]	0.81 [0.61, 1.04]	0.24 [-0.11, 0.59]	0.87 [0.77, 0.94]	0.95 [0.83, 1.08]	0.80 [0.67, 0.90]	0	4
<i>8xt50</i>	1.07 [0.78, 1.36]	0.81 [0.58, 1.07]	-0.47 [-0.82, -0.14]	0.91 [0.84, 0.95]	1.08 [0.94, 1.22]	0.80 [0.68, 0.89]	0	0
<i>nb013</i>	1.10 [0.72, 1.47]	0.80 [0.56, 1.09]	-0.15 [-0.55, 0.22]	0.88 [0.78, 0.95]	1.09 [0.90, 1.25]	0.79 [0.64, 0.90]	0	6
<i>nb015</i>	1.27 [0.98, 1.56]	1.04 [0.80, 1.31]	0.13 [-0.32, 0.56]	0.87 [0.80, 0.93]	1.16 [0.94, 1.34]	0.78 [0.66, 0.86]	0	0
<i>p0jba</i>	1.31 [0.69, 1.73]	1.08 [0.43, 1.72]	-0.92 [-1.72, -0.11]	0.91 [0.51, 1.00]	1.18 [0.36, 1.72]	0.80 [0.00, 1.00]	0	0
<i>37xm8</i>	1.41 [0.93, 1.84]	1.01 [0.68, 1.38]	-0.18 [-0.69, 0.32]	0.83 [0.70, 0.93]	1.16 [0.98, 1.33]	0.70 [0.56, 0.83]	1	1
<i>mkhqa</i>	1.60 [1.13, 2.05]	1.24 [0.90, 1.62]	-0.32 [-0.89, 0.21]	0.80 [0.67, 0.91]	1.14 [0.98, 1.34]	0.64 [0.44, 0.79]	0	6
<i>ttjd0</i>	1.64 [1.20, 2.06]	1.30 [0.96, 1.67]	-0.12 [-0.70, 0.45]	0.81 [0.69, 0.91]	1.2 [1.03, 1.40]	0.65 [0.47, 0.80]	0	5
<i>nb001</i>	1.68 [1.05, 2.37]	1.21 [0.84, 1.68]	0.44 [-0.10, 1.03]	0.80 [0.70, 0.90]	1.16 [0.95, 1.42]	0.72 [0.55, 0.85]	0	7
<i>nb002</i>	1.70 [1.08, 2.38]	1.25 [0.89, 1.70]	0.51 [-0.04, 1.10]	0.80 [0.70, 0.90]	1.15 [0.95, 1.42]	0.72 [0.56, 0.84]	0	7
<i>35bdm</i>	1.72 [0.66, 2.34]	1.44 [0.62, 2.26]	-1.01 [-2.18, 0.13]	0.92 [0.46, 1.00]	1.45 [0.73, 2.15]	0.80 [0.00, 1.00]	0	0
<i>ryzue</i>	1.77 [1.42, 2.12]	1.50 [1.17, 1.84]	1.30 [0.86, 1.72]	0.91 [0.86, 0.95]	1.23 [1.06, 1.41]	0.82 [0.71, 0.91]	0	0
<i>2ii2g</i>	1.80 [1.31, 2.24]	1.39 [1.01, 1.82]	-0.74 [-1.29, -0.15]	0.79 [0.65, 0.89]	1.15 [0.96, 1.37]	0.68 [0.59, 0.82]	0	2
<i>mpwiy</i>	1.82 [1.39, 2.23]	1.48 [1.14, 1.88]	0.10 [-0.54, 0.73]	0.82 [0.70, 0.91]	1.29 [1.12, 1.51]	0.66 [0.49, 0.80]	0	5
<i>5byn6</i>	1.89 [1.50, 2.27]	1.59 [1.24, 1.97]	1.32 [0.84, 1.80]	0.91 [0.85, 0.95]	1.28 [1.10, 1.48]	0.83 [0.72, 0.92]	0	0
<i>y75vj</i>	1.90 [1.50, 2.26]	1.58 [1.21, 1.97]	1.04 [0.46, 1.60]	0.89 [0.79, 0.95]	1.34 [1.16, 1.53]	0.75 [0.57, 0.88]	1	0
<i>w4iyd</i>	1.93 [1.53, 2.28]	1.58 [1.20, 1.98]	1.26 [0.72, 1.76]	0.85 [0.74, 0.92]	1.21 [1.00, 1.40]	0.73 [0.57, 0.85]	0	1
<i>np6b4</i>	1.94 [1.21, 2.71]	1.44 [1.04, 1.94]	-0.47 [-1.08, 0.24]	0.71 [0.60, 0.87]	1.08 [0.81, 1.43]	0.75 [0.62, 0.86]	0	8
<i>nb004</i>	2.01 [1.38, 2.63]	1.57 [1.16, 2.04]	0.56 [-0.10, 1.27]	0.82 [0.72, 0.90]	1.35 [1.15, 1.60]	0.71 [0.54, 0.84]	0	5
<i>nb003</i>	2.01 [1.39, 2.64]	1.58 [1.18, 2.04]	0.52 [-0.14, 1.22]	0.82 [0.73, 0.91]	1.36 [1.16, 1.61]	0.71 [0.54, 0.84]	0	5
<i>yc70m</i>	2.03 [1.73, 2.33]	1.80 [1.48, 2.13]	-0.41 [-1.09, 0.31]	0.47 [0.28, 0.64]	0.56 [0.35, 0.83]	0.53 [0.35, 0.68]	0	27
<i>hytjn</i>	2.16 [1.24, 3.06]	1.39 [0.86, 2.04]	0.71 [0.03, 1.48]	0.45 [0.13, 0.78]	0.62 [0.26, 1.00]	0.47 [0.16, 0.73]	1	27
<i>f0gew</i>	2.18 [1.38, 2.95]	1.58 [1.09, 2.16]	-0.73 [-1.42, 0.04]	0.77 [0.67, 0.89]	1.29 [1.01, 1.63]	0.76 [0.63, 0.86]	0	0
<i>q3pfp</i>	2.19 [1.33, 3.09]	1.51 [0.99, 2.13]	0.59 [-0.10, 1.37]	0.44 [0.13, 0.77]	0.66 [0.27, 1.07]	0.50 [0.20, 0.75]	1	22
<i>ds62k</i>	2.22 [1.62, 2.81]	1.78 [1.34, 2.27]	0.78 [0.06, 1.52]	0.82 [0.70, 0.90]	1.41 [1.20, 1.63]	0.72 [0.55, 0.85]	0	4
<i>xikp8</i>	2.35 [1.94, 2.73]	2.06 [1.66, 2.47]	0.77 [-0.02, 1.58]	0.89 [0.80, 0.95]	1.59 [1.40, 1.81]	0.76 [0.59, 0.89]	1	0
<i>nb005</i>	2.38 [1.79, 2.95]	1.91 [1.44, 2.43]	0.31 [-0.49, 1.15]	0.84 [0.74, 0.91]	1.56 [1.34, 1.82]	0.71 [0.54, 0.83]	0	0
<i>5nm4j</i>	2.45 [1.42, 3.34]	1.58 [0.94, 2.34]	0.05 [-0.80, 1.07]	0.19 [0.00, 0.70]	0.40 [-0.06, 0.81]	0.34 [-0.04, 0.67]	4	1
<i>ad5pu</i>	2.54 [1.68, 3.30]	1.83 [1.24, 2.49]	-0.65 [-1.48, 0.25]	0.76 [0.64, 0.88]	1.43 [1.12, 1.78]	0.77 [0.63, 0.88]	0	0
<i>pwn3m</i>	2.60 [1.45, 3.53]	1.54 [0.83, 2.37]	0.79 [-0.06, 1.77]	0.21 [0.00, 0.63]	0.37 [0.01, 0.78]	0.34 [0.04, 0.63]	1	3
<i>nb006</i>	2.98 [2.37, 3.56]	2.53 [2.00, 3.10]	0.42 [-0.60, 1.47]	0.84 [0.74, 0.92]	1.78 [1.55, 2.06]	0.71 [0.54, 0.84]	0	0
<i>0hxtm</i>	3.26 [1.81, 4.39]	1.92 [1.03, 2.98]	1.38 [0.37, 2.56]	0.08 [0.00, 0.48]	0.28 [-0.17, 0.83]	0.29 [-0.04, 0.61]	3	7

**Table S3. Evaluation statistics calculated for all microscopic pK<sub>a</sub> prediction submissions based on Hungarian match for 8 molecules with NMR data.** Methods are represented via their SAMPL6 submission IDs which can be cross referenced with Table 1 for method details. There are eight error metrics reported: the root-mean-squared error (RMSE), mean absolute error (MAE), mean (signed) error (ME), coefficient of determination ( $R^2$ ), linear regression slope (m), Kendall's Rank Correlation Coefficient ( $\tau$ ), unmatched experimental pK<sub>a</sub>s (number of missing pK<sub>a</sub> predictions) and unmatched predicted pK<sub>a</sub>s (number of extra pK<sub>a</sub> predictions between 2 and 12. This table is ranked by increasing RMSE. A CSV version of this table can be found in *SAMPL6-supplementary-documents.tar.gz*.

Submission ID	RMSE	MAE	ME	R <sup>2</sup>	m	Kendall's Tau	Unmatched exp. pK <sub>a</sub> s	Unmatched pred. pK <sub>a</sub> s [2,12]
nb011	0.47 [0.30, 0.64]	0.33 [0.22, 0.46]	-0.02 [-0.18, 0.14]	0.97 [0.94, 0.99]	1.01 [0.97, 1.06]	0.90 [0.78, 0.96]	0	36
hdlyq	0.62 [0.47, 0.76]	0.47 [0.33, 0.62]	0.13 [-0.09, 0.34]	0.95 [0.92, 0.97]	0.34 [0.92, 1.09]	0.87 [0.79, 0.93]	0	16
epvmk	0.63 [0.43, 0.81]	0.47 [0.32, 0.63]	-0.02 [-0.25, 0.21]	0.95 [0.89, 0.98]	0.21 [0.91, 1.04]	0.81 [0.68, 0.91]	0	37
xnoe0	0.65 [0.47, 0.82]	0.50 [0.36, 0.66]	-0.1 [-0.32, 0.13]	0.95 [0.89, 0.98]	0.13 [0.92, 1.05]	0.82 [0.69, 0.91]	0	36
gdqeg	0.65 [0.41, 0.89]	0.43 [0.27, 0.62]	0.11 [-0.10, 0.35]	0.94 [0.88, 0.98]	0.35 [0.87, 1.02]	0.83 [0.67, 0.95]	0	53
400ia	0.66 [0.44, 0.86]	0.47 [0.31, 0.64]	0.00 [-0.22, 0.24]	0.94 [0.88, 0.98]	0.24 [0.87, 1.05]	0.85 [0.73, 0.94]	0	35
nb008	0.76 [0.48, 1.02]	0.52 [0.34, 0.73]	-0.08 [-0.37, 0.17]	0.93 [0.85, 0.98]	0.17 [0.79, 0.93]	0.84 [0.73, 0.92]	0	35
ccpmw	0.79 [0.62, 0.94]	0.62 [0.46, 0.80]	-0.17 [-0.44, 0.11]	0.92 [0.86, 0.96]	0.11 [0.82, 1.05]	0.80 [0.67, 0.89]	0	7
0xi4b	0.84 [0.58, 1.07]	0.61 [0.42, 0.83]	0.22 [-0.07, 0.51]	0.92 [0.84, 0.97]	0.51 [0.91, 1.09]	0.81 [0.65, 0.92]	0	32
cwyk	0.86 [0.60, 1.10]	0.62 [0.42, 0.84]	0.13 [-0.16, 0.44]	0.90 [0.82, 0.96]	0.44 [0.86, 1.08]	0.81 [0.64, 0.92]	0	35
ftc8w	0.86 [0.51, 1.17]	0.59 [0.39, 0.83]	0.10 [-0.19, 0.41]	0.90 [0.77, 0.97]	0.41 [0.84, 0.98]	0.75 [0.57, 0.88]	0	35
nxaaw	0.89 [0.56, 1.25]	0.61 [0.41, 0.87]	-0.02 [-0.35, 0.28]	0.89 [0.75, 0.97]	0.28 [0.85, 1.00]	0.79 [0.63, 0.91]	0	29
nb016	0.95 [0.71, 1.18]	0.77 [0.57, 0.98]	-0.23 [-0.56, 0.12]	0.89 [0.83, 0.95]	0.12 [0.82, 1.07]	0.75 [0.62, 0.85]	0	3
kxzt	0.96 [0.56, 1.33]	0.64 [0.41, 0.92]	0.00 [-0.32, 0.36]	0.90 [0.76, 0.97]	0.36 [0.96, 1.13]	0.79 [0.63, 0.91]	0	37
eyetm	0.98 [0.69, 1.27]	0.72 [0.50, 0.97]	-0.32 [-0.65, 0.00]	0.91 [0.86, 0.96]	0.00 [0.94, 1.22]	0.78 [0.64, 0.88]	0	7
cm2yq	0.99 [0.44, 1.54]	0.56 [0.31, 0.90]	0.10 [-0.21, 0.50]	0.91 [0.83, 0.98]	0.50 [0.96, 1.25]	0.89 [0.80, 0.96]	0	36
2umai	1.00 [0.46, 1.54]	0.57 [0.33, 0.91]	0.07 [-0.25, 0.46]	0.91 [0.82, 0.98]	0.46 [0.96, 1.26]	0.87 [0.76, 0.95]	0	36
ko8yx	1.01 [0.76, 1.25]	0.78 [0.56, 1.01]	0.35 [0.01, 0.67]	0.91 [0.82, 0.96]	0.67 [0.96, 1.19]	0.78 [0.64, 0.89]	0	26
wuuvc	1.02 [0.51, 1.53]	0.62 [0.38, 0.93]	0.19 [-0.13, 0.58]	0.88 [0.80, 0.96]	0.58 [0.85, 1.19]	0.90 [0.81, 0.96]	0	36
ktpj5	1.02 [0.51, 1.56]	0.61 [0.37, 0.95]	0.17 [-0.16, 0.57]	0.88 [0.80, 0.96]	0.57 [0.87, 1.22]	0.89 [0.80, 0.96]	0	36
z7fhp	1.02 [0.49, 1.55]	0.61 [0.36, 0.94]	0.08 [-0.24, 0.48]	0.90 [0.82, 0.97]	0.48 [0.97, 1.26]	0.88 [0.80, 0.95]	0	28
arcko	1.04 [0.73, 1.32]	0.77 [0.53, 1.02]	0.37 [0.05, 0.72]	0.89 [0.80, 0.94]	0.72 [0.90, 1.14]	0.78 [0.62, 0.90]	0	24
y4wws	1.04 [0.70, 1.33]	0.74 [0.49, 1.00]	-0.31 [-0.66, 0.05]	0.91 [0.85, 0.96]	0.05 [1.02, 1.26]	0.79 [0.68, 0.88]	0	30
wcvnu	1.11 [0.80, 1.39]	0.84 [0.59, 1.11]	0.28 [-0.10, 0.66]	0.89 [0.77, 0.95]	0.66 [0.98, 1.22]	0.73 [0.54, 0.88]	1	27
8toyp	1.13 [0.61, 1.65]	0.70 [0.42, 1.05]	0.13 [-0.25, 0.56]	0.88 [0.81, 0.96]	0.56 [0.98, 1.29]	0.83 [0.72, 0.92]	0	27
qsicn	1.17 [0.30, 1.65]	0.88 [0.23, 1.54]	-0.76 [-1.54, 0.01]	0.91 [0.46, 1.00]	0.01 [0.52, 1.59]	0.80 [0.00, 1.00]	0	2
wexjs	1.30 [0.95, 1.62]	0.98 [0.68, 1.29]	0.27 [-0.17, 0.74]	0.86 [0.74, 0.93]	0.74 [1.00, 1.29]	0.73 [0.55, 0.86]	0	25
v8qph	1.37 [0.92, 1.79]	0.98 [0.66, 1.34]	-0.15 [-0.64, 0.34]	0.84 [0.70, 0.93]	0.34 [0.97, 1.32]	0.70 [0.55, 0.82]	0	6
w420e	1.57 [1.18, 1.94]	1.23 [0.90, 1.58]	0.09 [-0.48, 0.62]	0.85 [0.76, 0.91]	0.62 [1.08, 1.46]	0.72 [0.60, 0.82]	0	19
6tvf8	1.88 [0.87, 2.85]	1.02 [0.54, 1.66]	0.45 [-0.14, 1.18]	0.51 [0.16, 0.87]	1.18 [0.26, 0.89]	0.61 [0.34, 0.82]	0	55
0wfzo	2.89 [1.73, 3.89]	1.88 [1.17, 2.68]	0.76 [-0.15, 1.77]	0.48 [0.21, 0.75]	1.77 [0.60, 1.37]	0.51 [0.30, 0.70]	0	4
t8ewk	3.30 [1.89, 4.39]	1.98 [1.06, 3.00]	1.32 [0.27, 2.49]	0.07 [0.00, 0.45]	2.49 [-0.17, 0.79]	0.28 [-0.03, 0.6]	0	6
z3btx	4.00 [2.30, 5.45]	2.49 [1.47, 3.65]	1.48 [0.26, 2.86]	0.29 [0.04, 0.60]	2.86 [0.31, 1.44]	0.43 [0.19, 0.63]	0	1
758j8	4.52 [2.64, 6.18]	2.95 [1.85, 4.25]	1.85 [0.48, 3.38]	0.24 [0.02, 0.58]	3.38 [0.20, 1.51]	0.34 [0.08, 0.57]	0	2
hgn83	6.38 [4.04, 8.47]	4.11 [2.52, 5.93]	2.13 [0.07, 4.28]	0.08 [0.00, 0.39]	4.28 [-0.18, 1.43]	0.32 [0.07, 0.56]	0	0

**Table S4. Evaluation statistics calculated for all microscopic pK<sub>a</sub> prediction submissions based on microstate pair match for 8 molecules with NMR data.** Methods are represented via their SAMPL6 submission IDs which can be cross referenced with Table 1 for method details. There are eight error metrics reported: the root-mean-squared error (RMSE), mean absolute error (MAE), mean (signed) error (ME), coefficient of determination ( $R^2$ ), linear regression slope (m), Kendall's Rank Correlation Coefficient ( $\tau$ ), unmatched experimental pK<sub>a</sub>s (number of missing pK<sub>a</sub> predictions) and unmatched predicted pK<sub>a</sub>s (number of extra pK<sub>a</sub> predictions between 2 and 12. This table is ranked by increasing RMSE. A CSV version of this table can be found in *SAMPL6-supplementary-documents.tar.gz*.

Update this table with dominant microstate accuracy

Submission ID	RMSE	MAE	ME	$R^2$	m	Kendall's Tau	Unmatched exp. pK <sub>a</sub> s	Unmatched pred. pK <sub>a</sub> s [2,12]
nb016	0.52 [0.25, 0.71]	0.43 [0.23, 0.65]	-0.09 [-0.45, 0.30]	0.92 [0.05, 0.99]	0.99 [0.14, 1.16]	0.62 [-0.14, 1.00]	0	3
hdlyq	0.68 [0.49, 0.83]	0.60 [0.39, 0.80]	0.38 [0.02, 0.70]	0.86 [0.47, 0.98]	0.91 [0.45, 1.26]	0.78 [0.4, 1.00]	0	16
nb011	0.72 [0.35, 1.07]	0.54 [0.28, 0.86]	0.45 [0.14, 0.83]	0.86 [0.18, 0.98]	0.93 [0.50, 1.21]	0.64 [0.26, 0.95]	0	36
ftc8w	0.75 [0.52, 0.96]	0.68 [0.50, 0.89]	-0.31 [-0.68, 0.16]	0.87 [0.02, 0.99]	1.12 [-0.11, 1.39]	0.56 [-0.10, 1.00]	0	35
6tvf8	0.76 [0.55, 0.95]	0.68 [0.46, 0.90]	-0.63 [-0.89, -0.35]	0.92 [0.78, 0.99]	0.94 [0.69, 1.41]	0.87 [0.6, 1.00]	0	55
t8ewk	0.96 [0.65, 1.19]	0.81 [0.46, 1.13]	-0.77 [-1.12, -0.38]	0.80 [0.53, 0.96]	0.96 [0.76, 2.26]	0.78 [0.31, 1.00]	1	7
v8qph	0.99 [0.40, 1.52]	0.67 [0.29, 1.17]	-0.09 [-0.75, 0.45]	0.68 [0.11, 0.97]	0.96 [-1.26, 1.16]	0.38 [-0.3, 1.00]	0	6
ccpmw	1.07 [0.78, 1.27]	0.95 [0.60, 1.25]	-0.83 [-1.25, -0.37]	0.74 [0.43, 0.99]	0.95 [0.70, 2.32]	0.89 [0.52, 1.00]	1	8
0xi4b	1.15 [0.75, 1.50]	0.98 [0.63, 1.36]	-0.30 [-0.94, 0.44]	0.77 [0.02, 0.98]	1.26 [0.09, 2.10]	0.51 [-0.14, 1.00]	0	33
cywyk	1.17 [0.88, 1.41]	1.06 [0.74, 1.35]	-0.47 [-1.09, 0.24]	0.73 [0.02, 0.98]	1.15 [-0.04, 2.00]	0.56 [-0.08, 1.00]	0	36
eyetm	1.17 [0.77, 1.52]	1.00 [0.61, 1.41]	-0.89 [-1.38, -0.38]	0.67 [0.30, 0.94]	0.93 [0.65, 2.59]	0.72 [0.29, 1.00]	1	8
nb008	1.26 [0.74, 1.71]	1.09 [0.63, 1.57]	0.47 [-0.40, 1.32]	0.79 [0.01, 0.99]	1.21 [-0.59, 1.85]	0.52 [-0.2, 1.00]	0	38
y4wws	1.41 [0.95, 1.80]	1.22 [0.78, 1.66]	-0.71 [-1.44, 0.06]	0.87 [0.05, 0.98]	1.55 [0.41, 2.02]	0.56 [-0.11, 1.00]	0	31
ktpj5	1.46 [0.83, 2.10]	1.15 [0.67, 1.77]	0.94 [0.29, 1.68]	0.77 [0.01, 0.98]	1.28 [-0.26, 1.60]	0.42 [-0.27, 0.95]	0	37
wuuvc	1.47 [0.84, 2.09]	1.18 [0.70, 1.77]	0.99 [0.36, 1.68]	0.78 [0.01, 0.98]	1.27 [-0.24, 1.58]	0.47 [-0.20, 1.00]	0	37
xnoe0	1.54 [1.09, 2.00]	1.39 [1.02, 1.83]	0.91 [0.11, 1.64]	0.82 [0.01, 0.98]	1.47 [-0.30, 1.79]	0.42 [-0.27, 0.95]	0	37
qsicn	1.58 [1.44, 1.70]	1.57 [1.44, 1.70]	-1.57 [-1.7, -1.44]	1.00 [0.00, 1.00]	1.06		0	2
epvmk	1.66 [1.20, 2.15]	1.50 [1.07, 1.96]	1.12 [0.31, 1.82]	0.82 [0.02, 0.98]	1.47 [-0.21, 1.8]	0.42 [-0.25, 0.95]	0	37
400ia	1.73 [1.33, 2.17]	1.62 [1.29, 2.02]	1.31 [0.53, 1.93]	0.87 [0.03, 0.99]	1.50 [0.07, 1.84]	0.56 [-0.07, 1.00]	0	36
ko8yx	1.75 [1.08, 2.45]	1.44 [0.87, 2.12]	1.38 [0.74, 2.10]	0.97 [0.88, 1.00]	1.66 [1.46, 2.28]	0.91 [0.69, 1.00]	0	27
2umai	1.76 [1.21, 2.35]	1.54 [1.04, 2.11]	1.31 [0.55, 2.03]	0.82 [0.02, 0.98]	1.43 [-0.02, 1.77]	0.47 [-0.17, 0.95]	0	37
cm2yq	1.77 [1.22, 2.36]	1.55 [1.06, 2.12]	1.33 [0.57, 2.04]	0.82 [0.02, 0.98]	1.43 [-0.02, 1.76]	0.47 [-0.17, 0.95]	0	37
nxaaw	1.80 [0.84, 2.80]	1.34 [0.80, 2.18]	0.16 [-0.77, 1.41]	0.59 [0.02, 0.97]	1.37 [-0.08, 2.92]	0.6 [-0.05, 1.00]	0	30
wcvnu	1.90 [1.14, 2.64]	1.57 [0.97, 2.27]	1.44 [0.70, 2.24]	0.97 [0.91, 1.00]	1.78 [1.58, 2.48]	0.91 [0.69, 1.00]	0	27
kxzt	2.00 [1.13, 2.73]	1.64 [1.00, 2.39]	1.64 [1.00, 2.39]	0.83 [0.01, 0.98]	1.42 [-0.21, 1.99]	0.56 [-0.10, 1.00]	0	38
wexjs	2.05 [1.18, 2.93]	1.66 [1.01, 2.47]	1.48 [0.63, 2.39]	0.96 [0.55, 0.99]	1.87 [1.54, 2.29]	0.73 [0.20, 1.00]	0	26
z7fhp	2.14 [1.38, 2.87]	1.80 [1.12, 2.58]	1.28 [0.18, 2.34]	0.78 [0.02, 0.98]	1.71 [-0.41, 2.13]	0.42 [-0.25, 0.95]	0	30
gdqeg	2.38 [1.97, 2.71]	2.25 [1.74, 2.68]	-1.61 [-2.46, -0.37]	0.10 [0.00, 0.98]	0.31 [-0.60, 1.63]	0.29 [-0.45, 1.00]	0	53
8toyp	2.63 [1.89, 3.29]	2.34 [1.59, 3.07]	1.78 [0.47, 2.89]	0.82 [0.02, 0.98]	1.94 [-0.06, 2.39]	0.47 [-0.17, 0.95]	0	29
w420e	2.63 [1.81, 3.53]	2.34 [1.67, 3.18]	1.74 [0.46, 2.92]	0.98 [0.55, 1.00]	2.28 [1.52, 2.41]	0.73 [0.20, 1.00]	0	20
arcko	2.64 [1.23, 3.78]	2.08 [1.10, 3.24]	1.71 [0.44, 3.10]	0.57 [0.04, 0.95]	1.42 [0.56, 2.93]	0.56 [-0.06, 1.00]	0	28
0wfzo	18.72 [11.21, 25.03]	15.80 [9.9, 22.35]	15.09 [8.28, 22.12]	0.09 [0.01, 0.73]	2.35 [-10.18, 8.12]	0.02 [-0.65, 0.66]	0	12
z3btx	22.60 [15.03, 29.00]	19.70 [12.97, 26.69]	19.70 [12.97, 26.69]	0.09 [0.01, 0.72]	2.35 [-10.00, 8.28]	0.02 [-0.66, 0.66]	0	7
758j8	23.76 [16.33, 30.24]	21.00 [14.26, 28.00]	21.00 [14.26, 28.00]	0.09 [0.01, 0.71]	2.35 [-10.34, 8.12]	0.02 [-0.65, 0.65]	0	8
hgn83	27.91 [20.54, 34.52]	25.60 [18.9, 32.64]	25.60 [18.9, 32.64]	0.09 [0.01, 0.72]	2.35 [-10.21, 8.00]	0.02 [-0.65, 0.65]	0	5